UNIVERSITY OF SOUTHAMPTON

FACULTY OF PHYSICAL SCIENCES & ENGINEERING

Optoelectronics Research Centre

Inverse scattering designs of optical waveguides and fibres

by

Alexander Robinson May

Thesis for the degree of Doctor of Philosophy

November 2015

UNIVERSITY OF SOUTHAMPTON

ABSTRACT

FACULTY OF PHYSICAL SCIENCES & ENGINEERING

Optoelectronics Research Centre

Thesis for the degree of Doctor of Philosophy

INVERSE SCATTERING DESIGNS OF OPTICAL WAVEGUIDES AND FIBRES

Alexander Robinson May

Optical fibres and waveguides have become vital components in communication systems ranging from on-chip interconnects in datacentres, to trans-oceanic submarine communication cables. Typically, they are designed in a trial-and-error manner and the objective of this thesis was to investigate their inverse design using a method known as inverse-scattering. In contrast to methods of design optimisation where an initial refractive form of index profile of some kind must be chosen, inverse-scattering makes no such assumptions other than that of which modes are carried by the structure and what their respective propagation constants are.

Initially, the control over group-velocity dispersion in a single-mode planar waveguide with fixed propagation constant was investigated by considering the form of the transverse reflection response by which the modal properties of the waveguide may be specified, as discussed in the literature. It was demonstrated that common features of dispersion-engineered waveguides were obtained corroborating their use in the existing literature and further understanding of these features was developed.

Extending the study to multimode planar waveguides through the application of an inverse-scattering method rooted in the quantum mechanical community, the properties of multiple guided modes, such as their group-velocities and modal gain were controlled. The realisation that both gain and loss are required in a refractive index profile to have exact equalisation of modal gain across multiple modes was novel and differed from existing approaches using genetic algorithms. In addition to this, the design of waveguide couplers by which power can be transferred from one waveguide to another was considered by an approach differing from that of the increasingly popular supersymmetric (SUSY) approach in the literature.

Attention turned to the design of few-mode optical fibres which are at the forefront of technology. Since the planar waveguide designs above were found to contain ‘depressions’ and ‘rings’, similar such features were investigated in an optical fibre based upon the knowledge that there were similarities in the modal intensity profiles of the first few linearly polarised (LP) modes in a fibre, and that of the TE modes in planar waveguides. Core depressions and ‘rod-like’ refractive index perturbations were implemented and found to increase the spacing between mode groups.

Following on from the above successes, inverse-scattering techniques were applied directly to the cylindrical symmetry of optical fibres and their associated LP modes. A particular feature of this work was the realisation that the propagation constants of such modes can only be specified at the start of the design process for a fixed value of the azimuthal symmetry of the fibre mode. A finding by other researchers using the SUSY technique had been that the modes in coupled fibres (trunk-partner pairs) could only be ‘matched’ when the azimuthal symmetry of the trunk and partner modes differed. The inverse-scattering method in this thesis, on the other hand, does not have this limitation.

Table of Contents

List of Tables

List of Figures

DECLARATION OF AUTHORSHIP

I, Alexander Robinson May, declare that this thesis and the work presented in it are my own and have been generated by me as the result of my own original research.

Inverse scattering designs of waveguides and optical fibres

I confirm that:

1. This work was done wholly or mainly while in candidature for a research degree at this University;

2. Where any part of this thesis has previously been submitted for a degree or any other qualification at this University or any other institution, this has been clearly stated;

3. Where I have consulted the published work of others, this is always clearly attributed;

4. Where I have quoted from the work of others, the source is always given. With the exception of such quotations, this thesis is entirely my own work;

5. I have acknowledged all main sources of help;

6. Where the thesis is based on work done by myself jointly with others, I have made clear exactly what was done by others and what I have contributed myself;

7. Parts of this work have been published as [please see list of references below]:

[1] **A. R. May**, F. Poletti, and M. N. Zervas, "Inverse scattering designs of dispersion-engineered single-mode planar waveguides," in *SPIE Photonics West 2014-OPTO: Optoelectronic Devices and Materials*, 2014, vol. 8988, p. 89881S.

[2] **A. R. May**, F. Poletti, and M. N. Zervas, "Inverse scattering designs of dispersion-engineered single-mode planar waveguides," *Opt. Express*, vol. 23, no. 3, p. 3142, 2015.

[3] **A. R. May** and M. N. Zervas, "Group velocity equalisation in multimode waveguides using inverse scattering designs," in *Sixth International Conference on Optical, Optoelectronic and Photonic Materials and Applications (ICOOPMA '14)*, 2014.

[4] **A. R. May** and M. N. Zervas, "IS designs for mode selective waveguide couplers," in *23rd Int. Workshop OWTNM*, 2015.

[5] **A. R. May** and M. N. Zervas, "Inverse scattering designs of active multimode waveguides with tailored modal gain," *J. Sel. Top. Quantum Electron.*, 2015.

[6] **A. R. May** and M. N. Zervas, "Inverse scattering designs of mode-selective waveguide couplers," *Pending submission*

[7] **A. R. May** and M. N. Zervas, "Few-Mode Fibers with Improved Mode Spacing," in *European Conference on Optical Communication (ECOC)*, 2015.

[8] **A. R. May** and M. N. Zervas, "Inverse scattering designs of mode-selective fibre couplers", *Pending submission*

Signed:.....

Date: .....

Acknowledgements

The completion of a thesis is a task that involves not only academic study but also a good support network comprised of supervisors, friends and family. I am lucky that I have had a lot of freedom to explore this topic by my own devices but with the support of my supervisors when I have needed them. My main supervisor, Prof Michalis Zervas, has always been at hand to lend physical insight to the theoretical problems we have studied as well as keeping me grounded with a foot in the real world. I have greatly benefitted from this.

Without my friends Alberto Sposito and Zhihong Li, who have now departed for adventures in industry and academia elsewhere, life would have been a lot less fun. Together we have cried with laughter in good times as well as helped each other when things have not gone quite to plan. They have been there to celebrate my marriage to the wonderful Hannah, without whom I would never have been able to finish this PhD, and literally been there to 'hold the baby' when our wonderful and mischievous daughter Poppy arrived.

Finally I have to thank my parents Francine and Henry May as well as my brother "Dr Greg" who have listened to my incessant mutterings about PhD related work as well as rushed to my aid when I needed time away to get work done.

I dedicate this work to all of you!

Chapter 1: Introduction

1.1 Optical waveguide and fibre design

1.1.1 A historical context

Communication involves the transfer of information from one point to another, and, since the end of the nineteenth century, this has often been achieved using a transmitter modulated electromagnetic carrier wave, be it a radio wave, microwave or light wave. Once modulated, the carrier wave travels through a channel after which it eventually meets a receiver where it is demodulated and the imprinted signal obtained. It can be roughly stated that the rate of information that can be sent is approximately proportional to the difference between the maximum and minimum frequencies of the channel, otherwise known as its bandwidth. As such, the information capacity of a modulated optical beam with carrier frequency in the range of 10^{14} to 10^{15} Hz is much larger than that typically obtained using radio or microwaves.

The use of optical carrier waves for telecommunications was given a boost when the ruby laser was discovered in 1960 by Theodore Maiman [1.1]. Prior to this, no optical source was suitable for such use, and its discovery occurred at a time of significant growth in telecommunications traffic. Initial investigations examined the possibility of using optical beams in very much the same way as conventional communication systems, through the transmission of a laser beam through the atmosphere. However, it was soon found that laser beams, with their wavelength being shorter than that typically found in the radio spectrum, suffered from considerable attenuation due to scattering and absorption in the atmosphere. A solution to this problem would be the use of some form of guiding medium with which to protect the light beam.

Shortly after the development of the ruby laser, in 1965 Charles K. Kao and George A. Hockham [1.2] of the then British company, the Standard Telecommunications Laboratory, recognised that a fibre of glassy material could be used as a medium for guided transmission at optical frequencies. In addition, they reported that the most significant attenuation of such a fibre was caused by impurities and not by fundamental physical limits, and could therefore be reduced in time.

In 1970 the first practical optical fibre suitable for communications, with a new low loss of 17 dB/km, was developed at glassmaker Corning by Robert D. Maurer, Donald Keck, Peter Schultz and Frank Zimar [1.3]. Up to that time it was the purest glass that had ever been made and was a breakthrough for fibre-optic communications. As the 1970s went by, development continued and soon the best Silica laboratory fibres were approaching the fundamental scattering limit at 0.85 μm of two decibels per kilometre. At around this time on the 22nd April 1977, General Telephone and Electronics sent

the first live telephone traffic over a 10 kilometre route between Long Beach and Artesia, California, using fibre optics at 6.3 Mbit/s. It was a world first.

1.1.2 Fibre optic communication systems

The late 1970s saw the development of the first fibre optic communication systems. This began at a wavelength of 0.85 μm using GaAs semiconductor lasers. Combined with the discovery by Horiguchi [1.4] of fibre losses of ~1 decibel per kilometre at longer wavelengths between 0.95 and 1.37 μm, as well as the potential for near-zero material dispersion in the same region, was the development of a new family of InGaAsP semiconductor lasers operating at 1.3 μm. The combination of low loss and low material dispersion would allow signals to go not only further at the longer wavelength, but carry more information because shorter pulses could be spaced closer together. This was the opening of the new telecommunication window at 1.3 μm.

Up until this time single-mode fibres had had a bad reputation because coupling of light into them was difficult. In addition, the high material dispersion at 0.85 μm meant that any attraction of single-mode transmission was offset. However, the opening of the new 1.3 μm window with its relatively low loss and low material dispersion promised capacity increases many times that of the existing technology. The light coupling problem was also to become less of an issue because of the increased core size and improvements in splice and connector technology.

The 1980s saw the fibre-optics market take off with deregulation of the long-distance telephone service in the USA with many companies expanding their networks. In addition, it was decided that the next generation of coaxial cables would no longer be developed for submarine cabling purposes in favour of optical fibres. By the time the next transatlantic cable, TAT-8, was laid, the two pairs of single-mode fibres were each carrying 280 million bits per second of data, the combined equivalent of 35,000 phone calls.

With better technology came communications capacity at a lower cost per channel and there was an explosion in demand. As soon as TAT-8 was nearing completion, TAT-9 was under development, but this time in a further new telecommunications window. This new window was located at 1.55 μm where fibre loss was at its lowest. Combined with the then new development of the Erbium-doped fibre amplifier, it was possible to double transmission speed to 560 million bits per second and repeater spacing later reached 140 km.

1.2 The optical waveguide

An optical waveguide consists of a core in which light is confined, surrounded by a cladding as shown in Figure 1-1 below. The refractive index of the core n_1 is chosen to be higher than that of the

cladding n_0 such that a light beam coupled to the face of the waveguide is confined into the core by total internal reflection.

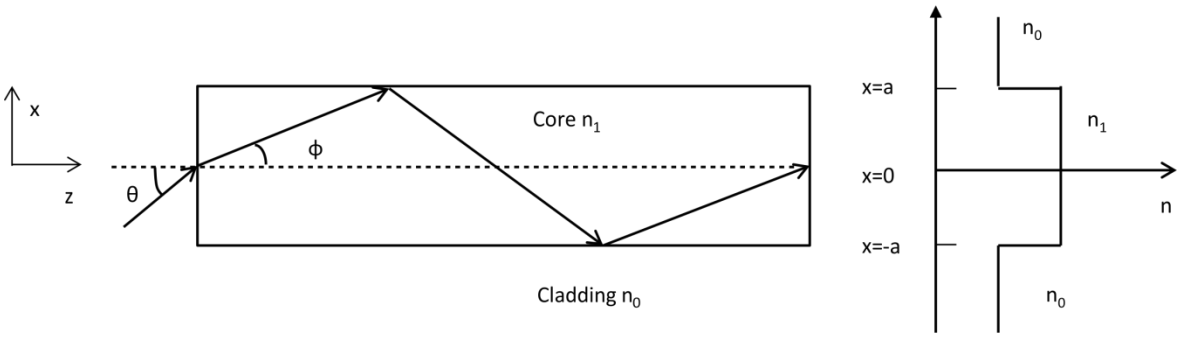

Figure 1-1: The basic structure and refractive index profile of an optical waveguide

In general, when an electromagnetic wave is incident upon a plane interface between two media of refractive indices n_1 and n_2 it gives rise to a reflected wave and a transmitted wave. The amplitudes of the reflection and transmission coefficients will be given later, but the relationship between the incident θ_1 and refracted θ_2 waves with respect to the normal at the boundary, is described through the use of Snell's Law,

$$n_1 \sin\theta_1 = n_2 \sin\theta_2 \tag{1.1}$$

The critical angle θ_c above which total internal reflection occurs is given by,

$$\theta_c = \arcsin\left(\frac{n_2}{n_1}\right) \tag{1.2}$$

The condition for total internal reflection at the core-cladding interface in Figure 1-1 is therefore given by,

$$n_1 \sin\left(\frac{\pi}{2} - \phi\right) \geq n_0 \tag{1.3}$$

and since the angle φ is related to the incident angle θ by,

$$\sin\theta = n_1 \sin\phi \leq \sqrt{n_1^2 - n_0^2} \tag{1.4}$$

we obtain the condition for the total internal reflection as,

$$\theta \leq \arcsin\sqrt{n_1^2 - n_0^2} \equiv \theta_{\max} \tag{1.5}$$

from which we arrive at the approximation for the maximum acceptance angle of the waveguide θ_{max}, otherwise known as the numerical aperture (NA),

$$\theta_{\max} \cong \sqrt{n_1^2 - n_0^2} \tag{1.6}$$

If the relative refractive index difference is defined as,

$$\Delta \equiv \frac{n_1^2 - n_0^2}{2n_1^2} \cong \frac{n_1 - n_0}{n_1} \tag{1.7}$$

Then the numerical aperture (NA) is related to the relative refractive index difference Δ by,

$$NA = \theta_{\max} \cong n_1\sqrt{2\Delta} \tag{1.8}$$

In the above we have described how waveguide modes may be confined provided the angle φ remains below a critical angle. However, it is important to note that not all modes with arbitrary angles lower than this critical value do not propagate in a waveguide. The angles that do propagate are discrete in nature and in order to elucidate what they are it is necessary to consider an example. Here we look at the ray picture of a planar slab waveguide as illustrated in Figure 1-2.

If we consider a plane wave propagating in the z-direction with an inclination angle φ, we see that the phase fronts are perpendicular to the direction of the light rays. Given an operating wavelength in vacuum λ we see that the wavelength and wavenumber in the core are given by the expressions λ/n_1 and kn_1 where $k=2\pi/\lambda$ is the vacuum wavenumber. The propagation constants in the

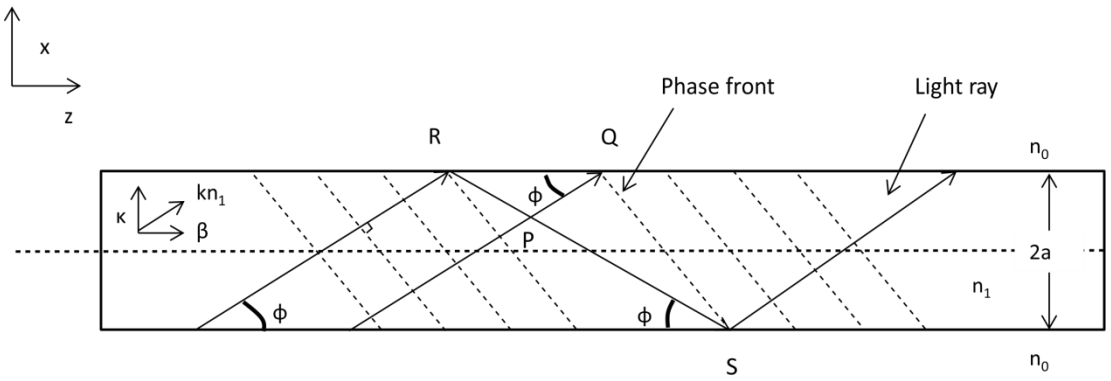

Figure 1-2: The light rays and their phase fronts in a waveguide

longitudinal (z-direction) and lateral (x-direction) are given by,

$$\beta = kn_1 \cos\phi \tag{1.9}$$

$$\kappa = kn_1 \sin\phi \tag{1.10}$$

Light ray PQ is assumed not to have suffered any phase change Φ on reflection, while the ray RS is reflected two times (once each at the upper and lower core-cladding interfaces). Since points P and R or points Q and S are on the same phase front, the optical path length between P and Q or R and S should be equal or a multiple of 2π. The path length l_1 between P and Q is given by,

$$l_1 = \left(\frac{2a}{\tan\phi} - 2a\tan\phi \right) \cos\phi \tag{1.11}$$

while path length between R and S is given by,

$$l_2 = \frac{2a}{\sin\phi} \tag{1.12}$$

The phase-matching condition is given by,

$$\left(kn_1 l_2 + 2\Phi\right) - kn_1 l_1 = 2m\pi \tag{1.13}$$

for integer m. The mode that satisfies m=0 is called the fundamental and those having larger values m≥1 are the higher-order modes. We simply state at this stage that the phase change on reflection at the interfaces, otherwise known as the Goos-Hanchen shift, is given by Okamoto [1.5],

$$\Phi = -2\arctan\sqrt{\frac{n_1^{\,2}\cos^2\phi - n_0^{\,2}}{n_1\sin\phi}} = -2\arctan\sqrt{\frac{2\Delta}{\sin^2\phi} - 1} \tag{1.14}$$

It is interesting to observe the formation of the modes and their standing waves through the interference of phase fronts. This is illustrated in Figure 1-3 for the fundamental mode and Figure 1-4 for the m=1 higher-order mode.

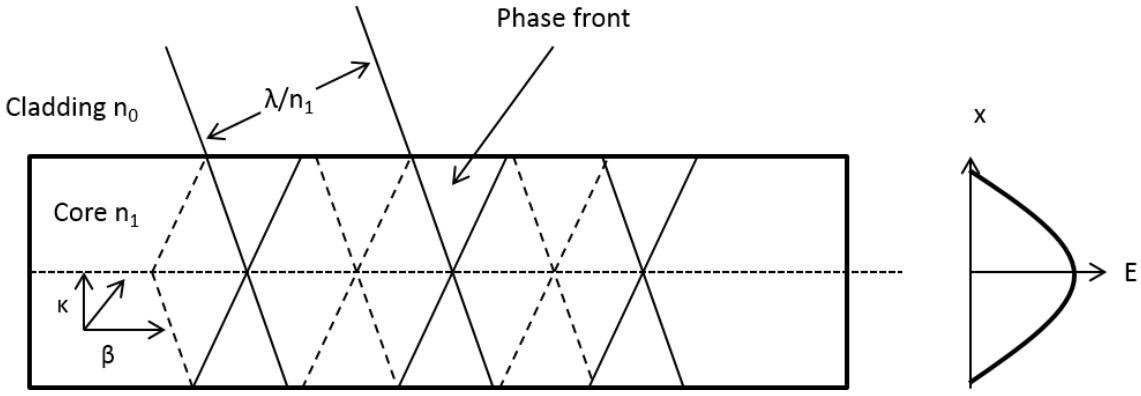

Figure 1-3: The formation of the fundamental mode standing-wave pattern

In each case the positive phase fronts are represented by solid lines, and the negative phase fronts by the dashed lines. Constructive interference between the solid lines leads to maxima and destructive interference between solid and dashed lines leads to minima. From Figure 1-3 and Figure 1-4, the value of the integer m is seen to correspond to the number of nodes of the lateral electric field profile.

A similar analysis can be applied to optical fibres, although it is necessary to introduce the concept of skew rays whereby rays travel in a helical path through the fibre and given the limitation of the above analysis to that of the high frequency limit and the fact that it is discussed in detail elsewhere such as by Snyder and Love [1.6], we do not discuss this approach further.

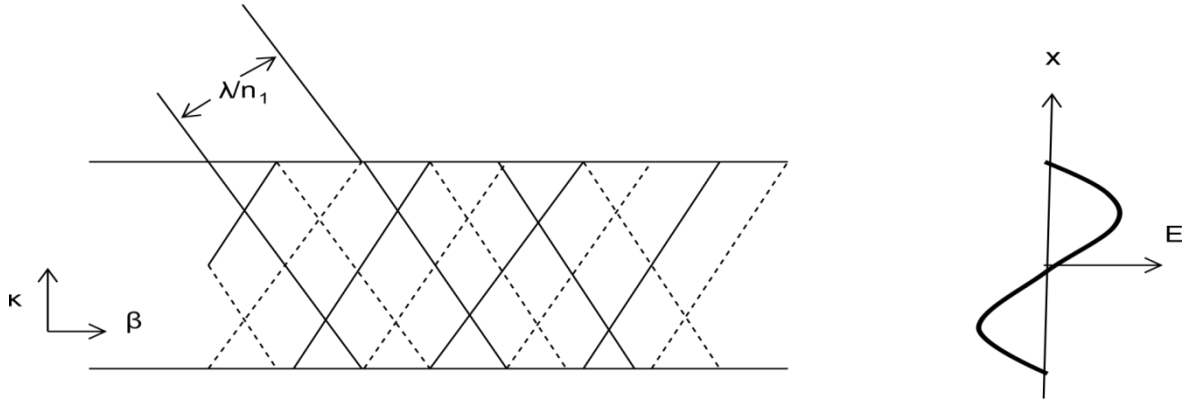

Figure 1-4: The formation of the m=1 higher-order mode standing wave pattern

1.3 Optical waveguide and fibre manufacture

As discussed above, optical waveguiding requires a variation in refractive index between the core and the cladding for the transmission of light. It is therefore necessary to identify at least two different materials which are transparent to light which exhibit relatively low optical attenuation. In order to avoid scattering losses greater than the fundamental limit, bubbles, strains and grain boundaries which act as scattering centres must be removed. The materials which satisfy these requires tend to be glasses and certain monocrystalline structure plastics [1.7]. In order to achieve graded refractive index profiles it is also necessary for the materials to be suitable for doping which in turn requires mutual solubility over a relatively wide range of doping concentrations. As a result of this, glass-like materials are chosen and plastics are thereby limited to the case of step-index fibres.

Vapour-phase deposition techniques are used in the production of silica-rich glasses which have optimal optical properties [1.7]. To begin with, volatile compounds such as $SiCl_4$, $GeCl_4$ and SiF_4, BCl_3, O_2, BBr_3 and $POCl_3$ are distilled to obtain raw materials with low concentrations of transition metal elements in order to reduce losses due to absorption. Modification of the refractive index is then possible by mixing gaseous mixtures of silica-containing compounds with a doping material such as TiO_2, GeO_2, P_2O_5, Al_2O_3, B_2O_3 and/or F, and oxygen in a vapour-phase oxidation reaction where the deposition of oxides results. This deposition is typically onto a substrate or within a hollow tube and is built up in successive layers. The variation possible in refractive index for a sample of dopant concentration is illustrated in Figure 1-5 where it can be seen that doping with Fluorine decreases the refractive index, while Germanium increases it.

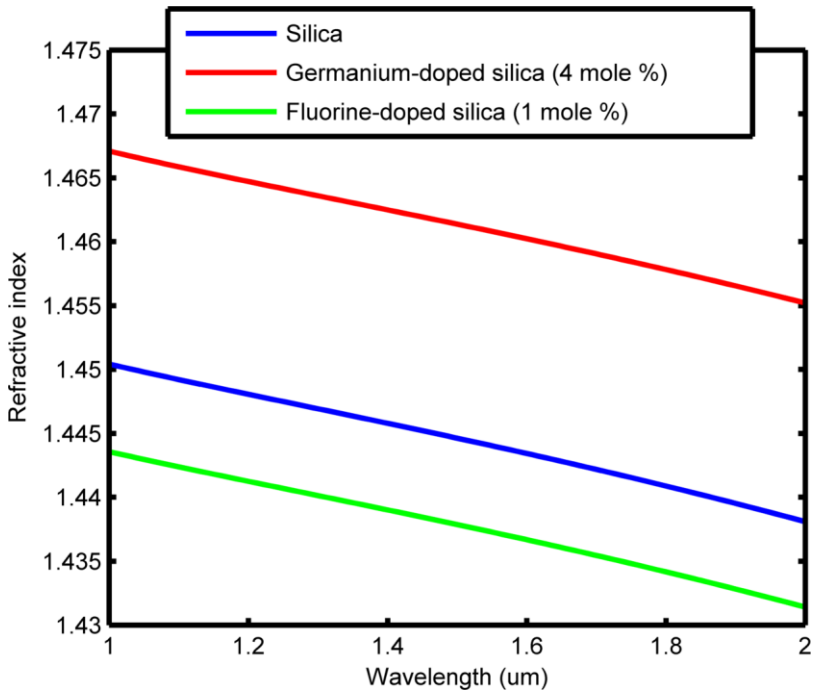

Figure 1-5: The variation in refractive index for a sample of dopant concentrations using data from [1.8]

1.4 Practical issues with optical waveguides and fibres

While optical waveguides and fibres bring with them huge potential benefits through their use in optical communications, it is necessary to consider their optical transmission characteristics in more detail. Here we briefly review two of their most important characteristics – their attenuation (loss) and bandwidth.

1.4.1 Attenuation in optical waveguides and fibres

The attenuation in optical waveguides and fibres is due to a combination of material absorption and scattering. Material attenuation can further be decomposed into intrinsic (caused by interaction of light with major components of the glass) or extrinsic (caused by impurities within the glass).

Pure silica glass has little intrinsic absorption in the near-infrared region due to its basic material structure. However, there are two major mechanisms at work, as shown in Figure 1-6, where fundamental absorption edges occur in the ultraviolet due to the stimulation of electronic transitions within the glass by high energy excitations, and in the infrared region where photons interact with molecular vibrations within the glass. In addition to the above, extrinsic absorption is due to transition element impurities within the glass. These impurities can lead to in excess of 1 dB/km attenuation in the near-infrared region. Another major loss mechanism is absorption due to water dissolved in the glass. The OH ions are bonded into the glass structure and have molecular stretching vibrations which give rise to overtones in the region of 1.38 μm as evidenced in the experimental curve.

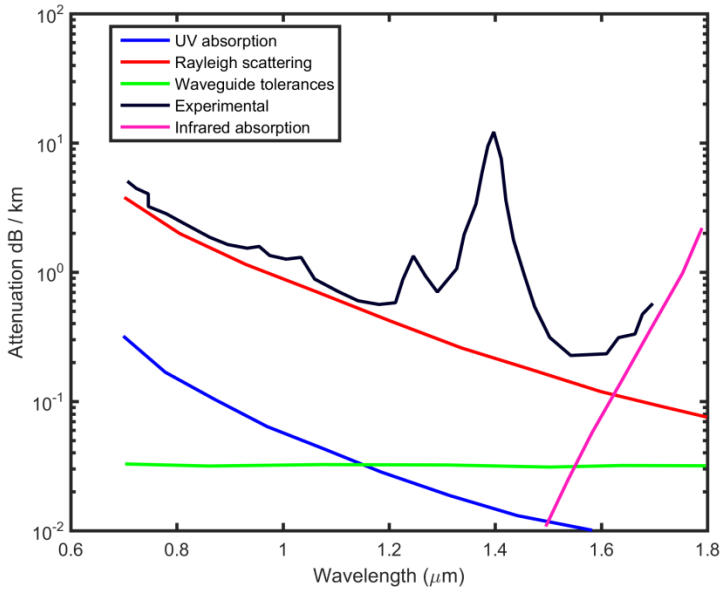

Figure 1-6: The attenuation spectrum for an ultra-low-loss fibre with calculated attenuation spectra for some of the loss mechanisms using data from [1.7]

Rayleigh scattering is a form of linear scattering whereby some or all of the optical power contained within a propagating mode is transferred proportionally into a different mode. Since it is possible for such power to transfer into leaky or radiation modes which do not continue to propagate within the core, it leads to attenuation. In particular, this form of scattering is the dominant loss mechanism in the low-absorption window between the ultraviolet and infrared absorption tails, and is due to random inhomogeneities in the refractive index due to density of compositional variations which have been frozen into the glass lattice on cooling. The scattering is found to occur in almost all directions and is proportional to $1/\lambda^4$.

Another form of scattering is known as Mie scattering and occurs at inhomogeneities comparable with the size of the guided wavelength. This typically occurs due to imperfections and irregularities in the fibre such as diameter fluctuations, strains and bubbles and is mainly directed in the forward direction.

Finally it is important to note that optical waveguides do not behave completely as linear channels where any increase in output optical power is proportional to the input power. This form of nonlinear scattering results in the transfer of optical power from one mode to another at a different frequency in either the forward or backward direction. The most important types are known as Brillouin and Raman scattering and are typically only observed at high optical power densities. Stimulated Brillouin scattering (SBS) is the modulation of light through the interaction of an incident photon with molecular vibrations within the fibre to produce a phonon of acoustic frequency and a scattered photon. As a result, the scattered light appears as upper and lower sidebands, of which the lower

appears mainly in the backward direction and the upper is lossy. Stimulated Raman scattering (SRS) is similar to SBS but involves the production of a high-frequency optical rather than acoustic phonon. It is observed in both the forward or backward directions with a threshold of up to three orders of magnitude higher than the Brillouin threshold in the same fibre. In each case the relevant non-linearities are members of the broader group of phenomena known as the Kerr effect.

1.4.2 Dispersion in optical waveguides and fibres

Dispersion is an effect that causes distortion of signal transmission along an optical waveguide thereby limiting the maximum transmission distance. As light pulses travel along the waveguide they are broadened by a variety of mechanisms, which can in general be split into two categories, one being intra-modal dispersion and the other being inter-modal dispersion. As the two names suggest, intra-modal dispersion, otherwise known as group-velocity dispersion, is the variation in the group velocity of a given signal mode with wavelength due to the wavelength dependence of both the confinement of the light in the waveguide and the material with which it is made. Inter-modal dispersion on the other hand is due to the differing group velocity of the various modes in a waveguide which carries multiple modes.

Input pulses are broadened as they travel along the optical waveguide, with the greatest broadening occurring for the case of the multimode step index fibre. An improvement in performance is seen in the graded-index multimode fibre, while the least broadening occurs for the final single-mode fibre.

As a simplification, for there to exist no overlapping of light pulses down an optical fibre link with bit rate B_T, it is necessary for this rate to be less than the reciprocal of the broadened pulse duration 2τ,

$$B_T \leq \frac{1}{2\tau} \tag{1.15}$$

The connection between bit rate and bandwidth depends upon the digital coding format used but a conservative measure results from nonreturn-to-zero (RZ) coding whereby the bandwidth B_{opt} is equal to the bitrate B_T. A measure of the performance of a fibre is therefore given by the product of the length L at which detection can still take place and the bandwidth of the optical link B (i.e B_{opt} x L). Typical bandwidth-length products of 20 MHz km, 1 GHz km and 100 GHz km are given for the multimode step index, multimode graded index and singlemode fibres respectively.

We now briefly discuss intramodal dispersion and intermodal dispersion in a little more detail.

1.4.3 Intramodal dispersion

As discussed above, intramodal dispersion is due to the dependence of the group velocity of a given mode on its wavelength. This dependence may be due to either material properties or the confinement

of the light in the waveguide. We first describe the effect of dispersion on a plane wave travelling through a material of refractive index n, and then adapt this to a guided wave.

The group delay τ_g of a plane wave is defined through its propagation constant β and angular frequency ω by [1.9],

$$\tau_g = \frac{L}{v_g} = L\frac{d\beta}{d\omega} = L\frac{d\beta}{d\lambda}\cdot\frac{d\lambda}{d\omega} \tag{1.16}$$

If we now write the propagation constant of the plane wave in terms of the refractive index n of the material and vacuum wavenumber k, we have,

$$\beta = nk = n\frac{2\pi}{\lambda} \tag{1.17}$$

We now derive,

$$\frac{d\beta}{d\lambda} = \frac{2\pi}{\lambda}\frac{dn}{d\lambda} - \frac{2\pi}{\lambda}n = -\frac{2\pi}{\lambda^2}\left(n - \lambda\frac{dn}{d\lambda}\right) \tag{1.18}$$

From which we obtain by inserting (1.18) into (1.16) and using the relationship $\omega=2\pi c/\lambda$,

$$\tau_g = L\cdot\frac{-2\pi}{\lambda^2}\left(n - \lambda\frac{dn}{d\lambda}\right)\cdot\left(\frac{-\lambda^2}{2\pi c}\right) = \frac{L}{c}\left(n - \lambda\frac{dn}{d\lambda}\right) \tag{1.19}$$

The light pulse will have a spectral width $\Delta\lambda$ and so different components in the pulse will travel with different delay times with the spread $\Delta\tau_g$ given by,

$$\Delta\tau_g = \frac{d\tau_g}{d\lambda}\cdot\Delta\lambda \tag{1.20}$$

With this in mind we derive,

$$\frac{d\tau_g}{d\lambda} = \frac{L}{c}\left[\frac{dn}{d\lambda} - \frac{dn}{d\lambda} - \lambda\frac{d^2n}{d\lambda^2}\right] = -\frac{L}{c}\lambda\frac{d^2n}{d\lambda^2} \tag{1.21}$$

finally giving the material dispersion,

$$\Delta\tau_g = -\frac{L}{c}\lambda\frac{d^2n}{d\lambda^2}\Delta\lambda \tag{1.22}$$

In order to investigate the effect of dispersion on a guided mode of propagation constant β, we consider relation (1.22) with the refractive index n replaced by the effective index n_{eff} of a guided mode defined through,

$$\beta = n_{eff}\frac{2\pi}{\lambda} = n_{eff}k \tag{1.23}$$

We then arrive at an expression for the total chromatic (intramodal) dispersion taking into account both material and waveguiding dependency,

$$D_c = \frac{1}{L}\frac{\Delta\tau_g}{\Delta\lambda} = -\frac{\lambda}{c}\frac{d^2 n_{eff}}{d\lambda^2} \tag{1.24}$$

An expression for a normalised propagation constant b is typically defined in terms of the effective index of the mode and the core n_1 and cladding materials n_2 by,

$$b = \frac{{n_{eff}}^2 - {n_2}^2}{{n_1}^2 - {n_2}^2} \approx \frac{n_{eff} - n_2}{n_1 - n_2} \tag{1.25}$$

With this in mind we may rewrite the above expression as,

$$n_{eff} = n_2 + (n_1 - n_2)b \tag{1.26}$$

From which we obtain a new expression for the total chromatic dispersion D_c in terms of two separate quantities, the material dispersion D_m and the waveguide dispersion D_w,

$$D_c = -\frac{\lambda}{c}\frac{d^2 n_2}{d\lambda^2} - \frac{\lambda}{c}\frac{d^2 (n_1 - n_2)b}{d\lambda^2} = D_m + D_w \tag{1.27}$$

We will discuss this further later in this chapter.

1.4.4 Intermodal dispersion

The broadening of pulses due to intermodal dispersion results from the differing group velocities between modes in a multimode waveguide. This form of dispersion can be considerable and dominates in multimode waveguides.

If we consider a ray theory model of a step-index fibre, we see that the minimum ray propagation time T_{min} is represented by an axial ray, while the maximum propagation time T_{max} would occur for an extreme meridional ray which is incident on the core-cladding interface at the critical angle.

As such we have,

$$T_{\min} = \frac{L}{c/n_1} = \frac{Ln_1}{c} \tag{1.28}$$

and,

$$T_{\max} = \frac{L/\cos\theta}{c/n_1} = \frac{Ln_1}{c\cos\theta} \tag{1.29}$$

Using Snell's law we also have,

$$\sin\phi_c = \frac{n_2}{n_1} = \cos\theta \tag{1.30}$$

From which we obtain a new expression for T_{max},

$$T_{\max} = \frac{Ln_1^2}{cn_2} \tag{1.31}$$

And from these expressions an approximation for the time difference between the two rays in terms of the refractive indices, their relative contrast Δ and the length of the waveguide L,

$$\delta T = T_{\max} - T_{\min} = \frac{Ln_1^2}{cn_2}\left(\frac{n_1 - n_2}{n_1}\right) = \frac{Ln_1^2\Delta}{cn_2} \tag{1.32}$$

Where the relative contrast Δ is approximately written as,

$$\Delta \approx \frac{n_1 - n_2}{n_1} \tag{1.33}$$

After some manipulation we obtain the time difference in terms of the numerical aperture (NA) of the fibre [1.7],

$$\delta T \approx \frac{L(NA)^2}{2n_2 c} \tag{1.34}$$

1.4.5 Maximising system performance

Here we briefly discuss how system performance can be maximised through the choice of optical fibre design. We then describe how the inverse scattering approach has evolved. The primary property of an optical fibre that can be modified is the dispersion curve which describes how an optical pulse of a given wavelength and spectral width will broaden in time as it propagates along the fibre. However, altering the dispersion curve alters the effective area of the fibre and also the cut-off wavelength.

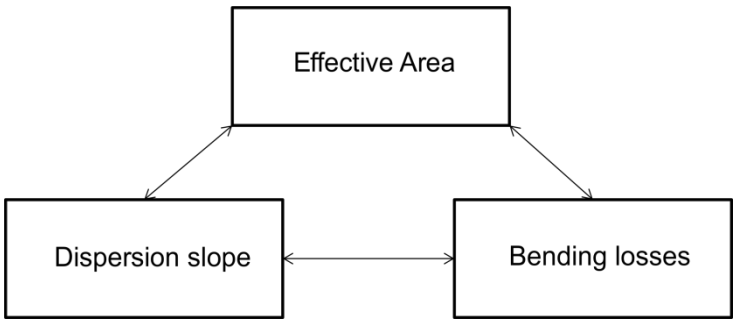

Figure 1-7: The trade-offs associated with optical fibre design

As can be seen in Figure 1-7 it is necessary to understand that design trade-offs occur and the properties of an optical fibre cannot be varied independently. System design dictates that the ideal fibre might be one with low dispersion as well as dispersion slope at 1.55 μm while maintaining a reasonable effective area A_{eff} of the fibre to control both non-linearity and bend losses, such as in the case of a wavelength-division-multiplexing (WDM) system. Here it is important that the dispersion is low, but non-zero, to control pulse broadening while limiting non-linear effects such as four-wave mixing (FWM) and cross-phase modulation (XPM) between channels. This is also helped by keeping a reasonably large mode effective area so that the power density is not confined to too small an area which would in turn make such a fibre more vulnerable to such non-linearities, while not so large as to make it sensitive to bend losses. It is also important that the dispersion is low across a band of channels and therefore the dispersion slope should also be low. If any two characteristics in Figure 1-7 are selected, Maxwell's equations control the third. It can be simply stated at this point to develop intuition that for paraxial waves, the propagation constant of a mode β may be expressed in terms of the mode field E(r,λ) as well as the refractive index n(r,λ) as [1.10],

$$\beta^2(\lambda) \leq \left(\frac{2\pi}{\lambda}\right)^2 \iint n^2(r,\lambda) \cdot \left|E(r,\lambda)\right|^2 \cdot dA \tag{1.35}$$

where the integration is performed over the fibre cross-section. This relationship demonstrates that the propagation constant and its derivatives, hence also dispersion, are inextricably linked to the mode field and refractive index profile. The rate at which the mode field expands and/or contracts with wavelength in turn determines the dispersive properties of the fibre. Since the equations which govern modal properties in optics are analogous to those which govern the wavefunction of a particle in a box in quantum mechanics it suggests that a certain amount of intuition in the design process is possible [1.10].

As might be expected in a field of work that crosses national boundaries, we now discuss briefly the international standardisation of optical fibres by the agency known as the ITU of the United Nations in order to obtain some consensus.

A fundamental way to group fibre designs is through the properties of the dispersion curve. The original standard single-mode fibre was known as the ITU G.652 and had a zero-dispersion-

wavelength (ZDW) at ~1.3 μm. With the development in the 1980s of the low-loss 1.55 μm window, the dispersion-shifted-fibre (DSF) was introduced and standardised under the name G.653. While it may appear that having zero dispersion in this new window is an advantage, the development of wavelength-division-multiplexing systems has meant that this fibre has limited application due to unwanted nonlinearities when optical channels are close to the ZDW. The G.654 was developed as a cutoff-shifted fibre with a larger mode field diameter in order to provide lower loss and allow higher optical power for transmission over longer distances. The family of G.655 fibres known as non-zero-dispersion-shifted fibres were developed to provide a balance of properties for high data transmission rates over long distances. The key property is low, but non-zero, dispersion at 1.55 μm. Finally, the G.656 was developed with the purpose of having low dispersion from 1.46-1.63 μm to decrease inter-symbol-interference (ISI) in wavelength-division-multiplexed systems. However, as can be seen, this fibre has properties similar to the medium dispersion category of G.655. The key feature of G.656 is its good performance with low nonlinearity for signal channels as well as Raman pumps at short wavelengths.

In addition to the control of dispersion in the single-mode case above, with the development of schemes designed to counter the upcoming 'capacity crunch', such as spatial-division-multiplexing (SDM) as discussed by Richardson et al. [1.11], it has become important to control the differential group delay between various modes in few-mode fibres to reduce complexity in the de-multiplexing process [1.12], [1.13], as well as control over the mode spacing [1.14], [1.15] in order to reduce coupling between modes. A good review of such approaches to the design of few-mode fibres is given by Sillard [1.16].

1.4.6 The advantages of optical waveguides and fibres

The merits and special features offered by optical communications can be summarised as has been done in the work of Senior and Jamro [1.7].

(a) Enormous potential bandwidth (~10^5 GHz in the near infrared) when compared with metallic systems such as coaxial cables (~20 MHz). By the year 2015, the length-bandwidth product of an optical fibre link was in the region of >100 GHz km whereas coaxial cable was 0.1 GHz km.

(b) Small size, weight and flexibility which is advantageous in crowded city network infrastructure. Light weight also allows for use in mobile situations including aircraft and satellites.

(c) Electrical isolation due to glass/plastic being an insulator. Problems involving earth loop and interface problems are removed and application in electrically hazardous environments is possible.

(d) Immunity to electrically noisy environments. Communications using optical fibres do not require shielding from electromagnetic interference (EMI) and crosstalk is negligible when compared with electrical conductors.

(e) Security of communications. Optical fibres do not radiate significantly and therefore provide for high signal security. Any interception would require invasive methods which could in theory be detected.

(f) High reliability and ease of maintenance due to a lower requirement for repeaters or amplifiers when compared with copper because of low optical fibre losses.

(g) Low cost. Optical fibres are made from derivatives of glass which are in abundance when compared with copper.

1.5 Applications of inverse scattering theory

Inverse scattering theory (IST) has been used in a variety of settings over the years. A seminal contribution to the field was made in the 1950s and 1960s when a closed-form solution to the fundamental Gel'fand-Levitan-Marchenko (GLM) integral equation of inverse scattering was found for rational reflection coefficients by Kay [1.17]. This particular technique was then later used to investigate the inversion of semiconductor charge carrier density profiles by Jordan and Kritikos [1.18] and then ionospheric and plasma profiles from scattering data by their group [1.19],[1.20] through the use of reflection coefficients approximated using Butterworth and three-pole rational functions respectively.

An important step forward was the consideration in Jordan's work [1.21] of a potential well for which one of the poles represented a bound state. At around the same time a general, efficient and exact method was being developed for the inversion of rational reflection coefficients of arbitrary order by Pechenick [1.22], [1.23]. Other numerical techniques were also being developed such as by Kritikos and Ge [1.24], [1.25]. Within a few years this general three-pole approach with a single bound state had been utilised in the design of both wide-core and general single-mode planar waveguides [1.26]-[1.28] and shortly afterwards a paper was published by Jordan and Xia [1.29] investigating the physical interpretation and meaning of various poles in the context of the modes in waveguides.

After a brief intermission, further design of single-mode and multi-mode waveguides and their modal fields were considered through numerical methods by authors such as Papachristos and Frangos [1.30] and Hirsch et al. [1.31]. However, no work had been done investigating control over either dispersive properties of waveguides, or mode spacing. In addition, although there had been some early work by on the design of circular waveguides under the weakly guiding approximation for which either the propagation constant was prescribed for modes of fixed azimuthal value, such as by Yukon and Bendow [1.32], or the propagation constant was fixed at a constant value for modes of

varying azimuthal value by Hooshyar [1.33], no work has been done investigating whether it is possible to control dispersion or mode spacing.

As alluded to in the previous section, there is an inherent link between the design of waveguides and potential wells in quantum mechanics. In addition to the inverse scattering techniques discussed above which rely upon solutions to the Gel'fand-Levitan-Marchenko (GLM) integral equations, the general construction of potential wells has also been considered using the Darboux/Crum-Krein transformations by Sakasi [1.34] as well as Rudyakm [1.35] and methods from supersymmetry (SUSY) which can importantly be shown to be a particular case of the Darboux transformation approach as was done by Suzko and Velicheva [1.36]. In particular, applied combinations of the transformations of the SUSY approach can be shown to be equivalent to the GLM approach [1.37].

1.6 Aims and objective of the thesis

The aim of the work undertaken in this thesis was to investigate the potential for the inverse design of optical fibres with a priori specified properties such as dispersion and mode spacing through the application of inverse scattering (IS) [1.38], [1.39] methods. The motivation behind this particular approach was the previous successful work done using IS methods in the design of Bragg gratings, some of which is described by Feced et al. and others [1.40]–[1.43]. There was also a precedent set for the IS design of planar waveguides in the works of Jordan and Lakshanasamy in the late 1980s [1.44],[1.45] where properties such as the waveguide width was maximised and optical interconnects were designed. However, little work had been done on the use of IS methods in the design of optical fibres. Some early work was done investigating the specification of propagation constants such as by Yukon in 1980 [1.46] and Hooshyar in 1992 [1.47] using circular dielectric waveguides but further approaches based on this method appeared to have stalled. More recently work had been done on the inverse design of optical fibres with tailored dispersion characteristics by Poletti [1.48] using optimisation methods such as Genetic Algorithms.

As a result of the above works it was decided that work on planar waveguides would be extended with a view to further understanding the IS approach and potential applications, and then following this, the IS approach or intuition derived from it would be applied to application to optical fibres. As little direct work had been performed in this area, it was very important at this stage to keep an open mind as to whether a direct solution actually existed to this problem, and to use intuition obtained from designs in the more mature field of planar slab waveguides to achieve the final goal.

1.7 Structure of the thesis

Chapter 2 introduces Maxwell's equations and the electromagnetic theory behind both waveguide and fibre modes. Following this there is further discussion of the spectral properties of fibre modes

in terms of normalised parameters and features such as the group delay and dispersion. The theory behind the methods of inverse scattering are then developed in the context of both waveguides and fibres and the connections between the various methods are discussed.

In Chapter 3 the methods of waveguide and fibre simulation are introduced, with particular emphasis on the transfer matrix method for the waveguide designs. The finite difference method implemented in the commercial mode solver MODE Solutions is then briefly developed for completeness as it is used to verify the results throughout this work. Finally coupled mode theory is developed for application in the later waveguide and fibre coupler designs.

Chapter 4 describes the initial work done on the dispersion-engineering of single-mode planar waveguides developed using the Gel'fand-Levitan-Marchenko equations as applied to rational reflection coefficients, and extended to those with larger numbers of poles. In particular, a general method of identifying the permissible domain of pole parameters is then developed using a computationally implemented Sturm's theorem in the symbolic algebra package MAPLE.

In Chapter 5 the initial work on the use of Darboux transformations as applied to multimode waveguides is developed and applied in the design of multimode waveguides with group velocity equalisation. Linked to this work, in Chapter 6 this same Darboux transformation approach was used in the design of multimode waveguides with tailored modal gain, and finally in Chapter 7 application was made to the design of multimode waveguide couplers where equalisation of coupling lengths was made using the addition of mode gain/loss.

Chapter 8 describes the use of physical intuition gained from the inverse scattering design of waveguides thus far to the design of optical fibres with improved LP mode group spacing through the addition of a core depression and non-azimuthally-symmetric 'rods' which preferentially 'lift' modes with similar such mode profiles.

In Chapter 9 the inverse scattering design of optical fibres is discussed through the solution of the Gel'fand-Levitan-Marchenko integral equations in cylindrical coordinates whereby mode effective indices can be specified for fixed azimuthal LP mode value. Using this technique, in contrast with state-of-the-art SUSY techniques, partner fibres can be designed to couple LP modes selectively, as well as with the same, or differing azimuthal l value. In the same way that Chapter 6 investigated the inverse scattering design of planar waveguides with tailored modal gain, and Chapter 7 used this in the development of mode-selective couplers with equalised coupling lengths, this same idea was now applied to fibre modes leading to the development of multimode mode-selective fibre couplers with equalized coupling lengths.

1.8 Summary of results and achievements

In the following two publications the work performed on the dispersion-engineering of planar waveguides through the solution of the Gel'fand-Levitan-Marchenko integral equations was described:

(1) **A. R. May**, F. Poletti, and M. N. Zervas, "Inverse scattering designs of dispersion-engineered single-mode planar waveguides," in *SPIE Photonics West 2014-OPTO: Optoelectronic Devices and Materials*, 2014, vol. 8988, p. 89881S.

(2) **A. R. May**, F. Poletti, and M. N. Zervas, "Inverse scattering designs of dispersion-engineered single-mode planar waveguides," *Opt. Express*, vol. 23, no. 3, p. 3142, 2015.

The novelty of engineering the dispersion of waveguides by this approach is in the ability to vary the dispersion of the waveguide while keeping the effective index and thus phase velocity of the guided mode constant. This is typically not possible in the waveguide design process where, as in the case of a step index design, the variation of parameters such as the refractive index contrast and core width varies the characteristic V-number of the guide and thus both its dispersion and propagation constant. While it may be possible to design more complex refractive index profiles for which there is more independent control of the above features, there is no way to know in advance what geometric assumptions must be made of such a profile to achieve these ends. An inverse scattering approach, on the other hand, provides the required profile directly.

In the following publications the initial work on the design of multimode waveguides through application of the Darboux transformation approach with equalised group velocity was described, followed by the initial work presented on the design of mode-selective waveguide couplers as an alternative to the more limited SUSY approach. Finally the tailoring of modal gain was investigated in multimode waveguides through the use of complex propagation constants in the design process:

(3) **A. R. May** and M. N. Zervas, "Group velocity equalisation in multimode waveguides using inverse scattering designs," in *Sixth International Conference on Optical, Optoelectronic and Photonic Materials and Applications (ICOOPMA '14)*, 2014.

(4) **A. R. May** and M. N. Zervas, "IS designs for mode selective waveguide couplers," in *23rd Int. Workshop OWTNM*, 2015.

(5) **A. R. May** and M. N. Zervas, "Inverse scattering designs of active multimode waveguides with tailored modal gain," *J. Sel. Top. Quantum Electron.*, 2015.

(6) **A. R. May** and M. N. Zervas, "Inverse scattering designs of mode selective waveguide couplers," *Pending submission*

In the above works the novelty lies first in the demonstration that the group velocity of modes may be controlled through their relative mode spacing, which until now has been described through Brown's identity, but not demonstrated explicitly in the design process, and secondly in the experimental determination through an inverse scattering approach that the optimal waveguide design for equalised group velocity is that with equally spaced mode effective indices and thus in fact belongs to the infinitely extended parabolic refractive index discussed in the literature by authors such as Adams [1.49].

The use of the Darboux transform in the design of mode-selective waveguide couplers is novel in its approach as it is not limited in its ability to 'select' modes through phase-matching in the same way as the current state-of-the-art SUSY technique. The Darboux approach neither requires the same development of a cascade of waveguides whereby modes are removed *singly* one at a time, nor the use of complex refractive index profiles to achieve only this. In addition, I demonstrate that it is possible to tailor and equalise the coupling lengths of *multiple* selected mode 'pairs' at once through the use of an imaginary (gain/loss) mismatch in effective index associated with each pair.

In the following publications the design of optical fibres was considered firstly by using physical intuition derived from the inverse scattering design of optical waveguides above through the use of perturbations to existing few-mode fibre designs, and then followed more completely by the solution of the Gel'fand-Levitan-Marchenko integral equations in cylindrical coordinates. As in the case of the Darboux transform approach discussed above for the design of multimode waveguides with tailored modal gain and its use in the design of mode-selective waveguide couplers with equalised coupling lengths, this was investigated in the context of fibres and has allowed for the design of mode-selective fibre couplers with an alternative and improved method to that of SUSY:

(7) **A. R. May** and M. N. Zervas, "Few-Mode Fibers with Improved Mode Spacing," in *European Conference on Optical Communication (ECOC)*, 2015.

(8) **A. R. May** and M. N. Zervas, "Inverse scattering designs of mode-selective fibre couplers", *Pending submission*

In the above works the novelty lies in the fact that intuition originally derived from observing patterns in refractive index profile behaviour with varying TE mode spacing in multimode inverse-scattered planar waveguide designs was carried across to LP modes in a few-mode optical fibre design. These patterns were further understood by considering the perturbation relation suggested by Snyder and Love [1.6] which definitively showed that mode spacing could be controlled by considering weighed integrals of the mode field and refractive index profile.

The result of this was a few-mode optical fibre which utilised high-index 'rods' in place of 'rings' in the planar waveguide cases and resulted in improved mode-spacing.Further to this, as described above, the solution of the Gel'fand-Levitan-Marchenko integral equations in cylindrical coordinates was then used to demonstrate a more complete method by which novel mode-selective fibre couplers could be developed as an extension to the aforementioned mode-selective waveguide couplers above.

1.9 References

[1.1] T. H. Maiman, "Stimulated Optical Radiation in Ruby," *Nature*, vol. 187, pp. 493–494, 1960.

[1.2] K. C. Kao and G. a Hockham, "Dielectric fiber surface waveguides for optical frequencies," *Procedings IEE*, vol. 7, no. 3, pp. 1151–1158, 1966.

[1.3] F. Kapron, D. Keck, and R. Maurer, "Radiation losses in glass optical waveguides," *Appl. Phys. Lett.*, vol. 17, pp. 423-425, 1970.

[1.4] M. Horiguchi and H. Osanai, "Spectral losses of low-OH-content optical fibres," *Electron. Lett.*, vol. 12, no. 12, pp. 310–312, 1976.

[1.5] K. Okamoto, *Fundamentals of Optical Waveguides*. London, UK, 2006.

[1.6] A. Snyder and J. Love, *Optical Waveguide Theory*. London: Chapman and Hall, 1983.

[1.7] J. M. Senior and M. Y. Jamro, *Optical Fiber Communications: Principles and Practice*. Harlow, Essex, UK: Pearson Education Limited, 2009.

[1.8] A. Mendez and T. Morse, *Speciality Optical Fibers Handbook*. London: Academic Press, 2007.

[1.9] R. S. Quimby, *Photonics and lasers: an introduction (Google eBook)*. John Wiley and Sons, 2006.

[1.10] S. Ramachandran, "Dispersion-Tailored Few-Mode Fibers : A Versatile Platform for In-Fiber Photonic Devices," *J. Light. Technol.*, vol. 23, no. 11, pp. 3426–3443, 2005.

[1.11] D. J. Richardson, J. M. Fini, and L. E. Nelson, "Space-division multiplexing in optical fibres," *Nat. Photonics*, vol. 7, no. April, pp. 354–362, 2013.

[1.12] L. Grüner-Nielsen and Y. Sun, "Few mode transmission fiber with low DGD, low mode coupling, and low loss," *J. Light. Technol.*, vol. 30, no. 23, pp. 3693–3698, 2012.

[1.13] T. Sakamoto, T. Mori, T. Yamamoto, N. Hanzawa, S. Tomita, F. Yamamoto, K. Saitoh, and M. Koshiba, "Mode-Division Multiplexing Transmission System With DMD-Independent Low Complexity MIMO Processing," *J. Light. Technol.*, vol. 31, no. 13, pp. 2192–2199, 2013.

[1.14] P. Sillard, M. Astruc, and D. Boivin, "Few-mode fiber for uncoupled mode-division multiplexing transmissions," *ECOC Tech. Dig.*, pp. 38–40, 2011.

[1.15] M. Bigot-Astruc, D. Boivin, and P. Sillard, "Design and fabrication of weakly-coupled few-modes fibers," *2012 IEEE Photonics Soc. Summer Top. Meet. Ser.*, vol. 1, no. 978, pp. 189–190, 2012.

[1.16] P. Sillard, M. Bigot-Astruc, and D. Molin, "Few-Mode Fibers for Mode-Division-Multiplexed Systems," *J. Light. Technol.*, vol. 32, no. 16, pp. 2824–2829, 2014.

[1.17] I. Kay, "The Inverse Scattering Problem When the Reflection Coefficient is a Rational Function," *Commun. Pure Appl. Math.*, vol. XIII, pp. 371–393, 1960.

[1.18] A. K. Jordan and H. N. Kritikos, "An Application of One-Dimensional Inverse-Scattering Theory for Inhomogeneous Regions," *IEEE Trans. Antennas Propag.*, vol. 21, no. 6, pp. 909-911, 1973.

[1.19] S. Ahn and A. K. Jordan, "Profile inversion of simple plasmas and nonuniform regions: Three-pole reflection coefficient," *IEEE Trans. Antennas Propag.*, vol. 24, no. 6, pp. 879–882, 1976.

[1.20] M. Reilly and A. K. Jordan, "The applicability of an inverse method for reconstruction of electron-density profiles," *IEEE Trans. Antennas Propag.*, vol. 29, no. 2, pp. 245–252, 1981.

[1.21] A. K. Jordan, D. Ph, and S. Ahn, "Inverse scattering theory and profile reconstruction," *Proc. Inst. Electr. Eng.*, vol. 126, no. 10, pp. 945–950, 1979.

[1.22] K. R. Pechenick, "Inverse scattering—exact solution of the Gel'fand-Levitan equation," *J. Math. Phys.*, vol. 22, no. 7, pp. 1513–1516, 1981.

[1.23] K. R. Pechenick, "Exact solutions to the valley problem in inverse scattering," *J. Math. Phys.*, vol. 24, no. 2, pp. 406–409, 1983.

[1.24] H. Kritikos, D. Jaggard, and D. Ge, "Numerical Reconstruction of Smooth Dielectric Profiles," *Proc. IEEE*, vol. 70, no. 3, pp. 1981–1983, 1982.

[1.25] D. Ge, "An iterative technique in one-dimensional profile inversion," *Inverse Probl.*, vol. 3, no. 3, pp. 399-406, 1987.

[1.26] A. K. Jordan and S. Lakshmanasamy, "Inverse scattering theory applied to the design of single-mode planar optical waveguides," *J. Opt. Soc. Am. A*, vol. 6, no. 8, pp. 1206–1212, 1989.

[1.27] S. Lakshmanasamy and A. K. Jordan, "Design of wide-core planar waveguides by an inverse scattering method.," *Opt. Lett.*, vol. 14, no. 8, pp. 411–413, 1989.

[1.28] D. B. Ge, A. K. Jordan, and L. S. Tamil, "Numerical inverse scattering theory for the design of planar optical waveguides," *J. Opt. Soc. Am. A*, vol. 11, no. 11, pp. 2809-2815, 1994.

[1.29] J. Xia and A. K. Jordan, "Inverse-scattering view of modal structures in inhomogeneous optical waveguides," *JOSA A*, vol. 9, no. 5, pp. 740–748, 1992.

[1.30] C. Papachristos and P. Frangos, "Synthesis of single-and multi-mode planar optical waveguides by a direct numerical solution of the Gel'fand-Levitan-Marchenko integral equation," *Opt. Commun.*, vol. 203, no. March, pp. 27–37, 2002.

[1.31] I. Hirsh, M. Horowitz, and A. Rosenthal, "Design of Planar Waveguides With Prescribed Mode-Profile Using Inverse Scattering Theory," *J. Quantum Electron.*, vol. 45, no. 9, pp. 1133–1141, 2009.

[1.32] S. P. Yukon and B. Bendow, "Design of waveguides with prescribed propagation constants," *J. Opt. Soc. Am.*, vol. 70, no. 2, pp. 172–179, 1980.

[1.33] M. Hooshyar, "Inverse scattering theory at fixed energy and the design of circular optical waveguides," *J. Math. Phys.*, vol. 33, pp. 663–669, 1992.

[1.34] R. Sasaki, "Exactly solvable potentials with finitely many discrete eigenvalues of arbitrary choice," p. 17, 2014.

[1.35] B. Rudyak, A. Suzko, and B. Zakhariev, "Exactly Solvable Models (Crum-Krein Transformations in the (λ2, E)-Plane)," *Phys. Scr.*, vol. 29, pp. 515–517, 1984.

[1.36] A. Suzko and E. Velicheva, "Supersymmetry and Darboux transformations," *J. Phys. Conf. Ser.*, vol. 343, p. 012120, 2012.

[1.37] C. V Sukumar, "Supersymmetric quantum mechanics and the inverse scattering method," *J. Phys. A. Math. Gen.*, vol. 18, pp. 2937–2955, 1985.

[1.38] P. Deift and E. Trubowitz, "Inverse scattering on the line," *Commun. Pure Appl. Math.*, vol. 32, pp. 121–251, 1979.

[1.39] K. . Hopcraft and P. . Smith, *An Introduction to Electromagnetic Inverse Scattering*. London: Kluwer Academic Publishers, 1992.

[1.40] R. Feced, M. N. Zervas, and M. A. Muriel, "An Efficient Inverse Scattering Algorithm for the Design of Nonuniform Fiber Bragg Gratings," *J. Quantum Electron.*, vol. 35, no. 8, pp. 1105–1115, 1999.

[1.41] M. Ibsen, M. K. Durkin, M. N. Zervas, A. B. Grudinin, and R. I. Laming, "Custom design of long chirped Bragg gratings: application to gain-flattening filter with incorporated dispersion compensation," *IEEE Photonics Technol. Lett.*, vol. 12, no. 5, pp. 498–500, 2000.

[1.42] J. Skaar, "Synthesis and characterization of fiber Bragg gratings," PhD Thesis, Norweigan University of Science and Technology, 2000.

[1.43] J. Skaar and L. Wang, "On the synthesis of fiber Bragg gratings by layer peeling," *J. Quantum Electron.*, vol. 37, no. 2, pp. 165–173, 2001.

[1.44] L. S. Tamil and A. K. Jordan, "Spectral Inverse Scattering Theory for Inhomogeneous Dielectric Waveguides and Devices," *Proc. IEEE*, vol. 79, no. 9103253, pp. 1519–1528, 1991.

[1.45] D. W. Mills and L. S. Tamil, "Synthesis of Guided Wave Optical Interconnects," *IEEE J. Quantum Electron.*, vol. 29, no. 11, pp. 2825–2834, 1993.

[1.46] S. P. Yukon and B. Bendow, "Design of waveguides with prescribed propagation constants," *J. Opt. Soc. Am.*, vol. 70, no. 2, pp. 172–179, 1980.

[1.47] M. Hooshyar, "Inverse scattering theory at fixed energy and the design of circular optical waveguides," *J. Math. Phys.*, vol. 33, pp. 663–669, 1992.

[1.48] F. Poletti, X. Feng, G. M. Ponzo, M. N. Petrovich, W. H. Loh, and D. J. Richardson, "All-solid highly nonlinear singlemode fibers with a tailored dispersion profile.," *Opt. Express*, vol. 19, no. 1, pp. 66–80, 2011.

[1.49] M. J. Adams, *An Introduction to Optical Waveguides*. New York: Wiley, 1981.

Chapter 2: **Theory**

2.1 I**ntroduction**

In this chapter we review the theory behind the guidance of electromagnetic modes in optical waveguides and fibres. In contrast to the ray theory approach described briefly earlier in this thesis to develop an intuition which is only valid in the high frequency limit, we now use the more accurate and general method of solving Maxwell's equations given the specific geometry of the guiding structure and assumptions regarding characteristics of the modes.

We first discuss the time-dependent and source-free Maxwell's equations and then investigate solutions for guided waves in planar optical waveguides. Following a review of the fundamental parameters and nomenclature associated with such structures, we then go on similarly to develop solutions as applied to optical fibres. Here we very much follow the description given by Kawana and Kitoh [2.1]

With an understanding of the modal features of both planar and fibre geometries in hand, we then develop the theory of inverse scattering as applied to such structures. We review the fundamental Gel'fand-Levitan-Marchenko integral equations and proceed to investigate solutions. Of particular interest are those associated with potentials, known in this context to be refractive index (RI) profiles, with rational reflection coefficients and those which are reflectionless. In each of these cases closed-form solutions exist which simplifies solution and develops intuition. Of particular interest is the development of an inverse spectral theory (IST) which allows for the perturbation of individual mode propagation constants at will.

2.2 **Maxwell's Equations**

We now describe Maxwell's equations which govern electromagnetic waves in a linear material. Inside such regions the electric field **E** (volts per metre), the magnetic field **H** (amperes per metre), the electric flux density **D** (coulombs per square metre) and magnetic flux density **B** (amperes per square metre) and current density **J** are related through,

$$\nabla \times \mathbf{E} = -\frac{\partial \mathbf{B}}{\partial t} \tag{2.1}$$

$$\nabla \times \mathbf{H} = \frac{\partial \mathbf{D}}{\partial t} + \mathbf{J} \tag{2.2}$$

$$\nabla \bullet \mathbf{B} = 0 \tag{2.3}$$

$$\nabla \bullet \mathbf{D} = \rho \tag{2.4}$$

$$\nabla \bullet \mathbf{J} = -\frac{\partial \rho}{\partial t} \tag{2.5}$$

With constitutive relations,

$$\mathbf{D} = \varepsilon \mathbf{E} \tag{2.6}$$

$$\mathbf{B} = \mu \mathbf{H} \tag{2.7}$$

The permittivity ε and permeability μ are defined in terms of the permittivity ε_0 and permeability μ_0 of free space as well as the relative permittivity ε_r and permeability μ_r of the material,

$$\varepsilon = \varepsilon_0 \varepsilon_r \tag{2.8}$$

$$\mu = \mu_0 \mu_r \tag{2.9}$$

Wave equations can be obtained by considering an electromagnetic field oscillating at an angular frequency ω. We may represent the field in complex notation as,

$$\mathbf{E}(\mathbf{r},t) = \mathrm{Re}\left[\bar{\mathbf{E}}(\mathbf{r})\exp\left(j\omega t\right)\right] \tag{2.10}$$

$$\mathbf{H}(\mathbf{r},t) = \mathrm{Re}\left[\bar{\mathbf{H}}(\mathbf{r})\exp\left(j\omega t\right)\right] \tag{2.11}$$

$$\mathbf{D}(\mathbf{r},t) = \mathrm{Re}\left[\bar{\mathbf{D}}(\mathbf{r})\exp\left(j\omega t\right)\right] \tag{2.12}$$

$$\mathbf{B}(\mathbf{r},t) = \mathrm{Re}\left[\bar{\mathbf{B}}(\mathbf{r})\exp\left(j\omega t\right)\right] \tag{2.13}$$

From which we obtain, where for simplicity we represent the time-independent terms $\bar{\mathbf{E}}$**,** $\bar{\mathbf{H}}$**,** $\bar{\mathbf{D}}$**,** $\bar{\mathbf{B}}$ in the phasor representation above again as **E**, **H**, **D** and **B**,

$$\nabla \times \mathbf{E} = -j\omega \mathbf{B} = -j\omega\mu_0 \mathbf{H} \tag{2.14}$$

$$\nabla \times \mathbf{H} = j\omega\varepsilon \mathbf{E} \tag{2.15}$$

$$\nabla \bullet \mathbf{H} = 0 \tag{2.16}$$

$$\nabla \bullet \left(\varepsilon_r \mathbf{E}\right) = 0 \tag{2.17}$$

In the above we have assumed that μ_r is 1 for all materials other than magnetic ones and ρ=0. A wave equation for the electric field E can then be obtained,

$$\nabla \times \left(\nabla \times \mathbf{E}\right) = -j\omega\mu_0 \nabla \times \mathbf{H} \tag{2.18}$$

Using,

$$\nabla \times \left(\nabla \times \mathbf{A} \right) = \nabla \left(\nabla \bullet \mathbf{A} \right) - \nabla^2 \mathbf{A} \tag{2.19}$$

we rewrite the LHS of (2.18) in the form,

$$\nabla \left(\nabla \bullet \mathbf{E} \right) - \nabla^2 \mathbf{E} \tag{2.20}$$

and since,

$$\nabla \bullet \left(\varepsilon_r \mathbf{E} \right) \equiv \nabla \varepsilon_r \bullet \mathbf{E} + \varepsilon_r \nabla \bullet \mathbf{E} = 0 \tag{2.21}$$

we obtain,

$$\nabla \bullet \mathbf{E} = -\frac{\nabla \varepsilon_r}{\varepsilon_r} \bullet \mathbf{E} \tag{2.22}$$

The LHS of (2.18) can therefore be written as,

$$-\nabla \left(\frac{\nabla \varepsilon_r}{\varepsilon_r} \bullet \mathbf{E} \right) - \nabla^2 \mathbf{E} \tag{2.23}$$

Using (2.15) and combining with (2.23) we obtain,

$$\nabla^2 \mathbf{E} + \nabla \left(\frac{\nabla \varepsilon_r}{\varepsilon_r} \bullet \mathbf{E} \right) + k_0{}^2 \varepsilon_r \mathbf{E} = \mathbf{0} \tag{2.24}$$

With the following definitions and introduction of the refractive index n,

$$k = k_0 n = k_0 \sqrt{\varepsilon_r} = k_0 n \tag{2.25}$$

And the relative permittivity taken as constant in the medium, the vectorial Helmholtz equation for the electric field is obtained,

$$\nabla^2 \mathbf{E} + k^2 \mathbf{E} = \mathbf{0} \tag{2.26}$$

In a similar manner a vectorial wave equation can be obtained for the magnetic field,

$$\nabla^2 \mathbf{H} + k^2 \mathbf{H} = \mathbf{0} \tag{2.27}$$

If we assume that the waveguiding structure is uniform in the z-direction, the derivative of the electromagnetic field with respect to z may be written as,

$$\frac{\partial}{\partial \mathrm{z}} = -j\beta \tag{2.28}$$

Where β is the propagation constant and signifies the z-directed component of the wavenumber k. The ratio of the propagation constant to the free-space wavenumber $k_0 = 2\pi/\lambda$, where λ is the wavelength, is defined as the effective index of the mode,

$$n_{eff} = \frac{\beta}{k_0} \tag{2.29}$$

Inserting this convention into the Helmholtz equation for the electric field **E** and magnetic field **H** gives,

$$\nabla^2{}_{\perp}\mathbf{E} + \left(k^2 - \beta^2\right)\mathbf{E} = 0 \tag{2.30}$$

$$\nabla^2{}_{\perp}\mathbf{H} + \left(k^2 - \beta^2\right)\mathbf{H} = 0 \tag{2.31}$$

where we have defined,

$$\nabla^2{}_{\perp} = \frac{\partial^2}{\partial x^2} + \frac{\partial^2}{\partial y^2} \tag{2.32}$$

2.2.1 The Poynting vector

In the following description we denote the time-dependent electric and magnetic fields by **E**(**r**,t) and **H**(**r**,t), and the time-independent electric and magnetic fields by $\bar{\mathbf{E}}$**(r)** and $\bar{\mathbf{H}}$**(r)**.

Due to the fact that the voltage is given by the integral of the electric field and because the magnetic field is created by a current, the product of the electric fields and the magnetic fields is related to the energy of the electromagnetic field. If we apply the divergence operator to the cross product we obtain,

$$\nabla\bullet\left(\mathbf{E}\times\mathbf{H}\right) = \mathbf{H}\bullet\nabla\times\mathbf{E} + \mathbf{E}\bullet\nabla\times\mathbf{H} \tag{2.33}$$

and if it then substitute this into Maxwell's equations (2.1-2.5) we get,

$$\begin{aligned}\nabla\bullet\left(\mathbf{E}\times\mathbf{H}\right) &= -\mu\mathbf{H}\bullet\frac{\partial\mathbf{H}}{\partial t} - \varepsilon\mathbf{E}\bullet\frac{\partial\mathbf{E}}{\partial t} - \sigma\mathbf{E}^2 \\ &= -\frac{\partial}{\partial t}\left(\frac{1}{2}\varepsilon\mathbf{E}^2 + \frac{1}{2}\mu\mathbf{H}^2\right) - \sigma\mathbf{E}^2\end{aligned} \tag{2.34}$$

Where we have used the relationship, **J**=σ**E,** relating the current density **J** to the electric field **E** through the electrical conductivity σ.

If we now integrate over an arbitrary volume V we get, using Gauss's theorem across a surface S,

$$\begin{aligned}\int_V \nabla\bullet(\mathbf{E}\times\mathbf{H})\,dV &= \int_S (\mathbf{E}\times\mathbf{H})\bullet\mathbf{n}\,dS \\ &= -\frac{\partial}{\partial t}\int_V\left(\frac{1}{2}\varepsilon\mathbf{E}^2+\frac{1}{2}\mu\mathbf{H}^2\right)dV-\int_V\sigma\mathbf{E}^2dV\end{aligned} \tag{2.35}$$

The first two terms can be identified as the rate of reduction of the energy stored in the electric and magnetic fields, while the third term is the rate of reduction of energy due to Joule heating in the volume V per unit time. As such we may identify the expression,

$$\int_S (\mathbf{E}\times\mathbf{H})\bullet\mathbf{n}\,dS \tag{2.36}$$

as being the rate of energy loss through the surface S. Therefore, the definition,

$$\mathbf{S}=(\mathbf{E}\times\mathbf{H}) \tag{2.37}$$

can be identified as the energy that passes through a unit area per unit time. This expression for **S** is known as the Poynting vector.

Considering an electromagnetic wave that oscillates at a single angular frequency, we may define the time-averaged Poynting vector <**S**> as,

$$\begin{aligned}\langle\mathbf{S}\rangle &= \langle\mathbf{E}\times\mathbf{H}\rangle \\ &= \left\langle \mathrm{Re}\left\{\bar{\mathbf{E}}(\mathbf{r})\exp(j\omega t)\right\}\times\mathrm{Re}\left\{\bar{\mathbf{H}}(\mathbf{r})\exp(j\omega t)\right\}\right\rangle \\ &= \left\langle \frac{\bar{\mathbf{E}}(\mathbf{r})\exp(j\omega t)+\bar{\mathbf{E}}(\mathbf{r})^*\exp(-j\omega t)}{2}\times\frac{\bar{\mathbf{H}}(\mathbf{r})\exp(j\omega t)+\bar{\mathbf{H}}(\mathbf{r})^*\exp(-j\omega t)}{2}\right\rangle \\ &= \frac{1}{4}\left\langle\left(\bar{\mathbf{E}}\times\bar{\mathbf{H}}^*\right)+\left(\bar{\mathbf{E}}^*\times\bar{\mathbf{H}}\right)+\bar{\mathbf{E}}\times\bar{\mathbf{H}}\exp(j2\omega t)+\bar{\mathbf{E}}^*\times\bar{\mathbf{H}}^*\exp(-j2\omega t)\right\rangle \\ &= \frac{1}{2}\mathrm{Re}\left\{\left\langle\bar{\mathbf{E}}\times\bar{\mathbf{H}}^*\right\rangle\right\}\end{aligned} \tag{2.38}$$

We may therefore write the energy propagating as the real part of the Poynting vector **S**.

2.2.2 Boundary conditions

In order to solve Maxwell's equations for electromagnetic fields we need the boundary conditions which may be summarised as

(a) Tangential components of the electric fields are continuous, that is

$$E_{1t}=E_{2t} \tag{2.39}$$

(b) If no current flows on the surface, tangential components of the magnetic fields are continuous, that is

$$H_{1t}=H_{2t} \tag{2.40}$$

If a current does flow on the surface, the magnetic fields are discontinuous and related to the current density J_S , that is

$$H_{1t} - H_{2t} = J_S \tag{2.41}$$

(c) If there is no charge on a surface, the normal components of the electric flux densities are continuous, that is

$$D_{1n} = D_{2n} \tag{2.42}$$

If there are charges on the surface, the electric flux densities are discontinuous and related to the charge density ρ_S, that is

$$D_{1n} - D_{2n} = \rho_S \tag{2.43}$$

(d) Normal components of the magnetic flux densities are continuous, such that

$$B_{1n} = B_{2n} \tag{2.44}$$

2.3 Theory of Optical Waveguides

Here we present the theory behind optical waveguides. We begin with a three layer slab waveguide with a one-dimensional structure. It has refractive indices n_1, n_2 and n_3 which are uniform in the y and z-directions, with regions 1 and 3 being cladding and region 2 the core. We know that tangential field components are connected at the interfaces and so we begin our analysis with the Helmholtz equations for each region of uniform material. Since we also assume that the structure is uniform in the y-direction we may assume that $\partial / \partial y = 0$

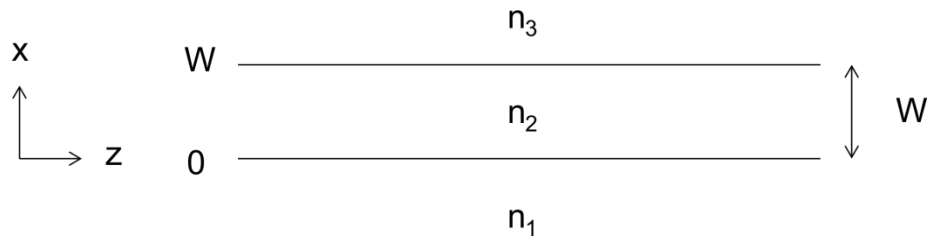

Figure 2-1: Geometry of a planar optical waveguide

The Helmholtz equation for the electric field may be written as,

$$\frac{d^2\mathbf{E}}{dx^2} + k_0^{\,2}\left(n^2 - n_{eff}^{\,2}\right)\mathbf{E} = 0 \tag{2.45}$$

and for the magnetic field,

$$\frac{d^2\mathbf{H}}{dx^2} + k_0^{\,2}\left(n^2 - n_{eff}^{\,2}\right)\mathbf{H} = 0 \tag{2.46}$$

It can be shown that two different forms of modes propagate in such a three-layer slab optical waveguide. These are known as the transverse electric modes (TE mode) and transverse magnetic modes (TM mode) and can be derived by considering Maxwell's equations,

$$\nabla \times \mathbf{E} = -j\omega\mu_0 \mathbf{H} \tag{2.47}$$

$$\nabla \times \mathbf{H} = j\omega\varepsilon_0\varepsilon_r \mathbf{E} \tag{2.48}$$

2.3.1 TE modes

If we assume the form of a mode where the electric field is not in the longitudinal direction (E_z=0) and is uniform in the y-direction, substitution into Equation (2.48) indicates that $\partial H_y / \partial x = 0$ and therefore H_y is constant and so may assume that H_y=0. Substituting E_z=H_y=0 into Equation (2.47) results in $\partial E_x / \partial z = 0$ from which we may assume constant E_x=0 and thus we have,

$$E_x = E_z = H_y = 0 \tag{2.49}$$

Using the above relationships we have,

$$H_x = -\frac{\beta}{\omega\mu_0} E_y \tag{2.50}$$

and,

$$H_z = \frac{j}{\omega\mu_0} \frac{\partial E_y}{\partial x} \tag{2.51}$$

Substituting these we obtain a wave equation for the principle electric field component E_y,

$$\frac{d^2 E_y}{dx^2} + \left(k_0{}^2 n^2 - n_{eff}{}^2\right) E_y = 0 \tag{2.52}$$

where we have written $k_0 = \omega\sqrt{\varepsilon_0\mu_0}$

We now know the form of the wave equation in each uniform layer and therefore assume solutions in each layer of the form,

$$E_y(x) = \begin{cases} C_1 \exp(\gamma_1 x) & \text{(region 1)} \\ C_2 \cos(\gamma_2 x + \alpha) & \text{(region 2)} \\ C_3 \exp(-\gamma_3 [x - W]) & \text{(region 3)} \end{cases} \tag{2.53}$$

Here the constants C_1,C_2 and C_3 are unknown constants, and we have defined,

$$\gamma_1 = k_0\sqrt{n_{eff}^{\ 2} - n_1^{\ 2}} \tag{2.54}$$

$$\gamma_2 = k_0\sqrt{n_2^{\ 2} - n_{eff}^{\ 2}} \tag{2.55}$$

$$\gamma_3 = k_0\sqrt{n_{eff}^{\ 2} - n_3^{\ 2}} \tag{2.56}$$

Using,

$$H_z = -\frac{1}{j\omega\mu_0}\frac{\partial E_y}{\partial x} \tag{2.57}$$

we may write the magnetic field in each region as,

$$H_z(x) = \begin{cases} -\dfrac{\gamma_1}{j\omega\mu_0}C_1\exp(\gamma_1 x) & \text{(region 1)} \\ \dfrac{\gamma_2}{j\omega\mu_0}C_2\sin(\gamma_2 x + \alpha) & \text{(region 2)} \\ \dfrac{\gamma_3}{j\omega\mu_0}C_3\exp(-\gamma_3[x - W]) & \text{(region 3)} \end{cases} \tag{2.58}$$

We see that there are five unknowns (n_{eff}, C_1, C_2 and C_3 and α) and by enforcing the boundary conditions of the tangential electric field component E_y and tangential magnetic field component H_z at x=0 and x=W,

$$E_{y1}(0) = E_{y2}(0) \tag{2.59}$$

$$H_{z1}(0) = H_{z2}(0) \tag{2.60}$$

$$E_{y2}(W) = E_{y3}(W) \tag{2.61}$$

$$H_{z2}(W) = H_{z3}(W) \tag{2.62}$$

we obtain the four equations,

$$C_1 = C_2\cos\alpha \tag{2.63}$$

$$-\gamma_1 C_1 = \gamma_2 C_2\sin\alpha \tag{2.64}$$

$$C_2\cos(\gamma_2 W + \alpha) = C_3 \tag{2.65}$$

$$-\gamma_2 C_2\sin(\gamma_2 W + \alpha) = -\gamma_3 C_3 \tag{2.66}$$

For a full solution the overall mode normalisation is required, but by letting C_1 be a free parameter, and thereby not specifying the amplitude of the mode, dividing (2.64) by (2.63) we obtain,

$$\alpha = -\tan^{-1}\left(\frac{\gamma_1}{\gamma_2}\right) + q_1\pi \qquad (q_1 = 0,1,2,...) \tag{2.67}$$

And dividing (2.66) by (2.65),

$$\gamma_2 W = \tan^{-1}\left(\frac{\gamma_3}{\gamma_2}\right) - \alpha + q_2\pi \qquad (q_2 = 0,1,2,...) \tag{2.68}$$

Substituting (2.67) into (2.68) we obtain,

$$\gamma_2 W = \tan^{-1}\left(\frac{\gamma_1}{\gamma_2}\right) + \tan^{-1}\left(\frac{\gamma_3}{\gamma_2}\right) + q\pi \qquad (q = 0,1,2,...) \tag{2.69}$$

Since all γ can be written in terms of the effective index n_{eff} this is a dispersion relation which can be solved numerically.

2.3.2 TM Modes

In TM modes the magnetic field component is now in the transverse direction. Since the structure is uniform in the y-direction we get $\partial E_y / \partial x = 0$ and therefore that E_y is a constant which we may take to be zero. Substituting H_z=E_y=0 we obtain $\partial H_x / \partial z = 0$ and so H_x=0. In summary,

$$H_x = H_z = E_y = 0 \tag{2.70}$$

Substituting the expressions,

$$E_x = \left(\frac{\beta}{\omega\varepsilon_0\varepsilon_r}\right) H_y \tag{2.71}$$

$$E_z = -\left(\frac{j}{\omega\varepsilon_0\varepsilon_r}\right)\frac{\partial H_y}{\partial x} \tag{2.72}$$

into (2.47) we obtain the wave equation for the principle magnetic field component H_y

$$\frac{d^2 H_y}{dx^2} + k_0{}^2\left(n^2 - n_{eff}{}^2\right) H_y = 0 \tag{2.73}$$

Again, the principle magnetic field components are assumed to be of the form,

$$H_y(x)=\begin{Bmatrix} C_1\exp(\gamma_1 x) & \text{(region 1)} \\ C_2\cos(\gamma_2 x+\alpha) & \text{(region 2)} \\ C_3\exp(-\gamma_3[x-W]) & \text{(region 3)} \end{Bmatrix} \tag{2.74}$$

with,

$$\gamma_1 = k_0\sqrt{n_{eff}{}^2 - n_1{}^2} \tag{2.75}$$

$$\gamma_2 = k_0\sqrt{n_2{}^2 - n_{eff}{}^2} \tag{2.76}$$

$$\gamma_3 = k_0\sqrt{n_{eff}{}^2 - n_3{}^2} \tag{2.77}$$

The tangential electric field component E_z is given by,

$$E_z = \frac{1}{j\omega\varepsilon_0\varepsilon_r}\frac{\partial H_y}{\partial x} \tag{2.78}$$

And so we may write the electric field in each region as,

$$E_z(x)=\begin{Bmatrix} \frac{\gamma_1}{j\omega\varepsilon_0\varepsilon_r}C_1\exp(\gamma_1 x) & \text{(region 1)} \\ -\frac{\gamma_2}{j\omega\varepsilon_0\varepsilon_r}C_2\sin(\gamma_2 x+\alpha) & \text{(region 2)} \\ \frac{\gamma_3}{j\omega\varepsilon_0\varepsilon_r}C_3\exp(-\gamma_3[x-W]) & \text{(region 3)} \end{Bmatrix} \tag{2.79}$$

Imposing the boundary conditions on the tangential fields at x=0 and x=W we obtain,

$$C_1 = C_2\cos\alpha \tag{2.80}$$

$$-\frac{\gamma_1}{\varepsilon_{r1}}C_1 = \frac{\gamma_2}{\varepsilon_{r2}}C_2\sin\alpha \tag{2.81}$$

$$C_2\cos(\gamma_2 W+\alpha) = C_3 \tag{2.82}$$

$$-\frac{\gamma_2}{\varepsilon_{r2}}C_2\sin(\gamma_2 W+\alpha) = -\frac{\gamma_2}{\varepsilon_{r2}}C_3 \tag{2.83}$$

Dividing (2.81) by (2.80) we obtain,

$$\alpha = -\tan^{-1}\left(\frac{\varepsilon_{r1}}{\varepsilon_{r2}}\frac{\gamma_1}{\gamma_2}\right) + q_1\pi \qquad (q_1 = 0,1,2,\ldots) \tag{2.84}$$

Dividing (2.83) by (2.82) we also obtain,

$$\gamma_2 W = \tan^{-1}\left(\frac{\varepsilon_{r2}}{\varepsilon_{r3}}\frac{\gamma_3}{\gamma_2}\right) - \alpha + q_2\pi \qquad (q_2 = 0,1,2,...) \tag{2.85}$$

Substituting (2.84) into (2.85) we obtain,

$$\gamma_2 W = \tan^{-1}\left(\frac{\varepsilon_{r2}}{\varepsilon_{r1}}\frac{\gamma_1}{\gamma_2}\right) + \tan^{-1}\left(\frac{\varepsilon_{r2}}{\varepsilon_{r3}}\frac{\gamma_3}{\gamma_2}\right) + q\pi \qquad (q = 0,1,2,...) \tag{2.86}$$

Since all γ can be written in terms of the effective index n_{eff} this is the dispersion relation which can be solved numerically.

2.4 Theory of Optical Fibres

In this section we discuss the analysis of a step-index optical fibre. An optical fibre consists of a core and a cladding and is axially symmetric as shown in Figure 2-2. The refractive index of the core is slightly larger than that of the cladding and so the optical field is largely confined in the core.

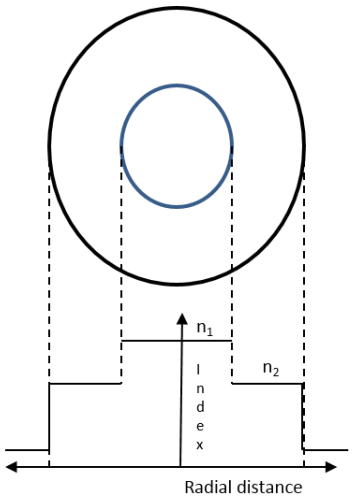

Figure 2-2: Geometry of an optical fibre illustrating the core n_1 and cladding n_2 refractive indices of a step-index optical fibre

Using the vectorial wave equations we may write for the transverse electric and magnetic fields,

$$\nabla^2{}_{\perp}\mathbf{E} + \nabla\left(\frac{\nabla\varepsilon_r}{\varepsilon_r}\bullet\mathbf{E}\right) + k_0{}^2\left(\varepsilon_r - n_{eff}{}^2\right)\mathbf{E} = 0 \tag{2.87}$$

$$\nabla^2{}_{\perp}\mathbf{H} + \frac{\nabla\varepsilon_r}{\varepsilon_r}\times\left(\nabla\times\mathbf{H}\right) + k_0{}^2\left(\varepsilon_r - n_{eff}{}^2\right)\mathbf{H} = 0 \tag{2.88}$$

Although the above equations can be solved using hybrid-mode analysis, in this work we only consider fibres for which the difference between the core and cladding indices is of the order of 1%. As such, the relative permittivity ε_r is small and ignoring the derivatives in the vectorial wave equations gives a good approximation. From this we obtain the scalar Helmholtz equations for the (weakly-guiding) transverse electric and magnetic fields,

$$\nabla^2{}_{\perp}\mathbf{E}_{\perp} + k_0{}^2\left(n(r)^2 - n_{eff}{}^2\right)\mathbf{E}_{\perp} = 0 \tag{2.89}$$

$$\nabla^2{}_{\perp}\mathbf{H}_{\perp} + k_0{}^2\left(n(r)^2 - n_{eff}{}^2\right)\mathbf{H}_{\perp} = 0 \tag{2.90}$$

The Laplacian in the above is written,

$$\begin{aligned}\nabla^2 &= \nabla^2{}_{\perp} + \frac{\partial^2}{\partial z^2} \\ &= \frac{1}{r}\frac{\partial}{\partial r}\left(r\frac{\partial}{\partial r}\right) + \frac{1}{r^2}\frac{\partial^2}{\partial\theta^2} + \frac{\partial^2}{\partial z^2} \\ &= \frac{\partial^2}{\partial r^2} + \frac{1}{r}\frac{\partial}{\partial r} + \frac{1}{r^2}\frac{\partial^2}{\partial\theta^2} + \frac{\partial^2}{\partial z^2}\end{aligned} \tag{2.91}$$

We may solve (2.89) for the electric field by assuming that the field $\mathbf{E}_{\perp}$ is oriented purely along either the x-axis or y-axis with zero axial z-component, henceforth known as a linearly-polarised mode, and of the form,

$$E_i(r,\theta) = R(r)\Theta(\theta) \tag{2.92}$$

Substituting this form into (2.89) and dividing by R(r)Θ(θ) gives,

$$\frac{1}{R(r)}\left(\frac{\partial^2 R(r)}{\partial r^2} + \frac{1}{r}\frac{\partial R(r)}{\partial r}\right) + r^2 k_0{}^2\left(n(r)^2 - n_{eff}{}^2\right) = -\frac{1}{\Theta(\theta)}\frac{\partial^2\Theta}{\partial\theta^2} \tag{2.93}$$

Since the LHS is a function of only r and the RHS is a function of only θ we find that both sides must be constants. We therefore get,

$$\frac{r^2}{R(r)}\left(\frac{d^2 R(r)}{dr^2} + \frac{1}{r}\frac{dR(r)}{dr}\right) + r^2 k_0{}^2\left(n(r)^2 - n_{eff}{}^2\right) = l^2 \tag{2.94}$$

and,

$$\frac{1}{\Theta(\theta)}\frac{d^2\Theta(\theta)}{d\theta^2} = -l^2 \tag{2.95}$$

With some rewriting these can be put in the more usual form,

$$\frac{d^2R(r)}{dr^2}+\frac{1}{r}\frac{dR(r)}{dr}+k_0{}^2\left(\varepsilon_r-n_{eff}{}^2-\frac{l^2}{r^2}\right)R(r)=0 \tag{2.96}$$

and,

$$\frac{d^2\Theta(\theta)}{d\theta^2}+l^2\Theta(\theta)=0 \tag{2.97}$$

The solution to (2.97) is an oscillation with a single frequency and may be expressed in the form,

$$\Theta\left(\theta\right)=\sin\left(l\theta+\phi\right) \tag{2.98}$$

and the solution to (2.96) are well known [2.1] and provided by the l'th-order Bessel functions. The solutions are,

$$R(r)=\begin{cases}AJ_l\left(\frac{ur}{a}\right)+BN_l\left(\frac{ur}{a}\right) & \text{for } r\le a\\ CK_l\left(\frac{wr}{a}\right)+DI_l\left(\frac{wr}{a}\right) & \text{for } r\ge a\end{cases} \tag{2.99}$$

where we have defined,

$$u^2=k_0{}^2a^2\left(\varepsilon_{r1}-n_{eff}{}^2\right) \tag{2.100}$$

$$w^2=k_0{}^2a^2\left(n_{eff}{}^2-\varepsilon_{r2}\right) \tag{2.101}$$

The $J_l(ur/a)$ and $N_l(ur/a)$ are the l-th order Bessel functions of the first and second kinds, and the $K_l(wr/a)$ and $I_l(wr/a)$ are the lth-order modified Bessel functions of the first and second kinds.

And notice the important relationships between the two expressions,

$$u^2+w^2=v^2 \tag{2.102}$$

Where we have defined the normalised frequency,

$$v=k_0a\sqrt{n_1{}^2-n_2{}^2} \tag{2.103}$$

In the above, the u and w are considered to be normalised lateral propagation constants in the core and cladding respectively.

Since the solution to (2.96) must be physically well-defined (finite) at r=0 and at r=∞, we must restrict the Bessel function solutions to,

$$R(r)=\begin{cases} AJ_l\left(\dfrac{ur}{a}\right) & \text{for } r \le a \\ CK_l\left(\dfrac{wr}{a}\right) & \text{for } r \ge a \end{cases} \tag{2.104}$$

2.4.1 The characteristic equation

In order to determine the values of the propagation constants of these linearly-polarised modes, we require a characteristic equation to solve. Firstly, we know that the tangential electric and magnetic fields should be continuous across the boundary between the core and cladding, and that the ratio of the normal components should be equal to that of the inverse ratio of refractive indices making up the boundary. Given the assumption that the electric and magnetic fields are linearly polarised, the conditions to be satisfied by the radial wave function R(r) are given under the weakly-guiding approximation by,

$$R(a-0)=R(a+0) \tag{2.105}$$

and,

$$\left.\frac{dR(r)}{dr}\right|_{a-0}=\left.\frac{dR(r)}{dr}\right|_{a+0} \tag{2.106}$$

We therefore require, using the solutions (2.104),

$$AJ_l(u)-CK_l(w)=0 \tag{2.107}$$

$$AuJ_l'(u)-CwK_l'(w)=0 \tag{2.108}$$

Or, in matrix notation,

$$\begin{pmatrix} J_l(u) & -K_l(w) \\ uU'(u) & -wK'(w) \end{pmatrix}\begin{pmatrix} A \\ C \end{pmatrix}=0 \tag{2.109}$$

If this is to hold of non-trivial A and C, we require the determinant of the matrix on the left to be zero, that is,

$$\left|\begin{pmatrix} J_l(u) & -K_l(w) \\ uU'(u) & -wK'(w) \end{pmatrix}\right|=0 \tag{2.110}$$

Or,

$$-wJ_l(u)K_l'(w)+uJ_l'(u)K_l(w)=0 \tag{2.111}$$

In all of the above the prime indicates differentiation. Rewriting, we may get the well-known characteristic equation,

$$\frac{uJ_l'(u)}{J_l(u)} = \frac{wK'(w)}{K_l(w)} \tag{2.112}$$

2.4.2 Particular solutions

It is interesting to note that for LP_{lm} modes, (2.112) has solutions only within limited ranges of the parameters u and w. If we investigate the limits of w->0 which also corresponds to u->v, we may obtain the values of the normalised frequency where a mode becomes cut-off.

We may investigate modes for which l=0 using the notation LP_{0m} and substituting into (2.112),

$$\frac{uJ_0'(u)}{J_0(u)} = \frac{wK_0'(w)}{K_0(w)} \tag{2.113}$$

If we make use of the Bessel function relations,

$$J_0'(z) = -J_1(z) \tag{2.114}$$

$$K_0'(z) = -K_1(z) \tag{2.115}$$

We may rewrite (2.113) as,

$$\frac{uJ_1(u)}{J_0(u)} = \frac{wK_1(w)}{K_0(w)} \tag{2.116}$$

Or,

$$\frac{J_0(u)}{uJ_1(u)} = \frac{K_0(w)}{wK_1(w)} \tag{2.117}$$

For the limit w->0 the zeroth-order and lth-order modified Bessel functions can be written asymptotically as,

$$K_0(z) \sim -\ln(z) \tag{2.118}$$

$$K_l(z) \sim \frac{1}{2}\Gamma(l)\left(\frac{1}{2}z\right)^{-1} \qquad \text{for } l > 0 \tag{2.119}$$

As such, we may rewrite (2.117) in this limit,

$$\frac{K_0(w)}{wK_1(w)} = \frac{\ln w}{w(1/2)\Gamma(1)\left[(1/2)w\right]^{-1}} = -\ln w \to +\infty \quad \text{for } w \to 0 \tag{2.120}$$

Since the left-hand-side must also go to +∞ we have,

$$\mathrm{v}\frac{J_0(v)}{vJ_1(v)} \to +\infty \tag{2.121}$$

We see that since J_0(v)->1 and J_1(v)->0 as v->0 it is implied that the LP_{01} mode has no cut-off and that the LP_{0m} modes for m>1 are the (m-1)'th zeros of the Bessel function of the first kind. That is

$$J_1\left(j_{1,m-1}\right) = 0 \tag{2.122}$$

and,

$$v_c = j_{1,m-1} \tag{2.123}$$

For modes with l>0 we use the Bessel function relations,

$$J_v'(z) = J_{v-1}(z) - vz^{-1}J_v(z) \tag{2.124}$$

$$zK_v'(z) = -zK_{v-1}(z) - vK_v(z) \tag{2.125}$$

and rewrite (2.112) as,

$$\frac{u\left(J_{l-1}(u) - lu^{-1}J_l(u)\right)}{J_l(u)} = \frac{-wK_{l-1}(w) - lK_l(w)}{K_l(w)} \tag{2.126}$$

So that we finally obtain,

$$\frac{J_l(u)}{uJ_{l-1}(u)} = -\frac{K_l(w)}{wK_{l-1}(w)} \tag{2.127}$$

If we again investigate the limit w->0 of the (l-1)th-order modified Bessel function of the first kind we have,

$$K_{l-1}(z) \sim \frac{1}{2}\Gamma(l-1)\left(\frac{1}{2}z\right)^{-l+1} \qquad \text{for } z \to 0 \tag{2.128}$$

Using this approximation we may rewrite the right-hand-side of (2.127) as,

$$
\begin{aligned}
-\frac{K_l(w)}{wK_{l-1}(w)} &= -\frac{1}{w}\frac{(1/2)\Gamma(l)\left[(1/2)w\right]^{-l}}{(1/2)\Gamma(l-1)\left[(1/2)w\right]^{-l+1}} \\
&= -\frac{1}{w}\frac{(l-1)!\left[(1/2)w\right]^{-l}}{(l-2)!\left[(1/2)w\right]^{-l+1}} \\
&= -\frac{1}{w}(l-1)\frac{2}{w} \\
&= -\frac{2(l-1)}{w^2} \to -\infty \qquad \text{for w} \to 0
\end{aligned}
\tag{2.129}
$$

The left-hand-side of (2.127) must also go -∞ and so,

$$\frac{J_l(v)}{vJ_{l-1}(v)} \to -\infty \tag{2.130}$$

We see that the possible solutions for this are that v->0 and $J_{l-1}(v)$->0. Since (2.130) would diverge to +∞ for v->0 we therefore have that $J_{l-1}(v)$->0. The signs of $J_l(v)$ and $J_{l-1}(v)$ differ for v->$j_{l-1,m}$ and so the cut-off conditions for the LP_{lm} modes for l>0 are,

$$J_{l-1}(v) \to 0 \tag{2.131}$$

$$v_c = j_{l-1,m} \tag{2.132}$$

2.4.3 Interpreting the dispersion relations

In both the case of the planar waveguides as well as the optical fibre, it is possible to write propagation constants in normalised form. If we now define a normalised longitudinal propagation constant b we may calculate dispersion curves which provide a description of how the propagation constant varies with normalised frequency.

$$b = \frac{(\beta/k_0)^2 - n_2^2}{n_1^2 - n_2^2} \tag{2.133}$$

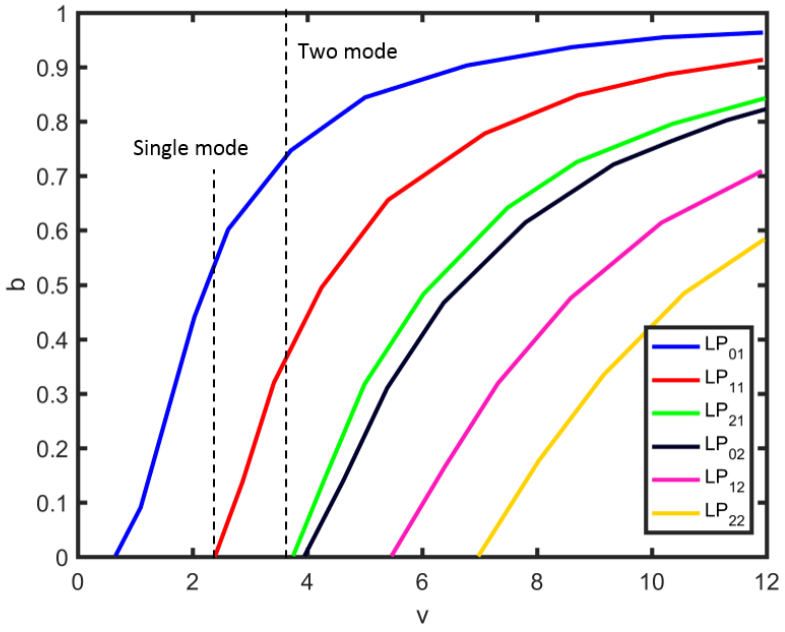

Figure 2-3: Dispersion curve for LP modes in a step-index fibre

In the case of a step-index optical fibre the locations of mode cut-off can be seen in Figure 2-3 as well as the dependence of the normalised propagation constant with normalised frequency. It makes sense that since such modes have a frequency dependence they are subject to dispersion. The propagation constant β can be written in terms of the normalised constant b as,

$$\beta = k_0\sqrt{n_0^2 + \left(n_1^2 - n_0^2\right)b} \approx k_0\left[n_0 + \left(n_1 - n_0\right)b\right] \tag{2.134}$$

If we substitute this into the expression for group delay we obtain,

$$\frac{d\beta}{dk_0} = N_0 + \left(N_1 - N_0\right)b + k_0\left(n_1 - n_0\right)b \tag{2.135}$$

where N_i are the material group indices. We may approximate this further and obtain,

$$\frac{d\beta}{dk_0} \approx N_0 + \left(N_1 - N_0\right)\frac{d\left(vb\right)}{dv} \tag{2.136}$$

If we take (2.112), invert it and differentiate both sides with respect to v we obtain,

$$\frac{d}{du}\left[\frac{uJ_{l-1}}{l}\right]\frac{du}{dv} = -\frac{d}{dw}\left[\frac{wK_{l-1}}{K_l}\right]\frac{dw}{dv} \tag{2.137}$$

Evaluating the left-hand and right-hand sides,

$$\frac{d}{du}\left[\frac{uJ_{l-1}}{J_l}\right] = u\left[\frac{J_{l-1}(u)J_{l+1}(u)}{J_l^2(u)} - 1\right] \tag{2.138}$$

$$\frac{d}{dw}\left[\frac{wK_{l-1}}{K_l}\right] = w\left[\frac{K_{l-1}(w)K_{l+1}(w)}{K_l^{\,2}(w)} - 1\right] \tag{2.139}$$

Using recurrence relations and equating (2.138) and (2.139) we obtain,

$$\frac{uJ_{l+1}(u)}{J_l(u)} = w\frac{K_{l+1}(w)}{K_l(w)} \tag{2.140}$$

If we now combine (2.140) and (2.112) ,

$$\frac{J_{l-1}(u)J_{l+1}(u)}{J_l^{\,2}(u)} = -\frac{w^2}{u^2}\frac{K_{l-1}(w)K_{l+1}(w)}{K_l^{\,2}(w)} \tag{2.141}$$

and use the relation $u^2+v^2=w^2$

$$\frac{du}{dv} = \frac{u}{v}\left[1-\xi_l(w)\right] \tag{2.142}$$

where we have defined,

$$\xi_l(w) = \frac{K_l^{\,2}(w)}{K_{l-1}(w)K_{l+1}(w)} \tag{2.143}$$

Now using,

$$u = v\sqrt{1-b} \tag{2.144}$$

we finally obtain the expression for use in the group delay expression (2.136),

$$\frac{d(vb)}{dv} = b + 2(1-b)\xi_l(w) \tag{2.145}$$

From this expression we can observe the behaviour of the group delay with normalised frequency v as shown in Figure 2-4 below

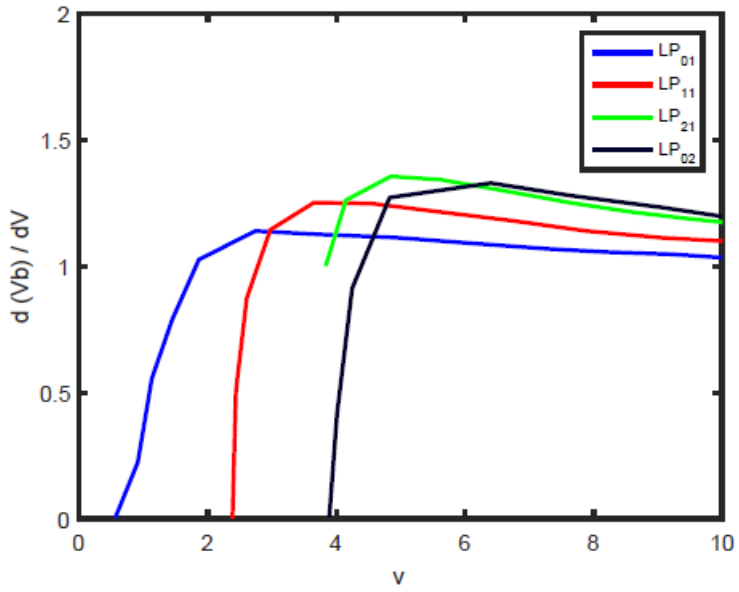

Figure 2-4: Group delay of the LP modes of a step-index fibre

We see that for low normalised frequency the group delay of a given mode is quickly increasing and as the normalised frequency increases the mode becomes more confined in the fibre and the group delay approaches unity. Multimode dispersion can be understood as the dispersion of the group delay time of a mode at a certain frequency. The multimode dispersion can therefore be calculated by considering the variance in the value of the normalised group delay at a fixed normalised frequency. In particular, the chromatic dispersion, which is defined as the sum of the material and waveguide dispersion is given by,

$$\delta t = \left[\frac{d^2\beta}{d\omega^2}\right]_{\omega=\omega_0} \cdot L\delta\omega \tag{2.146}$$

This may be rewritten using $\omega=k_0c$ and $k_0=2\pi/\lambda$ as,

$$\delta t = -\frac{\delta\lambda}{\lambda}\frac{L}{c}k_0\frac{d^2\beta}{dk_0^{\,2}} \tag{2.147}$$

Differentiating (2.136) for use in (2.147) we obtain,

$$k_0\frac{d^2\beta}{dk_0^{\,2}} = k_0\frac{dN_0}{dk_0} + k_0\frac{d\left(N_1-N_0\right)}{dk_0}\frac{d\left(vb\right)}{dv} + \left(N_1-N_0\right)v\frac{d^2\left(vb\right)}{dv^2} \tag{2.148}$$

We obtain the last term in (2.148) which is identified as waveguide dispersion, by differentiating (2.145) obtaining,

$$v\frac{d^2(vb)}{dv^2} = 2(1-b)\zeta_l(w)\left[(1-2\zeta_l)+\left(1+\frac{1-b}{b}\zeta_l\right)(2-\zeta_l)\right] \tag{2.149}$$

where we have defined,

$$\zeta_l(w) = w\left[\frac{K_{l-1}(w)}{K_l(w)}+\frac{K_{l+1}(w)}{K_l(w)}-\frac{K_l(w)}{K_{l+1}(w)}-\frac{K_l(w)}{K_{l-1}(w)}\right] \tag{2.150}$$

We calculate the waveguide dispersion in Figure 2-5 where it is observed that waveguide dispersion is largest for the LP_{01} mode at an intermediate v and that for the higher-order modes, dispersion is largest near the modal cut-off before passing through zero and becoming negative with increasing normalised frequency.

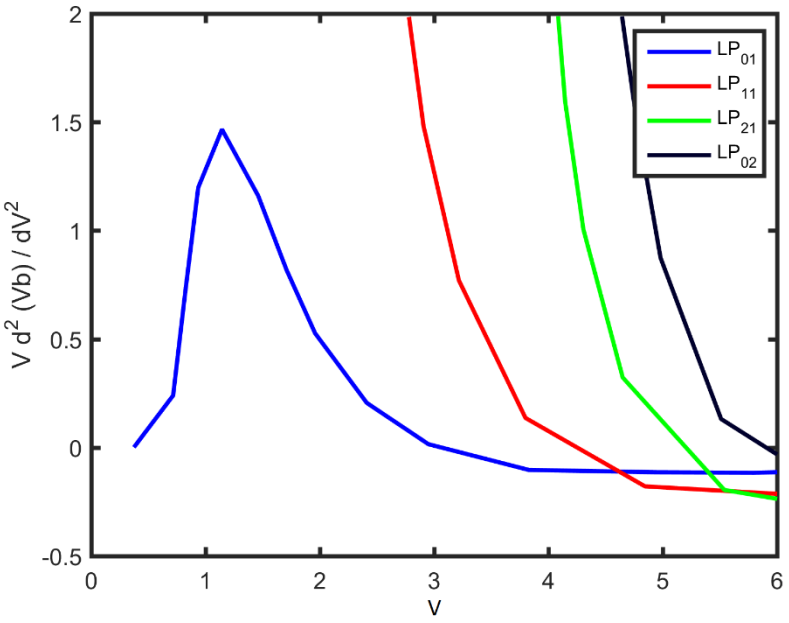

Figure 2-5: Waveguide dispersion of the LP modes of a step-index fibre

Looking at (2.148) we see that by combining the first two terms which we refer to as material dispersion and the third waveguide dispersion term which represents waveguide dispersion we may obtain optical fibres for which a range of dispersive properties are possible. The material dispersion, which is written in terms of the group index of the material, may be modelled through the use of an empirical fit for the refractive index against wavelength, which for Silica is well approximated by the Sellmeier polynomial,

$$n(\lambda) = \sqrt{1+\sum_1^3 \frac{a_i\lambda^2}{(\lambda^2-b_i)}} \tag{2.151}$$

Where the a's and b's are known as the Sellmeier coefficients and are given in references such as [2.2].

2.5 Inverse Scattering approaches

In this section we discuss the theory behind the approach of inverse scattering (IS) to the design of optical waveguides and fibres. As described earlier, the fundamental reason for this approach is the ability to design optical waveguides and fibres without making any initial assumptions as to the form of the refractive index profile as is the case with typically used optimisation methods. This could provide novel designs with modal characteristics such as dispersion and mode spacing unseen in existing designs. In particular, the success in the use of such a novel approach in the inverse design of Bragg gratings in the early 2000s [2.3]–[2.7] offered a great incentive to investigate this further. A review of the literature showed that one particular approach using a solution of the so-called Gel'fand-Levitan-Marchenko (GLM) integral equations had been successful in the IS design of waveguides with improved features such as waveguide width for single-mode operation [2.8]–[2.10]. Further work had shown that the inverse design of optical interconnects had been performed using a somewhat different technique known as Darboux transformations [2.11] derived from the theory of quantum mechanics. A feature of both of the above approaches was that the waveguide was designed 'from the side' by considering the transverse reflection response. It can be shown that the modal properties of a waveguide can be described in terms of such a reflection response, a particular practical example being in the case by which a recursive reflectance method is used to calculate the modes of thin-film waveguides [2.12]. A particular characteristic of this reflection response is that its denominator is identified as being the waveguide's dispersion relation, and thus satisfying it leads to poles in the reflection coefficient.

In the context of optical fibre design, the literature showed that early work was performed into their design by specification of modal propagation constants for a fixed azimuthal symmetry LP mode number, or fixed propagation constants for differing azimuthal symmetry LP mode number [2.13], [2.14]. In the context of quantum mechanics this is known as the solution to the problem for either fixed energy, or fixed angular momentum. This contrasted with the more recent work using pure optimisation of an assumed form of refractive index profile where optical fibres were designed with tailored dispersion characteristics [2.15] through the use of tools such as genetic algorithms. As a result, it made sense to investigate this area further but from the IS point of view with the hope that there could be potential control of modal characteristics such as mode spacing unseen in existing designs.

In addition, with the currentdeveloping interest in mode-division-multiplexing (MDM) methods, new approaches to the design of both waveguide and fibre optical couplers for the purpose of inserting and extracting modes using the approaches of supersymmetry (SUSY) [2.16] have been considered

recently. Here, the approach relies upon the development of cascades of phase-matched waveguides which are obtained as a direct result of the SUSY transformation. The limit of this approach is that each partner waveguide obtained from the SUSY transformation contained all of the modes except the fundamental, thereby removing one mode at a time. However, if a mode other than the fundamental needs to be removed it is necessary to use complex refractive index profiles. In addition, there is no way by which particular selected modes may be phase matched. We approached this problem from a different point of view using the aforementioned Darboux transformations for waveguide couplers and the Gel'fand-Levitan-Machenko equations once again but in cylindrical symmetry, respectively, and found different and more powerful solutions.

We now discuss the above inverse scattering techniques in more detail and observe the connections between them.

2.5.1 The Gel'fand-Levitan-Marchenko integral equations

In this subsection we develop the approach to the inverse design of optical waveguides and fibres using the solution to the Gel'fand-Levitan-Marchenko integral equations. It is shown that this equation relates the reflection response of a waveguide to a kernel K(x,t) by which which the refractive index profile may be obtained.

2.5.1.1 Optical Waveguides

The solution to the inverse scattering problem of based upon the solution of the Gel'fand-Levitan-Marchenko integral equations was discussed by Kay [2.17] and we follow a description from Jordan and Lakshmanasamy [2.8]. In the context of planar waveguide design the problem is stated as follows. We begin by considering a physical model in which electromagnetic radiation is scattered by an inhomogeneous planar optical waveguide as is depicted in Figure 2-6

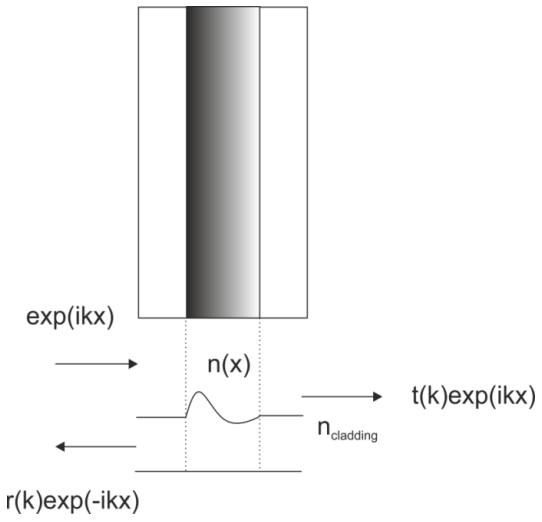

Figure 2-6: A physical model of a planar optical waveguide scattering electromagnetic radiation incident from the left

The modes of such a waveguide are the solutions to the wave equation discussed earlier in this chapter. That is,

$$\nabla^2{}_{\perp}\mathbf{E}+\left(k_0{}^2n(x)^2-\beta^2\right)\mathbf{E}=0 \tag{2.152}$$

The relationship between the reflection coefficient r(k) in Figure 2-6 and the refractive index profile in (2.152) is given by the Gel'fand-Levitan-Marchenko integral equation. It is possible to write (2.152) in the form of a Schrodinger equation containing a potential q(x) and energy k defined by,

$$q(x)=k_0{}^2\left[n_2{}^2-n(x)^2\right] \tag{2.153}$$

$$k^2=k_0{}^2n_2{}^2-\beta^2 \tag{2.154}$$

which puts the problem in a simpler form. If we assume we are dealing with a transverse electric (TE) mode, the field is of the form, **E**=0**,** $E_y(x)$,0], and (2.152) becomes,

$$\nabla^2{}_{\perp}E_y+\left(k^2-q(x)\right)E_y=0 \tag{2.155}$$

If we now consider the time-dependent formulation of the scattering problem, it can be shown that the Fourier transform $\tilde{E}(x,t)$ of $E(x,k)$ satisfies the time-dependent wave equation where the speed of light has been normalised, c=1,

$$\frac{\partial^2\tilde{E}(x,t)}{\partial x^2}-\frac{\partial^2\tilde{E}(x,t)}{\partial t^2}-q(x)\tilde{E}(x,t)=0 \tag{2.156}$$

If an incident plane wave to the waveguide is represented by a unit impulse,

$$\tilde{E}(x,t)=\delta(x-t)\qquad \text{for } x<0,\ t<0 \tag{2.157}$$

it in turn produces a reflected transient which may be written,

$$R(x+t)=\frac{1}{2\pi}\int_{-\infty}^{\infty}r(k)\exp\left[-ik(x+t)\right]dk-i\sum_{n=1}^{N}r_n\exp\left[-ik_n(x+t)\right] \tag{2.158}$$

with two terms, the first being the contribution from the continuous spectrum representing the radiation modes, and secondly the discrete spectrum representing propagating modes which may be written as a sum over the poles k_n on the positive imaginary axis with residues r_n. Causality requires that a reflected transient is not produced before the pulse has interacted with the inhomogeneous core of the waveguide and so we know that,

$$R(x+t)=0\qquad \text{for } x+t\le 0 \tag{2.159}$$

We may now relate the wave amplitude $\tilde{E}(x,t)$ in the core region to the wave amplitude $\tilde{E}_0(x,t)$ in the exterior region by a linear transformation and kernel K(x,t) independent of the spectral parameter k,

$$\tilde{E}(x,t)=\begin{Bmatrix}\tilde{E}_0(x,t)+\int_{-x}^{x}K(x,z')\tilde{E}_0(z',t)dz' & x\geq 0\\ \tilde{E}_0(x,t) & x\leq 0\end{Bmatrix} \tag{2.160}$$

where we have written,

$$\tilde{E}_0(x,t)=\delta(x-t)+R(x+t) \tag{2.161}$$

Since we know that $\tilde{E}(x,t)$ is a right-moving transient we also know that,

$$\tilde{E}(x,t)=0 \qquad \text{for } t<x \tag{2.162}$$

And so a condition on the kernel is that K(x,t)=0 for t>x, and K(x,t)=0 for t≤-x. Substituting (2.161) into (2.160) and using (2.159) and (2.162) we obtain the integral equation which the kernel must satisfy,

$$K(x,t)+R(x+t)+\int_{-t}^{x}K(x,z')R(z'+t)dz'=0 \quad \text{for } t<x \tag{2.163}$$

which is identified as Kay's version of the Gel'fand-Levitan-Marchenko integral equation. If we now substitute (2.160) into (2.156) we observe that the kernel K(x,t) also satisfies a differential equation of the same form as (2.156) if we impose the conditions

$$K(x,-x)=0 \tag{2.164}$$

and,

$$2\frac{dK(x,x)}{dx}=q(x) \tag{2.165}$$

It is now seen that solutions to (2.163) along with the conditions (2.164) and (2.165) provide a way in which to synthesise an optical waveguide from its reflected transient R(x,t) and in turn its reflection response r(k). Particular solutions to this integral equation are obtained in Chapter 4 for the case of 3,5 and 7-pole rational reflection coefficients where a numerical and general implementation of the solution to the GLM integral equation by Pechenick [2.18] is used.

2.5.1.2 Optical Fibres

In a similar vein to above, the Gel'fand-Levitan-Marchenko equations for a cylindrically symmetric fiber may be written for the l'th partial wave [2.12],

$$K^l(r,r') + B^l(r,r') + \int_0^r K^l(r,r'')B^l(r'',r')dr'' = 0 \tag{2.166}$$

where the reflected transient function B(r,t) for a fibre is now written in the form ,

$$B^l(r,r') = \frac{2rr'}{\pi}\int_{-\infty}^{\infty}\left[\left|f^l(k)\right|^2 - 1\right]J_l(kr)J_l(kr')\,dk + \sum_{i=1}^{N} c_i^{\,2} g_l(\chi_i r) g_l(\chi_i r') \tag{2.167}$$

In (2.167) the first term, once again, represents the contribution from radiation modes, and the second term that of the guided modes, and the functions $f^l(k)$ and $g_l(\chi_n r)$ represents the form of the modal solutions in a cylindrical geometry with $g_l(\chi_n r)$ being a solution of the homogeneous Bessel's equation,

$$\frac{d^2 g_l(\chi_n r)}{dr^2} - g_l(\chi_n r)\frac{\left(l^2 - \frac{1}{4}\right)}{r^2} - \chi_n^{\,2} g_l(\chi_n r) = 0 \tag{2.168}$$

giving,

$$g_l(\chi_n r) = c_n I_j(\chi_n r)\sqrt{r} \tag{2.169}$$

that is in terms of the transverse propagation constant in the cladding,

$$\chi_n = \sqrt{\beta_n^{\,2} - k_0^{\,2} n_2^{\,2}} \tag{2.170}$$

If we assume phaseless scattering in 2D [2.13], we set the absolute value of the solution $f^l(k)$ equal to 1 and we obtain a separable equation for the kernel $K^l(r,r')$ which we may solve by setting,

$$K^l(r,r') = -\sum_{n=1}^{N}\psi_n(\chi_n r) g_l(\chi_n r) \tag{2.171}$$

where the $\psi_n(\chi_n r)$ are the eigenfunctions of the bound modes which are normalized according to,

$$\int_0^{\infty}\psi_j(\chi_j r)\psi_j(\chi_n r) = \delta_{mn} \tag{2.172}$$

The solution is given by,

$$q^l(r) = 2\frac{dK^l(r,r)}{dr} \tag{2.173}$$

where,

$$K^l(r,r) = -\frac{d}{dr}\ln\left\{\det\left[\Delta^{(l)}\right]\right\} \tag{2.174}$$

with,

$$\left[\Delta^{(l)}\right]_{mn} = \delta_{mn} + c_m c_n \int_0^r I_l(\chi_m r') I_l(\chi_n r') r' dr' \tag{2.175}$$

It is important to note that exact closed-form solutions exist for the particular integral in (2.175) and may be found tables such as that compiled by Gradshteyn and Ryzhik [2.19].

The refractive index profile is then given by,

$$n(r) = \sqrt{n_2^2 k_0^2 - q^l(r)} \tag{2.176}$$

2.5.2 The Darboux transformation

While the GLM technique above provides a way by which the refractive index profile can be obtained from the transverse reflection response of a waveguide, when multimode designs are to be considered in the form of rational reflection coefficients, there is considerable complexity involved in the solution to the problem. However, an alternative and simpler approach exists that allows an N-mode structure to be obtained in terms of an existing and initial refractive index profile.

Fundamentally the electromagnetic problem being investigated can be represented by a one-dimensional quantum mechanical problem which satisfies the time-independent Schrodinger equation. In operator notation this may be written as,

$$H\psi_n = E_n\psi_n \tag{2.177}$$

Where the operator H, known as the Hamiltonian, is defined by,

$$H \equiv -\frac{d^2}{dx^2} + U(x) \tag{2.178}$$

The eigenvalue problem is to find all the discrete eigenvalues E_n and the corresponding eigenfunctions. The eigenvalues may be numbered in increasing order,

$$E_0 < E_1 < E_2 < \ldots \tag{2.179}$$

and the eigenfunctions are mutually orthogonal,

$$(\psi_n, \psi_m) \equiv \int_{-\infty}^{\infty} \psi_n(x)\psi_m(x)dx = h_n\delta_{nm}, \quad 0 < h_n < \infty,\ n,m = 0,1,\ldots \tag{2.180}$$

Given a solution $\{\psi(x), \mathrm{E}\}$ in addition to $\left\{\varphi_j(x), \bar{E}_j\right\}$, $j=1,...,M$ of

$$H\psi(x)=E\psi(x), \quad H\varphi_j(x)=\bar{E}_j\varphi_j(x), \ j=1,...,M \tag{2.181}$$

we may take the solution $\varphi_1(x)$ and define,

$$W[f_1,...,f_n](x)=\begin{vmatrix} f_1(x) & f_2(x) & \cdots & f_n(x) \\ f_1'(x) & f_2'(x) & \cdots & f_n'(x) \\ \vdots & \vdots & \ddots & \vdots \\ f_1^{(n-1)}(x) & f_2^{(n-1)}(x) & \cdots & f_n^{(n-1)}(x) \end{vmatrix} \tag{2.182}$$

$$\psi^{(1)}(x)\equiv\frac{W[\varphi_1,\psi](x)}{\varphi_1(x)} \tag{2.183}$$

$$\varphi_1^{(1)}(x)\equiv\frac{1}{\varphi_1}, \ \varphi_k^{(1)}(x)\equiv\frac{W[\varphi_1,\varphi_k](x)}{\varphi_1(x)}, \ k=2,...,M \tag{2.184}$$

It can then be shown that they are solutions to a new Schrodinger equation with the deformed Hamiltonian $\mathrm{H}^{(1)}$,

$$H^{(1)}(x)=-\frac{d^2}{dx^2}+U^{(1)}(x), \ U^{(1)}(x)\equiv U(x)-2\frac{d^2\left(\log\left|\varphi_1(x)\right|\right)}{dx^2} \tag{2.185}$$

and energies E and $\mathrm{E_k}$,

$$H^{(1)}\psi^{(1)}(x)=E\psi^{(1)}(x), \ H^{(1)}\varphi_j^{(1)}(x)=\bar{E}_j\varphi_j^{(1)}(x), \ j=1,...,M \tag{2.186}$$

If this is repeated M-times we arrive at,

$$\psi^{(M)}(x)\equiv\frac{W[\varphi_1,...,\varphi_M,\psi](x)}{W[\varphi_1,...,\varphi_M](x)} \tag{2.187}$$

$$\varphi_j^{(M)}(x)\equiv\frac{W[\varphi_1,...,\varphi_j,\varphi_M](x)}{W[\varphi_1,...,\varphi_M](x)}, \ j=1,...,M \tag{2.188}$$

These then satisfy the M-th deformed Schrodinger equation with the same energy,

$$H^{(M)}\psi^{(M)}(x)=E\psi^{(M)}(x), \ H^{(M)}\varphi_j^{(M)}(x)=\bar{E}\varphi_j^{(M)} \tag{2.189}$$

$$H^{(M)}=-\frac{d^2}{dx^2}+U^{(M)}(x), \ U^{(M)}(x)\equiv U(x)-2\frac{d^2\left(\log\left|W[\varphi_1,...,\varphi_M](x)\right|\right)}{dx^2} \tag{2.190}$$

As such, given an initial refractive index profile or potential U(x), M additional guided modes may be added to it. A particularly simple design approach is found when U(x) is chosen to be identically zero everywhere, that is, it is reflectionless.

At this point it is interesting to note that reflectionless potentials of the Schrodinger equation have been found to be of use in the design of planar waveguides by authors such as Papachristos et al. [2.20] following a particular solution to the above described GLM integral equations. In general, a reflectionless potential which has N discrete eigenstates,

$$\begin{aligned} &H = -\frac{d^2}{dx^2} + U_N(x),\ H\psi_k(x) = k^2\psi_k(x) \\ &H\phi_{N,j}(x) = E_j\phi_{N,j}(x),\ E_j = -k_j{}^2,\ j = 1,...,N,\ 0 < k_1 < k_2,...,< k_N \end{aligned} \tag{2.191}$$

has an inverse scattering solution given by Moses and Kay [2.21],

$$\begin{aligned} &U_N \equiv -2\frac{d^2 \log u_N(x)}{dx^2} \\ &u_N \equiv \det A_N(x),\ \left[A_N(x)\right]_{mn} \equiv \delta_{mn} + \frac{c_m \mathrm{e}^{-(k_m+k_n)x}}{k_m + k_n},\ m,n = 1,...,N \end{aligned} \tag{2.192}$$

with arbitrary positive constants $\{c_m\}$. However, the form of U_N above suggests that the refectionless potential can be obtained from the trivial potential U(x)=0 by multiple Darboux transformations. To investigate this further we assume seed solutions to the Schrodinger equation when the potential is identically zero,

$$\psi_j(x) = e^{k_j x} + c_j e^{-k_j x},\ 0 < k_1 < k_2,...,k_N,\ (-1)^{j-1} c_j > 0 \tag{2.193}$$

$$-\frac{d^2\psi_j(x)}{dx^2} = -k_j{}^2\psi_j(x),\ j = 1,...,N \tag{2.194}$$

The Wronskian of these seed solutions is given by,

$$W[\psi_1,...,\psi_N](x) = \prod_{j>l}^{N}(k_j - k_l)\exp\left(\sum_{j=1}^{N} k_j x\right) u_N(x) \tag{2.195}$$

$$U_N(x) = -2\frac{d^2 W[\psi_1,...,\psi_N](x)}{dx^2} = -2\frac{d^2 \log u_N(x)}{dx^2} \tag{2.196}$$

As such, the solution for the reflectionless potential using both the GLM and Darboux approaches is identical.

2.5.3 The SUSY transformations

There has been a recent surge of interest in a different approach to waveguide design using the so-called supersymmetric (SUSY) transformations. In particular, this has been applied to the problem of mode extraction in proposed mode-division multiplexing systems [2.16]. However, to the author's knowledge there has been little discussion in the optics community of the comparisons between the SUSY, Darboux and the Gel'fand-Levitan-Marchenko approach that was used in the early parts of this thesis. In the following we follow the excellent description given by [2.22]

It can be shown that the Hamiltonian operator H discussed above can be factorised in the form,

$$H^{[0]} = H = A^{\dagger}A \tag{2.197}$$

with,

$$A = \frac{d}{dx} - \frac{dw(x)}{dx},\ A^{\dagger} = -\frac{d}{dx} - \frac{dw(x)}{dx},\ w(x) \in R,\ \psi_0(x) = e^{w(x)} \tag{2.198}$$

$$H = -\frac{d^2}{dx^2} + U(x),\ U(x) = \left(\frac{dw(x)}{dx}\right)^2 + \frac{d^2 w(x)}{dx^2} \tag{2.199}$$

The function $\psi_0(x)$ is the ground state eigenfunction and w(x) is known as the prepotential. It is also possible to write a partner Hamiltonian in the form,

$$H^{[1]} \equiv AA^{\dagger} \tag{2.200}$$

The Darboux-Crum transformations state that the Hamiltonians $H^{[0]}$ and $H^{[1]}$ are related through the so-called intertwining relations,

$$AH^{[0]} = AA^{\dagger}A = H^{[1]}A, \qquad A^{\dagger}H^{[1]} = A^{\dagger}AA^{\dagger} = H^{[0]}A^{\dagger} \tag{2.201}$$

and the pair are essentially iso-spectral and their eigenfunctions are related by,

$$H^{[0]}\psi_n^{[0]}(x) = E_n\psi_n^{[0]}(x), \quad n = 0,1,... \tag{2.202}$$

$$H^{[1]}\psi_n^{[1]}(x) = E_n\psi_n^{[1]}(x), \quad n = 1,2,... \tag{2.203}$$

$$\psi_n^{[1]} = A\psi_n^{[0]}, \quad \psi_n^{[0]} = \frac{A^{\dagger}}{E_n}\psi_n^{[1]}, \quad n = 1,2,... \tag{2.204}$$

As such, the Hamiltonian $H^{[1]}$ has the eigenvalue E_0 missing. In the quantum mechanical community, a system with the Hamiltonian factorised as $H = A^{\dagger}A$ and an associated one $H^{[1]} = AA^{\dagger}$ is called

supersymmetric. This shows that SUSY is purely a particular application of the Darboux transformations where $\varphi_j = \varphi_{j-1}$.

2.6 Conclusions

In this chapter we have introduced three main methods of inverse scattering whereby the refractive index profile of a waveguide or fibre may be obtained from its transverse reflection response. An important feature of the transverse reflection response was its ability to characterise the modal properties of a waveguide through its poles, in a similar way in which the poles of the reflection response of a multilayer waveguide may be used to obtain the same. In addition, the case for the cylindrical geometry of an weakly-guiding optical fibre is then developed.

The GLM technique was introduced and the procedure for its use demonstrated. From the reflection response R(x,t) an integral equation was obtained involving a kernel K(x,t). Upon solving for this kernel it was then possible to obtain the refractive index profile. The Darboux transformation was then developed utilising the operator notation of quantum mechanics. It was shown that through the use of an initial solution to the Schrodinger equation as well as further 'seed solutions', it was possible to add further modes or bound states to the waveguide. A particular application of the Darboux approach to the case of an initial and trivial reflectionless potential led to the demonstration that in this case the GLM and Darboux approaches yield exactly the same solution.

Further to this, the recently popular SUSY technique was then developed and it was made clear that it is purely a particular case of the Darboux transformation where the ordering of the seed solutions is rearranged to remove the fundamental mode.

Compared with genetic algorithms and other such optimisation methods, the above inverse scattering approaches make no assumptions as to the geometric structure of the waveguide or fibre. The only assumptions made are those of the characteristics of the guided modes supported. If a genetic algorithm were chosen, the refractive index profile would have to be split into differing 'genes' which could be switched 'on' or 'off' as the process progressed. However, in order to do this either the refractive index profile must be split into very many such genes to cover a significant proportion of the possibilities, each with many different potential values and with associated high computational cost, or a specific set must be chosen at the start. While some of the work later in this thesis does require some level of 'trial and error' in the design progress, it is expected that the dimensionality and cost of this optimisation problem will be much lower and potentially show physical insights that would otherwise be lost by 'brute-force' methods.

2.7 References

[2.1] K. Kawano and T. Kitoh, *Introduction to optical waveguide analysis: solving Maxwell's equations and the Schrodinger equation*. Chichester, UK: John Wiley & Sons Ltd, 2001.

[2.2] K. Okamoto, *Fundamentals of Optical Waveguides*. London, UK, 2006.

[2.3] R. Feced, M. N. Zervas, and M. A. Muriel, "An Efficient Inverse Scattering Algorithm for the Design of Nonuniform Fiber Bragg Gratings," *J. Quantum Electron.*, vol. 35, no. 8, pp. 1105–1115, 1999.

[2.4] R. Feced and M. N. Zervas, "Efficient inverse scattering algorithm for the design of grating-assisted codirectional mode couplers," *JOSA A*, vol. 17, pp. 1573–1582, 2000.

[2.5] M. Ibsen, M. K. Durkin, M. N. Zervas, A. B. Grudinin, and R. I. Laming, "Custom design of long chirped Bragg gratings: application to gain-flattening filter with incorporated dispersion compensation," *IEEE Photonics Technol. Lett.*, vol. 12, no. 5, pp. 498–500, 2000.

[2.6] J. Skaar, "Synthesis and characterization of fiber Bragg gratings," PhD Thesis, Norweigan University of Science and Technology, 2000.

[2.7] J. Skaar and L. Wang, "On the synthesis of fiber Bragg gratings by layer peeling," *J. Quantum Electron.*, vol. 37, no. 2, pp. 165–173, 2001.

[2.8] A. K. Jordan and S. Lakshmanasamy, "Inverse scattering theory applied to the design of single-mode planar optical waveguides," *J. Opt. Soc. Am. A*, vol. 6, no. 8, pp. 1206–1212, 1989.

[2.9] S. Lakshmanasamy and A. K. Jordan, "Design of wide-core planar waveguides by an inverse scattering method.," *Opt. Lett.*, vol. 14, no. 8, pp. 411–413, 1989.

[2.10] L. S. Tamil and A. K. Jordan, "Spectral Inverse Scattering Theory for Inhomogeneous Dielectric Waveguides and Devices," *Proc. IEEE*, vol. 79, no. 9103253, pp. 1519–1528, 1991.

[2.11] D. W. Mills and L. S. Tamil, "Synthesis of Guided Wave Optical Interconnects," *IEEE J. Quantum Electron.*, vol. 29, no. 11, pp. 2825–2834, 1993.

[2.12] S. A. Shakir and A. F. Turner, "Method of poles for multilayer thin-film waveguides," *Appl Phys A.*, vol. 29, no. 3, pp. 151-155, 1982.

[2.13] S. P. Yukon and B. Bendow, "Design of waveguides with prescribed propagation constants," *J. Opt. Soc. Am.*, vol. 70, no. 2, pp. 172–179, 1980.

[2.14] M. Hooshyar, "Inverse scattering theory at fixed energy and the design of circular optical waveguides," *J. Math. Phys.*, vol. 33, pp. 663–669, 1992.

[2.15] F. Poletti, X. Feng, G. M. Ponzo, M. N. Petrovich, W. H. Loh, and D. J. Richardson, "All-solid highly nonlinear singlemode fibers with a tailored dispersion profile.," *Opt. Express*, vol. 19, no. 1, pp. 66–80, 2011.

[2.16] M. Heinrich, M.-A. Miri, S. Stützer, R. El-Ganainy, S. Nolte, A. Szameit, and D. N. Christodoulides, "Supersymmetric mode converters.," *Nat. Commun.*, vol. 5, 3698, pp. 1-7, 2014.

[2.17] I. Kay, “The Inverse Scattering Problem When the Reflection Coefficient is a Rational Function,” *Commun. Pure Appl. Math.*, vol. XIII, pp. 371–393, 1960.

[2.18] K. R. Pechenick, “Inverse scattering—exact solution of the Gel’fand-Levitan equation,” *J. Math. Phys.*, vol. 22, no. 7, pp. 1513–1516, 1981.

[2.19] I. Gradshteyn and I. Ryzhik, *Table of integrals, series and products*, Seventh Ed. London, UK: Academic Press, 2007.

[2.20] C. Papachristos and P. Frangos, “Synthesis of single-and multi-mode planar optical waveguides by a direct numerical solution of the Gel’fand-Levitan-Marchenko integral equation,” *Opt. Commun.*, vol. 203, pp. 27–37, 2002.

[2.21] H. Moses and I. Kay, “Reflectionless transmission through dielectrics and scattering potentials,” *J. Appl. Phys.*, vol. 27, pp. 1503-1508, 1956.

[2.22] R. Sasaki, "Exactly solvable potentials with finitely many discreet eigenvalues of arbitrary choice," *J. Math. Phys.*, vol. 55, 062101, pp. 1-11, 2014

Chapter 3: **Methods of analysis and simulation**

3.1 **Introduction**

In this chapter we briefly discuss the methods by which the modal properties of waveguides and fibres can be obtained. Throughout this thesis the commercial mode solver MODE Solutions by Lumerical has been used to verify our results. This particular mode solver is based upon the work of Zhu and Brown [3.1]. In addition to this approach, we have utilised the well-known transfer matrix method (TMM) in order to evaluate the reflection response of the planar waveguides in Chapter 4 of this thesis. We also derive the basic formulae of coupled-mode theory which is used in Chapters 7 and 9 which discuss mode-selective coupler design.

3.2 **Transfer matrix method analysis of optical structures**

Following the description given by Anemogiannis et al. [3.2], the transfer matrix method can be approached by considering the geometry in Figure 3-1 below.

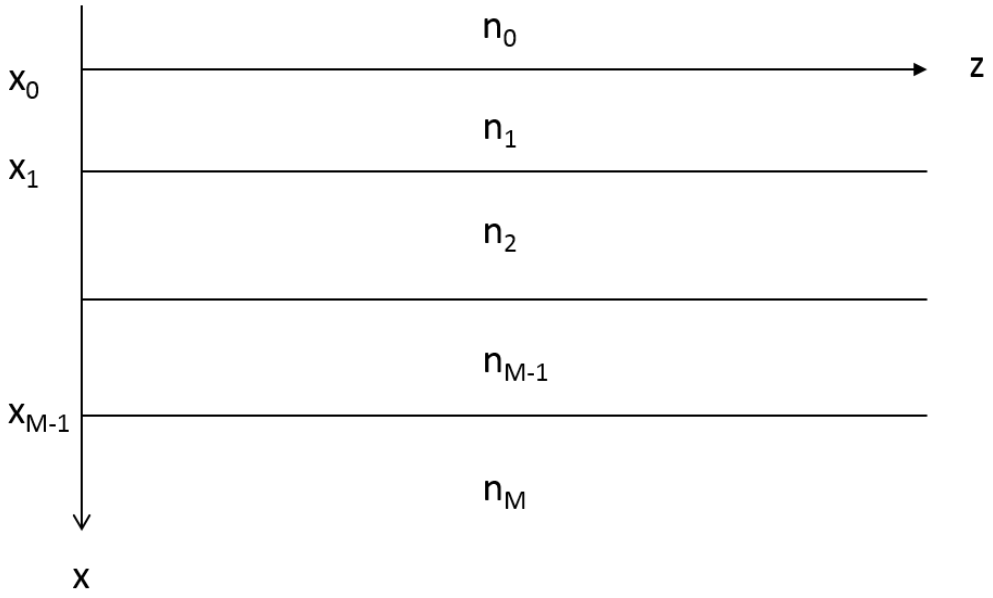

Figure 3-1: Geometry of a multilayer waveguide

For a transverse electric (TE) mode propagating in the z-direction the electric field in the i'th layer for which $x_{i-1} \le x \le x_i$ may be given as

$$\bar{E}_i = \hat{y} E_{y,i}(x) \exp\left[j\left(\omega t - \beta z\right)\right] \tag{3.1}$$

where $\hat{y}$ is the unit vector in the +y direction, β is the propagation constant in the z-direction and ω is the angular frequency. In each layer the field $E_{y,i}(x)$ may be written as the sum of a forward and backward propagating wave in the form

$$E_{y,i}(x) = A_i \exp\left[-i\kappa_i\left(x - x_{i-1}\right)\right] + B_i \exp\left[+i\kappa_i\left(x - x_{i-1}\right)\right] \tag{3.2}$$

where A_i and B_i are the complex coefficients in the +x and –x directions respectively. Here κ_i is the transverse propagation constant given by $\kappa_i = \sqrt{\beta^2 - k_0^{\,2} n_i^{\,2}}$ with $k_0=2\pi/\lambda$ the free-space wavenumber. By matching the tangential field components at each layer interface the field expansion coefficients at the cover and substrate layer may be given in terms of the matrix product

$$\begin{aligned}\begin{pmatrix} A_S \\ B_S \end{pmatrix} &= Q_{M-1} Q_{M-2} Q_{M-3} \ldots Q_0 \begin{pmatrix} A_C \\ B_C \end{pmatrix} \\ &= \begin{pmatrix} q_{11} & q_{12} \\ q_{21} & q_{22} \end{pmatrix} \begin{pmatrix} A_C \\ B_C \end{pmatrix}\end{aligned} \tag{3.3}$$

The matrix Q_i is given by

$$Q_i = \frac{1}{2}\begin{pmatrix} \left[1 + f_i \frac{\kappa_i}{\kappa_{i+1}}\right]\exp\left(-i\kappa_i d_i\right) & \left[1 - f_i \frac{\kappa_i}{\kappa_{i+1}}\right]\exp\left(i\kappa_i d_i\right) \\ \left[1 - f_i \frac{\kappa_i}{\kappa_{i+1}}\right]\exp\left(-i\kappa_i d_i\right) & \left[1 + f_i \frac{\kappa_i}{\kappa_{i+1}}\right]\exp\left(i\kappa_i d_i\right) \end{pmatrix} \tag{3.4}$$

where $f_i=1$ for TE modes and $f_i=n^2_{i+1}/n^2_i$ for TM modes and d_i is the thickness of the i'th layer. Assuming cover incidence, the relation for the global reflection coefficient R_C is,

$$R_C = \left|R_C\right| \exp\left(j\phi_C\right) = \frac{-q_{21}}{q_{22}} \tag{3.5}$$

In addition, the value of β for which R_C is infinite ($q_{22}=0$) corresponds to a guided mode of the multilayer structure.

3.3 Finite difference analysis of optical structures

In order to determine the modal properties of the waveguides investigated in this thesis a finite difference approach was used which is implemented in the commercial mode solver MODE Solutions. It is based upon the work of Zhu and Brown [3.1] and we now briefly discuss the theory behind it. For completeness we supply the expressions but provide no proof.

This solver is a full-vector finite difference mode solver based upon the discretization scheme proposed by Yee [3.3]. The structure of the mesh is shown in Figure 3-2. The mesh is discretised such that the coordinates (j,l)=(jΔx,lΔy) where Δx and Δy are the spacings along the x and y-axes respectively. It is important to note that the electric and magnetic fields are staggered so that the magnetic field components are located midway between their associated electric field components, and vice versa, thereby providing a discretisation amenable to 2nd-order central differencing and one that is naturally divergence free and thereby satisfying Gauss's laws.

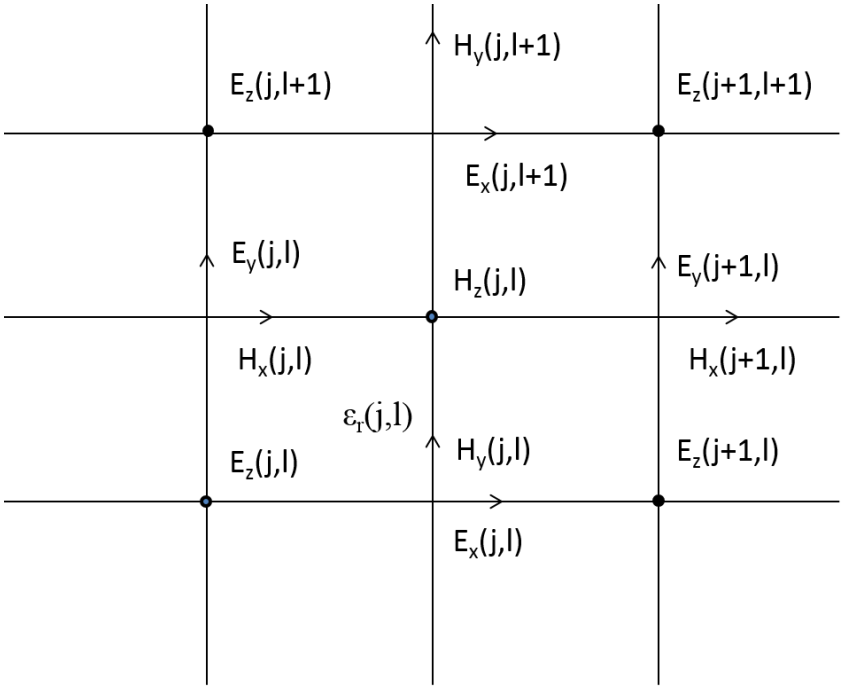

Figure 3-2: The Yee grid adapted from [3.1]

Maxwell's curl equations give,

$$\nabla \times \mathbf{E} = -\frac{\partial \mathbf{B}}{\partial t} \tag{3.6}$$

$$\nabla \times \mathbf{H} = \frac{\partial \mathbf{D}}{\partial t} \tag{3.7}$$

and assuming that the fields have the usual $\exp\left[i\left(\beta z - \omega t\right)\right]$ dependence, following scaling **E** by the free space impedance $Z_0 = \sqrt{\mu_0 / \varepsilon_0}$ we have,

$$ik_0 H_x = \frac{\partial E_z}{\partial y} - i\beta E_y \tag{3.8}$$

$$ik_0 H_y = i\beta E_x - \frac{\partial E_z}{\partial x} \tag{3.9}$$

$$ik_0 H_z = \frac{\partial E_y}{\partial x} - \frac{\partial E_x}{\partial y} \tag{3.10}$$

$$-ik_0 \varepsilon_r E_x = \frac{\partial H_z}{\partial y} - i\beta H_y \tag{3.11}$$

$$-ik_0 \varepsilon_r E_y = i\beta H_x - \frac{\partial H_z}{\partial x} \tag{3.12}$$

$$-ik_0 \varepsilon_r E_z = \frac{\partial H_y}{\partial x} - \frac{\partial H_x}{\partial y} \tag{3.13}$$

Discretising the above we have,

$$ik_0 H_x(j,l) = [E_z(j,l+1) - E_z(j,l)]/\Delta y - i\beta E_y(j,l) \tag{3.14}$$

$$ik_0 H_y(j,l) = i\beta E_x(j,l) - [E_z(j+1,l) - E_z(j,l)]/\Delta x \tag{3.15}$$

$$ik_0 H_z(j,l) = \left[E_y(j+1,l) - E_y(j,l)\right]/\Delta x - \left[E_x(j,l+1) - E_x(j,l)\right]/\Delta y \tag{3.16}$$

$$-ik_0 \varepsilon_{rx}(j,l) E_x(j,l) = [H_z(j,l) - H_z(j,l-1)]/\Delta y - i\beta H_y(j,l) \tag{3.17}$$

$$-ik_0 \varepsilon_{ry}(j,l) E_y(j,l) = i\beta H_x(j,l) - [H_z(j,l) - H_z(j-1,l)]/\Delta x \tag{3.18}$$

$$-ik_0 \varepsilon_{rz}(j,l) E_z(j,l) = \left[H_y(j,l) - H_y(j-1,l)\right]/\Delta x - \left[H_x(j,l) - H_x(j,l-1)\right]/\Delta y \tag{3.19}$$

where we have defined,

$$\varepsilon_{rx}(j,l) = \left[\varepsilon_r(j,l) + \varepsilon_r(j,l-1)\right]/2 \tag{3.20}$$

$$\varepsilon_{ry}(j,l) = [\varepsilon_r(j,l) + \varepsilon_r(j-1,l)]/2 \tag{3.21}$$

$$\varepsilon_{rz}(j,l) = \left[\varepsilon_r(j,l) + \varepsilon_r(j-1,l-1) + \varepsilon_r(j,l-1) + \varepsilon_r(j-1,)\right]/4 \tag{3.22}$$

The above definitions have approximated the refractive indices by averaging the indices of adjacent cells. The discretised equations (3.14) -(3.19) can be written in matrix form as,

$$\mathrm{ik}_0 \begin{bmatrix} \mathbf{H}_x \\ \mathbf{H}_y \\ \mathbf{H}_z \end{bmatrix} = \begin{pmatrix} 0 & -\mathbf{i}\beta\mathbf{I} & \mathbf{U}_y \\ \mathbf{i}\beta\mathbf{I} & 0 & -\mathbf{U}_x \\ -\mathbf{U}_y & \mathbf{U}_x & 0 \end{pmatrix} \begin{bmatrix} \mathbf{E}_x \\ \mathbf{E}_y \\ \mathbf{E}_z \end{bmatrix} \tag{3.23}$$

$$-ik_0\begin{pmatrix}\boldsymbol{\varepsilon}_{rx} & 0 & 0\\ 0 & \boldsymbol{\varepsilon}_{ry} & 0\\ 0 & 0 & \boldsymbol{\varepsilon}_{rz}\end{pmatrix}\begin{bmatrix}\mathbf{E}_x\\ \mathbf{E}_y\\ \mathbf{E}_z\end{bmatrix}=\begin{pmatrix}0 & -i\beta\mathbf{I} & \mathbf{V}_y\\ i\beta\mathbf{I} & 0 & -\mathbf{V}_x\\ -\mathbf{V}_y & \mathbf{V}_x & 0\end{pmatrix}\begin{bmatrix}\mathbf{H}_x\\ \mathbf{H}_y\\ \mathbf{H}_z\end{bmatrix} \tag{3.24}$$

In the above, $\mathbf{I}$ is the square identity matrix, $\boldsymbol{\varepsilon}_{rx}$, $\boldsymbol{\varepsilon}_{ry}$ and $\boldsymbol{\varepsilon}_{rz}$ are diagonal matrices determined by (3.21) – (3.23). $\mathbf{H}_x$, $\mathbf{H}_y$, $\mathbf{H}_z$ are the discretised forms of the H_x, H_y and H_z components of the magnetic field, and $\mathbf{E}_x$, $\mathbf{E}_y$, $\mathbf{E}_z$ are the discretised forms of the E_x, E_y and E_z components of the electric field. In addition, $\mathbf{U}_x$, $\mathbf{U}_y$, $\mathbf{V}_x$ and $\mathbf{V}_y$ are square matrices and depend upon the boundary conditions at the computational window edges. When the zero-boundary condition is applied we have,

$$\mathbf{U}_x=\frac{1}{\Delta x}\begin{pmatrix}-1 & 1 & & & & \\ & -1 & 1 & & & \\ & & \ddots & \ddots & & \\ & & & \ddots & \ddots & \\ & & & & -1 & 1\\ & & & & & -1\end{pmatrix} \tag{3.25}$$

$$\mathbf{U}_y=\frac{1}{\Delta y}\begin{pmatrix}-1 & 1 & & & & \\ & -1 & 1 & & & \\ & & \ddots & \ddots & & \\ & & & \ddots & \ddots & \\ & & & & -1 & 1\\ & & & & & -1\end{pmatrix} \tag{3.26}$$

$$\mathbf{V}_x=\frac{1}{\Delta x}\begin{pmatrix}-1 & 1 & & & & \\ & -1 & 1 & & & \\ & & \ddots & \ddots & & \\ & & & \ddots & \ddots & \\ & & & & -1 & 1\\ & & & & & -1\end{pmatrix} \tag{3.27}$$

$$\mathbf{V}_y=\frac{1}{\Delta y}\begin{pmatrix}-1 & 1 & & & & \\ & -1 & 1 & & & \\ & & \ddots & \ddots & & \\ & & & \ddots & \ddots & \\ & & & & -1 & 1\\ & & & & & -1\end{pmatrix} \tag{3.28}$$

As such we may obtain an eigenvalue equation in terms of the transverse electric fields of the form,

$$\mathbf{P}\begin{bmatrix}\mathbf{E}_x\\ \mathbf{E}_y\end{bmatrix}=\begin{pmatrix}\mathbf{P}_{xx} & \mathbf{P}_{xy}\\ \mathbf{P}_{yx} & \mathbf{P}_{yy}\end{pmatrix}\begin{bmatrix}\mathbf{E}_x\\ \mathbf{E}_y\end{bmatrix}=\beta^2\begin{bmatrix}\mathbf{E}_x\\ \mathbf{E}_y\end{bmatrix} \tag{3.29}$$

with,

$$\mathbf{P}_{xx} = -k_0^{-2}\mathbf{U}_x\boldsymbol{\varepsilon}_{rz}^{-1}\mathbf{V}_y\mathbf{V}_x\mathbf{U}_y + \left(k_0^2\mathbf{I} + \mathbf{U}_x\boldsymbol{\varepsilon}_{rz}^{-1}\mathbf{V}_x\right)\left(\boldsymbol{\varepsilon}_{rx} + k_0^{-2}\mathbf{V}_y\mathbf{U}_y\right) \tag{3.30}$$

$$\mathbf{P}_{yy} = -k_0^{-2}\mathbf{U}_y\boldsymbol{\varepsilon}_{rz}^{-1}\mathbf{V}_x\mathbf{V}_y\mathbf{U}_x + \left(k_0^2\mathbf{I} + \mathbf{U}_y\boldsymbol{\varepsilon}_{rz}^{-1}\mathbf{V}_y\right)\left(\boldsymbol{\varepsilon}_{rx} + k_0^{-2}\mathbf{V}_x\mathbf{U}_x\right) \tag{3.31}$$

$$\mathbf{P}_{xy} = \mathbf{U}_x\varepsilon_{rz}^{-1}\mathbf{V}_y\left(\boldsymbol{\varepsilon}_{ry} + k_0^{-2}\mathbf{V}_x\mathbf{U}_x\right) - k_0^{-2}\left(k_0^2\mathbf{I} + \mathbf{U}_x\boldsymbol{\varepsilon}_{rz}^{-1}\mathbf{V}_x\right)\mathbf{V}_y\mathbf{U}_x \tag{3.32}$$

$$\mathbf{P}_{yx} = \mathbf{U}_y\boldsymbol{\varepsilon}_{rz}^{-1}\mathbf{V}_x\left(\boldsymbol{\varepsilon}_{rx} + k_0^{-2}\mathbf{V}_y\mathbf{U}_y\right) - k_0^{-2}\left(k_0^2\mathbf{I} + \mathbf{U}_y\boldsymbol{\varepsilon}_{rz}^{-1}\mathbf{V}_y\right)\mathbf{V}_x\mathbf{U}_y \tag{3.33}$$

We may also alternatively write an eigenvalue equation in terms of the transverse magnetic fields,

$$\mathbf{P}\begin{bmatrix}\mathbf{H_x}\\ \mathbf{H_y}\end{bmatrix} = \begin{pmatrix}\mathbf{Q}_{xx} & \mathbf{Q}_{xy}\\ \mathbf{Q}_{yx} & \mathbf{Q}_{yy}\end{pmatrix}\begin{bmatrix}\mathbf{H}_x\\ \mathbf{H}_y\end{bmatrix} = \beta^2\begin{bmatrix}\mathbf{H}_x\\ \mathbf{H}_y\end{bmatrix} \tag{3.34}$$

with,

$$\mathbf{P}_{xx} = -k_0^{-2}\mathbf{V}_x\mathbf{U}_y\mathbf{U}_x\boldsymbol{\varepsilon}_{rz}^{-1}\mathbf{V}_y + \left(\varepsilon_{rz} + k_0^{-2}\mathbf{V}_x\mathbf{U}_x\right)\left(k_0^2\mathbf{I} + \mathbf{U}_y\varepsilon_{rz}^{-1}\mathbf{V}_y\right) \tag{3.35}$$

$$\mathbf{P}_{yy} = -k_0^{-2}\mathbf{V}_y\mathbf{U}_x\mathbf{U}_y\boldsymbol{\varepsilon}_{rz}^{-1}\mathbf{V}_x + \left(\varepsilon_{rx} + k_0^{-2}\mathbf{V}_y\mathbf{U}_y\right)\left(k_0^2\mathbf{I} + \mathbf{U}_x\varepsilon_{rz}^{-1}\mathbf{V}_x\right) \tag{3.36}$$

$$\mathbf{P}_{xy} = -\left(\boldsymbol{\varepsilon}_{ry} + k_0^{-2}\mathbf{V}_x\mathbf{U}_x\right)\mathbf{U}_y\boldsymbol{\varepsilon}_{rz}^{-1}\mathbf{V}_x + k_0^{-2}\mathbf{V}_x\mathbf{U}_y\left(k_0^2\mathbf{I} + \mathbf{U}_x\boldsymbol{\varepsilon}_{rz}^{-1}\mathbf{V}_x\right) \tag{3.37}$$

$$\mathbf{P}_{yx} = -\left(\boldsymbol{\varepsilon}_{rx} + k_0^{-2}\mathbf{V}_y\mathbf{U}_y\right)\mathbf{U}_x\boldsymbol{\varepsilon}_{rz}^{-1}\mathbf{V}_y + k_0^{-2}\mathbf{V}_y\mathbf{U}_x\left(k_0^2\mathbf{I} + \mathbf{U}_y\boldsymbol{\varepsilon}_{rz}^{-1}\mathbf{V}_y\right) \tag{3.38}$$

3.4 Coupled-mode theory

In order to evaluate the behaviour of our later coupler designs, it was necessary to make use of coupled mode theory. Here we follow Okamoto [3.4] in deriving the coupled mode equations.

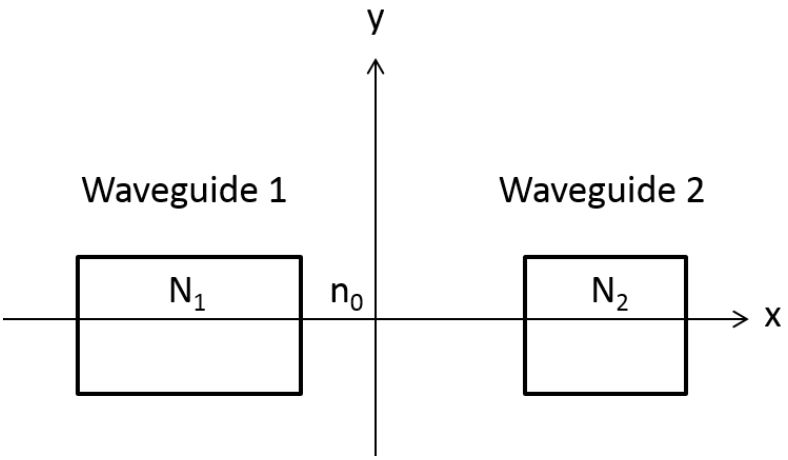

Figure 3-3: An illustration of two coupled waveguides

If we consider two waveguides each of which have modes that satisfy Maxwell's equations as is depicted in Figure 3-3,

$$\nabla \times \mathbf{E}_p = -j\omega\mu_0 \mathbf{H}_p \tag{3.39}$$

$$\nabla \times \mathbf{H}_p = j\omega\varepsilon_0 N_p{}^2 \mathbf{E}_p \tag{3.40}$$

where N_p (x,y) represents the refractive index of each waveguide, then we make the assumption that the fields of the coupled structure can be expressed as the sum of the eigenmodes of each waveguide,

$$\mathbf{E} = A(z)\mathbf{E}_1 + B(z)\mathbf{E}_2 \tag{3.41}$$

$$\mathbf{H} = A(z)\mathbf{H}_1 + B(z)\mathbf{H}_2 \tag{3.42}$$

This solution is also required to satisfy Maxwell's equations and so,

$$\nabla \times \mathbf{E} = -j\omega\mu_0 \mathbf{H} \tag{3.43}$$

$$\nabla \times \mathbf{H} = j\omega\varepsilon_0 N^2 \mathbf{E} \tag{3.44}$$

Using the vector identity,

$$\nabla \times (A\mathbf{E}) = A\nabla \times \mathbf{E} + \nabla A \times \mathbf{E} = A\nabla \times \mathbf{E} + \frac{dA}{dz}\mathbf{u}_z \times \mathbf{E} \tag{3.45}$$

we may derive the relations,

$$(\mathbf{u}_z \times \mathbf{E}_1)\frac{dA}{dz} + (\mathbf{u}_z \times \mathbf{E}_2)\frac{dB}{dz} = 0 \tag{3.46}$$

$$\left(\mathbf{u}_z \times \mathbf{H}_1\right)\frac{dA}{dz} - j\omega\varepsilon_0\left(N^2 - N_1^{\,2}\right)A\mathbf{E}_1 + \left(\mathbf{u}_z \times \mathbf{H}_2\right)\frac{dB}{dz} - j\omega\varepsilon_0\left(N^2 - N_2^{\,2}\right)B\mathbf{E}_2 = 0 \qquad (3.47)$$

with $N^2(x,y)$ the refractive index in the entire coupled waveguide. If we now perform the following integrations,

$$\int_{-\infty}^{\infty}\int_{-\infty}^{\infty}\left[\mathbf{E}_1 \cdot (3.48) - \mathbf{H}_1 \cdot (3.47)\right] dxdy = 0 \qquad (3.48)$$

$$\int_{-\infty}^{\infty}\int_{-\infty}^{\infty}\left[\mathbf{E}_2 \cdot (3.48) - \mathbf{H}_2 \cdot (3.47)\right] dxdy = 0 \qquad (3.49)$$

We obtain the equations,

$$\begin{aligned}
&\frac{dA}{dz} + \frac{dB}{dz}\frac{\int_{-\infty}^{\infty}\int_{-\infty}^{\infty}\mathbf{u}_z \cdot \left(\mathbf{E}^*_1 \times \mathbf{H}_2 + \mathbf{E}_2 \times \mathbf{H}^*_1\right)dxdy}{\int_{-\infty}^{\infty}\int_{-\infty}^{\infty}\mathbf{u}_z \cdot \left(\mathbf{E}^*_1 \times \mathbf{H}_1 + \mathbf{E}_1 \times \mathbf{H}^*_1\right)dxdy} \\
&+ jA\frac{\omega\varepsilon_0\int_{-\infty}^{\infty}\int_{-\infty}^{\infty}\left(N^2 - N_1^{\,2}\right)\mathbf{E}^*_1 \cdot \mathbf{E}^*_1 dxdy}{\int_{-\infty}^{\infty}\int_{-\infty}^{\infty}\mathbf{u}_z \cdot \left(\mathbf{E}^*_1 \times \mathbf{H}_1 + \mathbf{E}_1 \times \mathbf{H}^*_1\right)dxdy} \\
&+ jB\frac{\omega\varepsilon_0\int_{-\infty}^{\infty}\int_{-\infty}^{\infty}\left(N^2 - N_2^{\,2}\right)\mathbf{E}^*_1 \cdot \mathbf{E}^*_2 dxdy}{\int_{-\infty}^{\infty}\int_{-\infty}^{\infty}\mathbf{u}_z \cdot \left(\mathbf{E}^*_1 \times \mathbf{H}_1 + \mathbf{E}_1 \times \mathbf{H}^*_1\right)dxdy} = 0
\end{aligned} \qquad (3.50)$$

and,

$$\begin{aligned}
&\frac{dB}{dz} + \frac{dA}{dz}\frac{\int_{-\infty}^{\infty}\int_{-\infty}^{\infty}\mathbf{u}_z \cdot \left(\mathbf{E}^*_2 \times \mathbf{H}_1 + \mathbf{E}_1 \times \mathbf{H}^*_2\right)dxdy}{\int_{-\infty}^{\infty}\int_{-\infty}^{\infty}\mathbf{u}_z \cdot \left(\mathbf{E}^*_2 \times \mathbf{H}_2 + \mathbf{E}_2 \times \mathbf{H}^*_2\right)dxdy} \\
&+ jA\frac{\omega\varepsilon_0\int_{-\infty}^{\infty}\int_{-\infty}^{\infty}\left(N^2 - N_1^{\,2}\right)\mathbf{E}^*_2 \cdot \mathbf{E}^*_1 dxdy}{\int_{-\infty}^{\infty}\int_{-\infty}^{\infty}\mathbf{u}_z \cdot \left(\mathbf{E}^*_2 \times \mathbf{H}_2 + \mathbf{E}_2 \times \mathbf{H}^*_2\right)dxdy} \\
&+ jB\frac{\omega\varepsilon_0\int_{-\infty}^{\infty}\int_{-\infty}^{\infty}\left(N^2 - N_2^{\,2}\right)\mathbf{E}^*_2 \cdot \mathbf{E}^*_2 dxdy}{\int_{-\infty}^{\infty}\int_{-\infty}^{\infty}\mathbf{u}_z \cdot \left(\mathbf{E}^*_2 \times \mathbf{H}_2 + \mathbf{E}_2 \times \mathbf{H}^*_2\right)dxdy} = 0
\end{aligned} \qquad (3.51)$$

If we assume that the individual electromagnetic fields are of the form,

$$\mathbf{E}_p = \mathbf{E}_p \exp\left(-j\beta_p z\right) \tag{3.52}$$

$$\mathbf{H}_p = \mathbf{H}_p \exp\left(-j\beta_p z\right) \tag{3.53}$$

Then substituting this form into (3.50) and (3.51) we obtain,

$$\frac{dA}{dz} + c_{12}\frac{dB}{dz}\exp\left[-j\left(\beta_2 - \beta_1\right)z\right] + j\chi_1 A + j\kappa_{12} B\exp\left[-j\left(\beta_2 - \beta_1\right)z\right] = 0 \tag{3.54}$$

and,

$$\frac{dB}{dz} + c_{12}\frac{dA}{dz}\exp\left[+j\left(\beta_2 - \beta_1\right)z\right] + j\chi_2 B + j\kappa_{21} A\exp\left[+j\left(\beta_2 - \beta_1\right)z\right] = 0 \tag{3.55}$$

where we have defined the coupling coefficients,

$$\kappa_{pq} = \frac{\omega\varepsilon_0 \int_{-\infty}^{\infty}\int_{-\infty}^{\infty}\left(N^2 - {N_q}^2\right)\mathbf{E}^*{}_p \cdot \mathbf{E}_q \, dxdy}{\int_{-\infty}^{\infty}\int_{-\infty}^{\infty}\mathbf{u}_z \cdot \left(\mathbf{E}^*{}_p \times \mathbf{H}_p + \mathbf{E}_p \times \mathbf{H}^*{}_p\right)dxdy} \tag{3.56}$$

$$c_{pq} = \frac{\int_{-\infty}^{\infty}\int_{-\infty}^{\infty}\mathbf{u}_z \cdot \left(\mathbf{E}^*{}_p \times \mathbf{H}_q + \mathbf{E}_q \times \mathbf{H}^*{}_p\right)dxdy}{\int_{-\infty}^{\infty}\int_{-\infty}^{\infty}\mathbf{u}_z \cdot \left(\mathbf{E}^*{}_p \times \mathbf{H}_p + \mathbf{E}_p \times \mathbf{H}^*{}_p\right)dxdy} \tag{3.57}$$

$$\chi_p = \frac{\omega\varepsilon_0 \int_{-\infty}^{\infty}\int_{-\infty}^{\infty}\left(N^2 - {N_p}^2\right)\mathbf{E}^*{}_p \cdot \mathbf{E}_p \, dxdy}{\int_{-\infty}^{\infty}\int_{-\infty}^{\infty}\mathbf{u}_z \cdot \left(\mathbf{E}^*{}_p \times \mathbf{H}_p + \mathbf{E}_p \times \mathbf{H}^*{}_p\right)dxdy} \tag{3.58}$$

Here κ_{pq} is known as the mode coupling coefficient, c_{pq} represents the butt-coupling coefficients. The term χ_p involves the integration of the field of a waveguide p over the refractive index region occupied by the other waveguide q. As such, since the field in this region is likely to be very small, it can typically be neglected unless the waveguides are very close together. It can be noted immediately that the terms in the denominator of the above expressions can be rewritten in terms of the power in each individual mode which is given by,

$$P_p = \frac{1}{2}\int_{-\infty}^{\infty}\int_{-\infty}^{\infty}\left(E_p \times H^*{}_p\right)\cdot \mathbf{u}_z dxdy \tag{3.59}$$

Therefore we have,

$$\int_{-\infty}^{\infty}\int_{-\infty}^{\infty}\mathbf{u}_z\cdot\left(\mathbf{E}^*_p\times\mathbf{H}_p+\mathbf{E}_p\times\mathbf{H}^*_p\right)dxdy=4P_p \tag{3.60}$$

Assuming unit power in each mode we can then easily obtain from the above coupling expressions,

$$c_{21}=c_{12}^* \tag{3.61}$$

$$\chi_p=\chi^*_p \tag{3.62}$$

The power in the entire coupled waveguide structure can then be obtained as,

$$\begin{aligned}P&=\frac{1}{2}\int_{-\infty}^{\infty}\int_{-\infty}^{\infty}\left(\mathbf{E}\times\mathbf{H}^*\right)\cdot\mathbf{u}_z dxdy\\&=\frac{1}{2}\left[|A|^2+|B|^2+A^*Bc_{12}\exp(-j2\delta z)+AB^*c^*_{12}\exp(j2\delta z)\right]\end{aligned} \tag{3.63}$$

As useful expression can be obtained under the condition of loss-less waveguides by considering that optical power must remain constant,

$$\begin{aligned}\frac{dP}{dz}&=jA^*B\left(\kappa^*_{21}-\kappa_{12}-2\delta c_{12}\right)\exp(-j2\delta z)\\&\quad-jAB^*\left(\kappa_{21}-\kappa^*_{12}-2\delta c^*_{12}\right)\exp(j2\delta z)=0\end{aligned} \tag{3.64}$$

For this to be true for any z we therefore require that,

$$\kappa_{21}=\kappa^*_{12}+2\delta c^*_{12} \tag{3.65}$$

This tells us that under the condition of phase-matched waveguides or when the waveguides are sufficiently separated $\kappa_{21}=\kappa^*_{12}$.

3.5 Conclusions

In this chapter, the transfer matrix method was introduced for the purpose of evaluating and verifying the reflection responses of planar waveguides against their a priori prescribed values. In addition, the finite difference analysis of waveguides was described following the work of Zhu and Brown [3.1], as implemented in the Lumerical MODE Solutions solver. This is used extensively in this thesis to verify the modal properties of both the waveguide and fibres designs. Finally, coupled-mode theory was discussed so that it could be used in the modelling of the coupler designs later in this thesis.

3.6 References

[3.1] Z. Zhu and T. Brown, "Full-vectorial finite-difference analysis of microstructured optical fibers.," *Opt. Express*, vol. 10, no. 17, pp. 853–864, 2002.

[3.2] E. Anemogiannis, E. N. Glytsis, and T. K. Gaylord, "Determination of guided and leaky modes in lossless and lossy planar multilayer optical waveguides: reflection pole method and wavevector density method," *J. Light. Technol.*, vol. 17, no. 5, pp. 929–941, 1999.

[3.3] K. Yee, "Numerical solution of initial boundary value problems involving Maxwell's equations in isotropic media," *Antennas and Propagation, IEEE Transactions on*, vol. 14, no. 3. pp. 302–307, 1966.

[3.4] K. Okamoto, *Fundamentals of Optical Waveguides*. London, UK, 2006.

Chapter 4: Inverse scattering designs of dispersion-engineered single-mode planar waveguides

The work in this chapter was published in Optics Express, Vol 23(3), 2015 as "Inverse scattering designs of dispersion-engineered planar waveguides"

4.1 Introduction

Optical waveguides, in addition to controlling the propagation losses through total internal reflections and efficient power confinement in the core, offer the unique ability to control the group velocity of the propagating light. These two main attributes have rendered optical waveguides indispensable parts in any advanced optical system. So far, the largest control and highest performance has been achieved with optical fibres. Tailoring the core shape has been used to control both modality and group velocity dispersion in optical fibres [4.1].

While the control of dispersion in optical fibres is usually associated with dispersion compensation in optical communications networks [4.2] there has also been increasing interest in its control for the purposes of harnessing and optimising nonlinear optical effects. Parametric processes [4.3] and supercontinuum generation [4.4] rely upon tailoring the dispersion profile of the fibre to enhance energy transfer in certain spectral regions. Therefore, significant effort has been put over the last decade to develop technologies to fine control waveguide dispersion [4.5].

Silica-based highly nonlinear fibres (HNLF) feature very low attenuation characteristics and so by using long lengths of these fibres a large nonlinear effect can be realised. Small mode effective areas and thereby large nonlinearity are produced by increasing the refractive index (RI) difference between the core and the cladding which enhances the confinement of the light. This may be achieved by utilizing a highly germanium-doped core and a fluorine-doped cladding. In addition to creating a small mode effective area, nonlinear processes such as four-wave mixing (FWM) require the pump wavelength to coincide with the zero-dispersion wavelength of the fibre. Further control of the dispersion slope is advantageous in controlling dispersion and increasing operating bandwidth. An example of a HNLF with a zero-dispersion wavelength near 1550nm, a mode field diameter (MFD) of 4.3μm and a low dispersion slope of 0.0032ps/nm^2/km was realised through the use of a W-shape RI profile [4.6] . The index and thickness of these RI features determines the rate as a function of wavelength at which the mode transitions from the core to the ring. It is this, as well as, the average RI over which the mode extends that controls the propagation constant and its derivatives and thereby the dispersion properties of the fibre.

Control of dispersion has been achieved by modifying the inner-core shape and adding features, such as rings and trenches into the overall core design [4.1], [4.7]. While the dispersion-engineering of

fibres is typically approached through a trial and error method and parametric study, a powerful method for designing dispersion-engineered devices is *inverse scattering* (IS). Such methods have been used extensively to design fibre Bragg gratings with prescribed dispersion characteristics [4.8]–[4.10]. These methods have provided non-intuitive designs with advanced performance [4.11].

Also, authors have in the past studied the design of planar waveguides, as well as fibres from the IS point of view [4.12]–[4.17]. In these works, the modal properties of the waveguide such as a prescribed mode-profile [4.15], or the number of propagating modes [4.14] have been considered and specified at the start and through the inverse design process the waveguide with these properties is obtained. In particular, in the latter work the starting point of a truncated reflectionless potential is used. However, in each case, waveguide dispersion has not been considered from the point of view of the selection of (a variable number of) leaky poles and their approximation to the associated radiation modes. In our work, a transverse reflection coefficient of the structure is defined and the guiding properties of the waveguides are defined by the positions of reflection coefficient poles on the complex plane, representing guided and leaky modes of the waveguide under consideration. Similar IS techniques have also been used for the determination of the ionosphere characteristics from reflection data [4.18], [4.19].

In this work, we extend IS techniques, used in the ionosphere characterization, for the design of optical planar waveguides and study their dispersion characteristics. To our knowledge this is the first time that the connection between a transverse reflection coefficient and waveguide dispersion has been investigated. New designs are obtained with RI features which are generalizations to the ones considered previously. As a starting point to a more general analysis with fibres, we describe the dispersion characteristics of IS designed planar waveguides. We begin by considering design cases for which exact solutions exist which have previously been discussed in the literature, before extending this to a set of new cases. In each case the waveguide design is first obtained from the IS theory before the effective indices of the modes are solved (the forward problem) using the Lumerical MODE solver. This data is then used to map the dispersion characteristics of the waveguides. We then show that typical dispersion-engineered waveguide features such as rings and trenches come naturally from this theory. Finally, we discuss what benefits the new extended cases bring to the literature.

4.2 Designs using rational reflection coefficients

A general reflection coefficient can be approximated by rational functions of different degree [4.19]. The three-pole case is amenable to analytic solutions and has been studied extensively in the past in the context of ionospheric simulations [4.17] and waveguide modality [4.12], [4.13]. So far, waveguide examples are based upon either the GLM procedure or the application of the Crum-Krein or Darboux transformations [4.22] to reflectionless potentials. Here we focus on the GLM technique

where we note that to date the majority of waveguide examples are based upon a rational three-pole formulation. While numerical GLM techniques exist for non-rational reflection coefficients, these methods bring with it the possibility of roundoff errors and instabilities [4.23] and there is therefore an advantage in solving the GLM equation exactly using a generalization of the seminal work of Kay [4.20]. In addition, the complexity of the solutions, however, increases quickly with the number of poles and in view of Galois' proof that 5th and higher-order polynomial equations are insoluble by radicals, the previous analytic solutions cannot be implemented. In this case, the semi-analytical numerical technique, described by Pechenick in the context of ionospheric reflection data inversion [4.23], provides a powerful alternative. We have used this general technique throughout our study. It is worth noting that this is, to our knowledge, the first time this technique has been applied to waveguiding structures and the lack of significant development of the inversion of potentials with bound states is acknowledged in the work of Ge et al. [4.24].

We begin our study by considering first the simplest case of three-pole reflection coefficients and then proceed by progressively increasing the number of poles to five and seven.

4.2.1 Three-pole reflection coefficients

First we consider waveguide designs associated with the three-pole reflection coefficients:

$$r(k) = \frac{k_1 k_2 k_3}{(k-k_1)(k-k_2)(k-k_3)} \tag{4.1}$$

with poles k_1, k_2 and k_3 given by,

$$k_1 = -c_1 - ic_2; \quad k_2 = c_1 - ic_2; \quad k_3 = +ia \tag{4.2}$$

for which $c_1, c_2, a \in R^+$. The choice of poles k_1, k_2 and k_3 controls the shape and dispersion of reflection coefficient of the scattering layered medium and is expected to define the dispersion of the resulting waveguide. Pole k_3 corresponds to the propagation constant of the fundamental guided mode through $\beta = \sqrt{k_0^2 n_2^2 + a^2}$. Poles k_1 and k_2 on the other hand, result in leaky modes, which are necessary for the full description of the waveguide. Poles k_1 and k_2 are hereafter referred to as "leaky poles".

In order for a solution to exist, the reflection coefficient must obey a set of conditions [4.25], which are indeed satisfied by the general forms given in (4-11). However, it is necessary to restrict the position of the poles in the complex plane in order to satisfy energy conservation, $r(k) \leq 1$, for all real k. Previous authors [4.12], [4.13] have satisfied this requirement by considering the discriminant of a conservation-of-energy condition to be positive, thus giving the allowed regions A and B shown in Figure 4-1. Region A is bounded above by the line $c_2 = 0.5$ and below by the lemniscate of Bernoulli [4.25]. Region B is bounded below by $c_2 = 0.5$, but it is unbounded above.

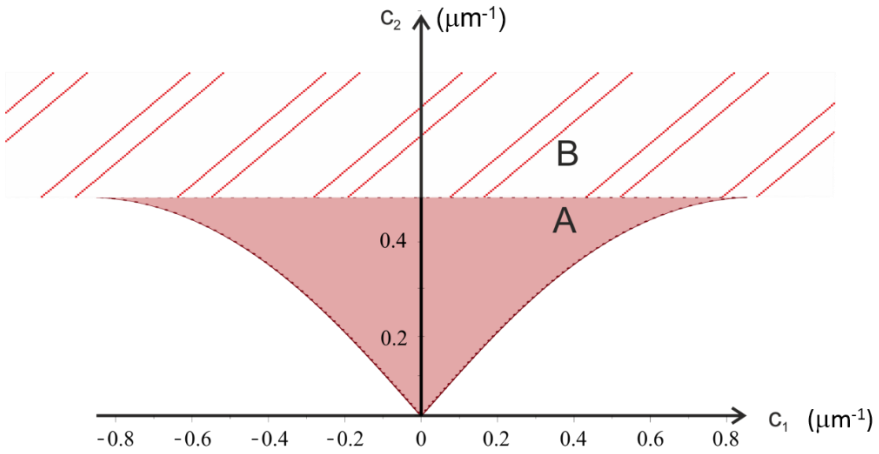

Figure 4-1: The allowed regions designed by A and B for the three pole case with a guided mode located at $|k_3|=1\mu m^{-1}$ derived by previous authors [4.12], [4.13]

In order to generalize this procedure to higher numbers of poles, we adopt a different approach by using Sturm's Theorem [4.26] from which we are able to determine whether the conservation-of-energy condition is satisfied or not (see Sec. 4.4 for details). The conjugate symmetric leaky poles k_1, k_2 maybe placed anywhere in Region A or Region B but must not be placed at the origin as this would result in the trivial reflection coefficient $r(k)=0$. The study of the dispersive properties of the designed waveguides was restricted in a region defined by $c_1=0.1$, $c_2=0.1$ as the inner limit and $c_1=4$, $c_2=4$ as the outer limit. In all subsequent calculations we assume cladding RI $n_2=1.444$, operating wavelength $\lambda = 1.55\mu m$ and guided mode pole $|k_3|=1\mu m^{-1}$.

Figure 4-2(a) shows two representative waveguide RI distributions, obtained by inverse scattering the three-pole reflection coefficient with ($c_1=0.1$, $c_2=0.1$ – design#1) and ($c_1=0.85$, $c_2=0.4999$ – design#2), using the semi-analytical technique of Pechenick [4.23]. Design#2 is also compared with the one derived by Lakshmanasamy and Jordan previously using an analytical technique [4.12], showing an excellent agreement. Figure 4-2(b) shows the variation of the effective index ($n_{eff}=\beta/k_0$) as function of $k_0=2\pi/\lambda$ for guided modes TE_0 and TE_1, for the two designs. It must be noted that for each design the TE_0 mode effective index at the design wavelength $\lambda = 1.55\mu m$ ($k_0=4.05\mu m^{-1}$) is $n_{eff}=1.4649$, as predicted by the expression above for β with a guided mode pole $|k_3|=1\mu m^{-1}$. It can be seen that designs with small leaky poles (design#1) resemble more closely a simple quasi-parabolic design. On the other hand, designs with larger conjugate symmetric poles (leaky poles), like design#2, result in features loosely resembling a fibre W-type RI profile and is associated with larger dispersion, as evidenced by the larger slopes of the associated n_{eff}-vs-k_0 curve in Figure 4-2(b). In addition, design#2 shows single-mode operation over a much wider range of wavelengths.

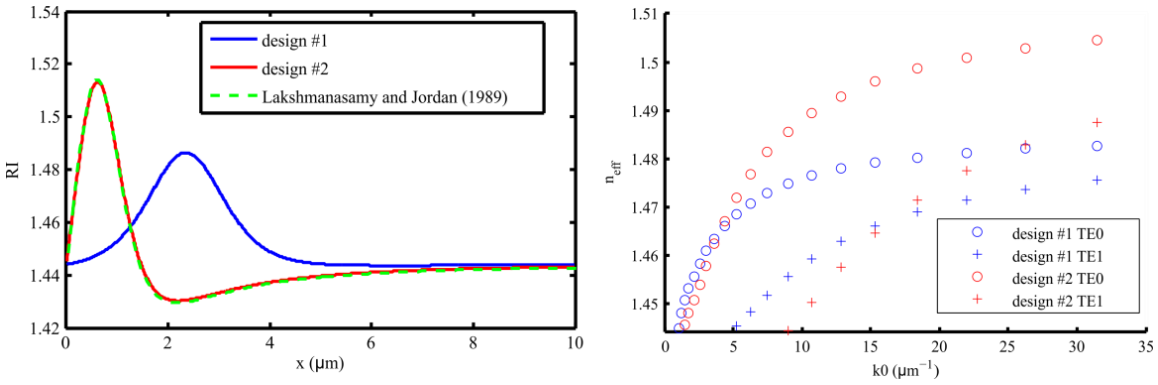

Figure 4-2: (a) RI profiles with three-pole rational reflection coefficient designs in region A with c_1=0.1, c_2=0.1 (design#1) and c_1=0.85, c_2=0.499 (design#2). The exact design#2 obtained by Lakshmanasamy and Jordan [4.12] (dotted green curve) is also shown for comparison. (b) effective index variation with k_0 for design#1 and #2 (the design point is demarcated by the dashed lines).

So far, in the literature inverse-scattering waveguide designs have been limited to region A [4.13]. In this work, in order to evaluate the effect of the leaky poles thoroughly, we have studied direct scattered designs, located in both Region A and B, to determine the waveguide dispersion and dispersion slope. The results are summarized in Figure 4-3.

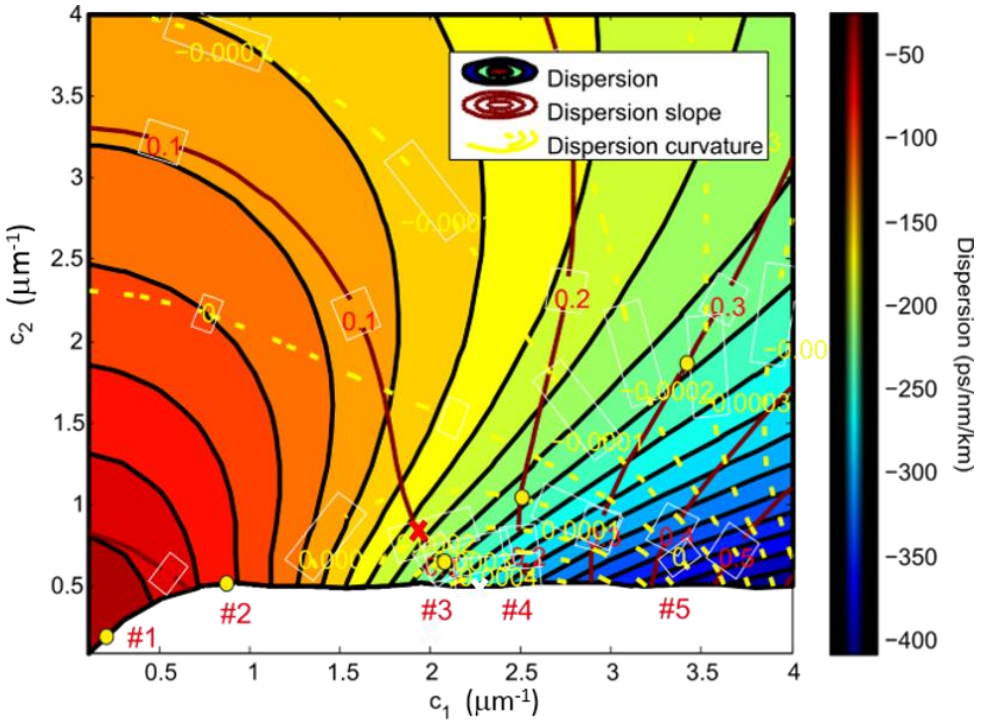

Figure 4-3: Waveguide dispersion D_2 (in ps/nm/km), dispersion slope D_3 (in ps/nm^2/km), and dispersion curvature D_4 (in ps/nm^3/km) as a function of leaky pole positions. (designs #1 to #5 are designated by yellow dots)

The second order dispersion coefficient D_2 is defined in terms of the mode effective index $n_{eff}=\beta/k_0$ as,

$$D_2 = -\frac{\lambda}{c}\frac{d^2 n_{eff}}{d\lambda^2} \tag{4.3}$$

The higher order dispersion coefficients D_n is given by,

$$D_n = \mathrm{d}D_{(n-1)} / \mathrm{d}\lambda, \quad n > 2 \tag{4.4}$$

D_3 and D_4 are also known as dispersion slope and dispersion curvature expressed in ps/nm^2/km and ps/nm^3/km, respectively. The dispersion map in Figure 4-3 can be used to provide the appropriate c_1 and c_2 values for a target D_2, D_3 and D_4 combination.

It can be seen that as previously surmised leakier poles (i.e. larger c_1 and c_2) lead to waveguides with higher waveguide dispersion. In particular, moving out of region A (bottom-left corner of allowed region in Figure 4-4) into region B (c_2>0.5) the waveguide dispersion increases from <50ps/nm/km to >400ps nm/km with more positive dispersion slopes and more negative dispersion curvature. In particular there appears a region close to the edge of the considered region B, on the lower-right hand side, where the largest dispersions are observed.

We also note that designs exist for which the dispersion is constant, and the dispersion slope and dispersion curvature differ. As an example, Figure 4-4(a) shows waveguide designs for which D_2= -215ps/nm/km is constant and D_3 is 0.1ps/nm^2/km (design#3), 0.2ps/nm^2/km (design#4), and 0.3ps/nm^2/km (design#5). The corresponding parameters (c_1,c_2) are (2.0588,0.6541-design#3), (2.5014,1.0885-design#4), and (3.5810,2.1803-design#5). Designs #1 to #5 are designated by yellow dots in Figure 4-4.

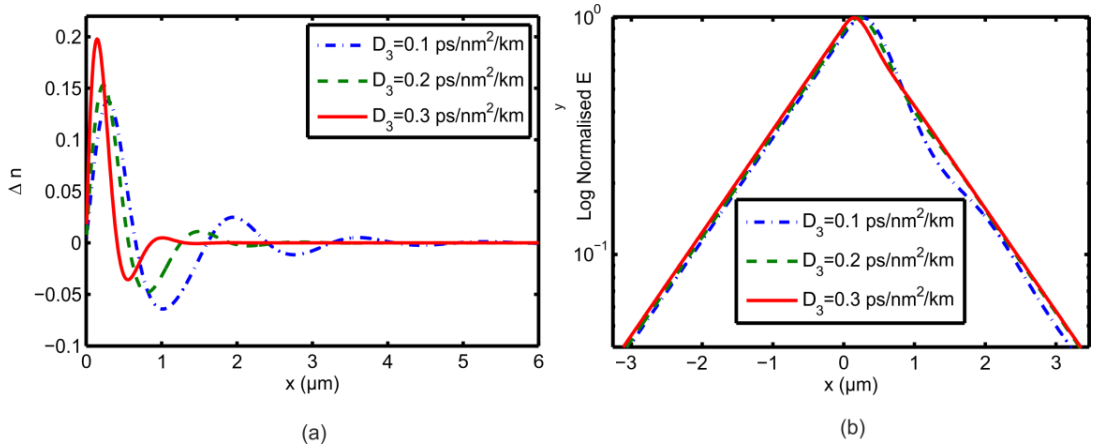

Figure 4-4: (a) Waveguide designs and (b) corresponding TE_0 normalized electric field profiles with D_2 = -215ps/nm/km and D_3= 0.1ps/nm^2/km (design#3), 0.2ps/nm^2/km (design#4) and 0.3ps/nm^2/km (design#5).

We observe from Figure 4-4(a) that, for a constant dispersion, increasing the magnitude of the dispersion slope causes the RI profile to narrow and steepen. It is particularly interesting to note that the design with the smallest dispersion slope contains significant trench and ring features, as well as oscillations, which result in substantial dispersion flattening. It should be mentioned that the inversed-scattered profiles can be considered as generalizations of commonly used triple-cladding dispersion compensating fibres. It is well known that for a fixed phase velocity changes in the electric-field/RI overlap are associated with changes in group velocity through the integrals of the scalar approximation method [4.27]. This is demonstrated in Figure 4-4 (b) where the electric field of design#3 varies noticeably, when compared with design #5, in accordance with the RI distribution which results in substantial dispersion slope reduction.

In order to further explore the significance of the leaky pole positions on the IS waveguide designs, we have considered separately the effect of their modulus $R=|k_1|=|k_2|$ and their real part magnitude c_1. Figure 4-5(a) and 6(b) plot the RI modulation profiles for R=3 and 4, respectively. This demonstrates that while an increase in leaky pole modulus does increase the dispersion, through a narrowing and steepening of the design, it is the increase of parameter c_1 that causes the development of strong RI modulation and larger dispersion.

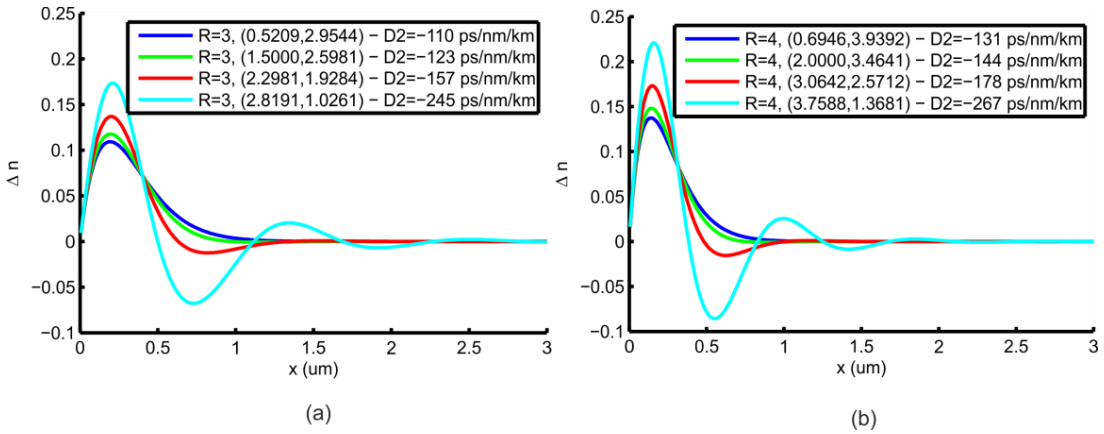

Figure 4-5: Effect of leaky pole modulus $R=|k_1|=|k_2|$ on IS waveguide RI modulation. (a) R=3 and (b) R=4.

The dispersion curves of the TE_0 and TE_1 modes for the designs shown in Figure 4-5 are plotted in Figure 4-6. In addition to higher dispersion, manifested by the increased slope of the dispersion curves at the design wavelength (indicated by dotted lines), the designs with the largest c_1 parameter show wider single mode operation bandwidth (marked by the TE1 cut-off point). Compared with the low dispersion design#1 in Figure 4-3, these high dispersion designs show about three time wider single-mode operation bandwidths. This is because of the presence of the RI depression adjacent to the main RI lobe.

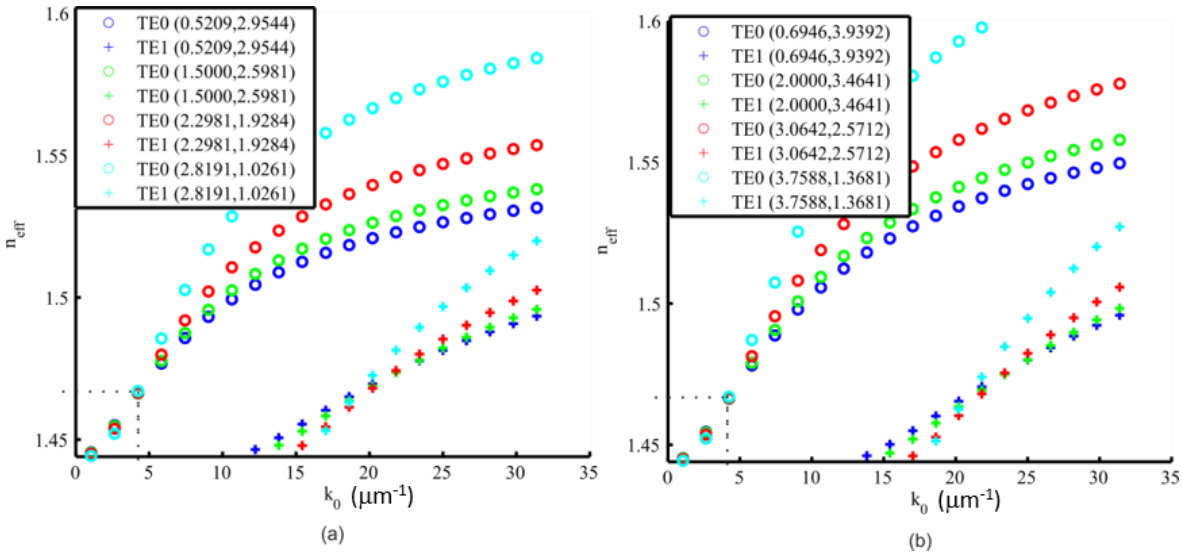

Figure 4-6: The dispersion curves (TE_0, TE_1) for (a) R=3 and (b) R=4 designs (the design point is demarcated by the dashed lines).

Figure 4-7(a) shows the effect of c_1 on the waveguide RI profile, for constant c_2. It demonstrates that increasing the c_1 parameter introduces strong RI oscillations with varying period. This also increases the waveguide dispersion as evidenced from the increased slope of the dispersion curves shown in Figure 4-8 (b).

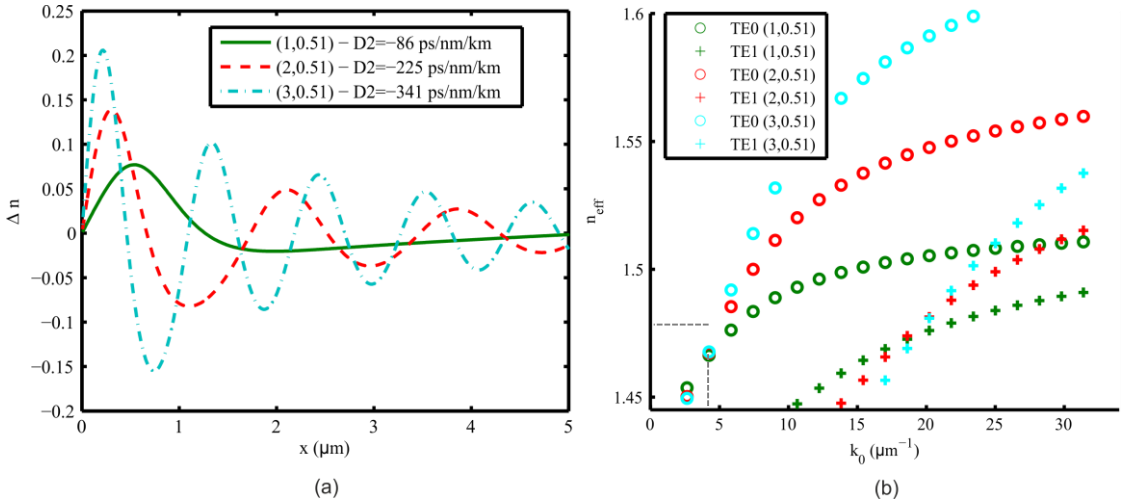

Figure 4-7: (a) RI modulation profiles for different c_1 and fixed c_2=0.51. (b) n_{eff} variation for TE_0 and TE_1 with k_0 (the design point is demarcated by the dashed lines)

In addition to dispersion, RI modulation affects the guided mode field distribution (see Figure 4-4(b)), and therefore, the effective mode area. Effective mode area is another important parameter since it defines the strength on waveguide nonlinear effects and the losses between different waveguide structures. The fundamental TE_0 mode effective mode area is calculated by $A_{eff} = (\int |E_y|^2 dA)^2 / \int |E_y|^4 dA$ and is plotted over the entire (c_1,c_2) parameter space in Figure 4-8. It is clearly shown that high dispersion is associated with smaller effective mode areas. The low dispersion designs, located close to the origin within region A, show the largest effective mode areas

(of order of 2.8μm^2), while the most dispersive designs, located close to region B lower boundary, show effective mode areas of the order of 1.8μm^2. Such inter-dependence has also been observed in highly dispersive fibres [4.2], [4.7].

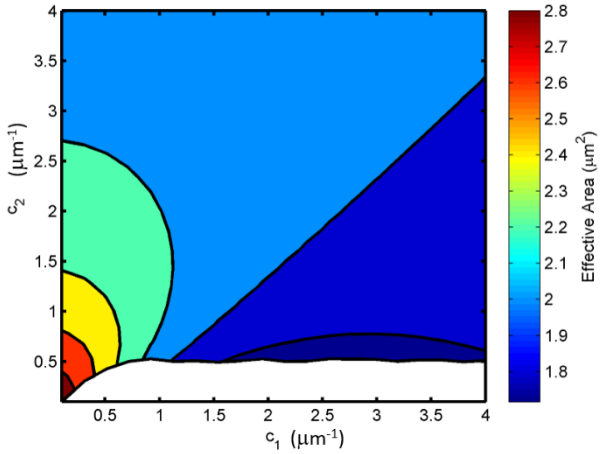

Figure 4-8: TE_0 effective mode area over the entire (c_1,c_2) parameter space.

4.2.2 Five- & Seven-pole reflection coefficients

We have extended the waveguide IS designs to rational reflection coefficients with five poles of the form,

$$r(k)=\frac{k_1k_2k_3k_4k_5}{(k-k_1)(k-k_2)(k-k_3)(k-k_4)(k-k_5)} \tag{4.5}$$

with poles k_1,k_2,k_3,k_4,k_5 for which $c_1,\ c_2,\ d_1,\ d_2,\ a\in\mathbb{R}$, and

$$k_1=-c_1-ic_2,\ k_2=c_1-ic_2;\quad k_3=-d_1-id_2,k_4=d_1-id_2;\quad k_5=+ia \tag{4.6}$$

It is once again possible to use the semi-analytical IS numerical technique [4.21] to solve for waveguide designs. This is now a multi-dimensional problem and we only consider specific cases to demonstrate the effect of extra leaky poles.

We first fix two of the leaky poles to $k_{1,2}$ = ±0.85-i0.4999 and the guided mode pole to $|k_5|$=1μm^{-1}; as per the leakiest case for three poles in region A considered previously (design#2 in Figure 4-2(a) with D_2= -72ps/nm/km, D_3= 0.0042ps/nm^2/km & D_4= 0.000049 ps/nm^3/km). Using Sturm's Theorem, we obtain in Figure 4-9 the allowable domain and dispersion contours of d_1 and d_2, defining the positions of the other two leaky poles k_3 and k_4. In this case, the allowable domain is totally different to the three-pole case shown in Figure 4-3. We notice that in this case the introduction of two extra leaky poles does not change dramatically the waveguide dispersion. Actually, the dispersion for these designs has been limited in magnitude by the size of the initial leaky poles c_1 and c_2 to a value of the order of D_2= -72ps/nm/km.

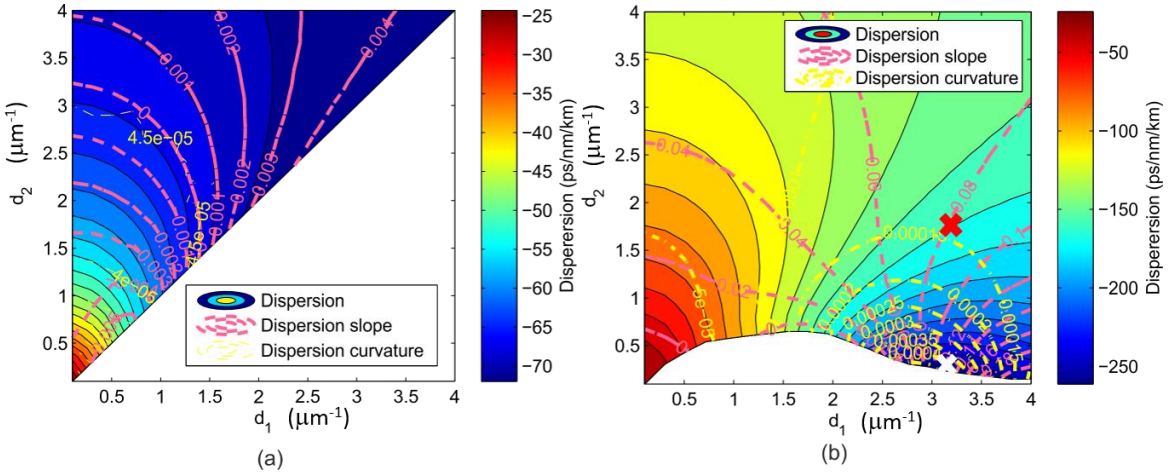

Figure 4-9: Waveguide dispersion map as a function of additional leaky pole positions for a five-pole case. (a) (c_1,c_2)=(0.85,0.4999) and (b) (c_1,c_2)=(1.7,1), $|k_5|$=1μm^{-1}, n_2=1.444 and λ=1.55 μm

Figure 4-9 (b) shows the allowable region and dispersion map with varying d_1, d_2, when the fixed leaky pole position is moved into region B to (c_1,c_2)=(1.7,1). In the three-pole case (see Figure 4-3 red cross) this corresponds to D_2= -145ps/nm/km, D_3= 0.08/nm^2/km & D_4= 0.00010/nm^3/km. The allowable (d_1,d_2) region in this case resembles the three-pole one. Once again, though, the obtained waveguide dispersion shows a limited variation around the three-pole values. From the two examples shown in Figure 4-9, we deduce that the addition of two extra leaky poles provides very similar results for dispersion tuning as that around the values achieved by the corresponding three-pole case. To demonstrate this, consider a design in Figure 4-9 (b) with identical waveguide dispersion and dispersion curvature to that of the three-pole case above, which we also denote by a red cross. We then find that the waveguide dispersion, slope and curvature here are all very similar to those in the existing three-pole case.

To explore this even further, we may choose a three-pole case and a five-pole case indicated by the white crosses in Figure 4-3 and Figure 4-9 (b) respectively, both with waveguide dispersion D_2= -261ps/nm/km and dispersion slope D_3= 0.13ps/nm^2/km but ever so slightly differing dispersion curvature D_4 of 4.41x10^{-4} ps/nm^3/km & 4.29x10^{-4} ps/nm^3/km, respectively. The designs are obtained with (c_1,c_2)=(2.2775,0.5269) and (c_1,c_2,d_1,d_2)=(1.7,1,3.18,0.22), respectively, and the resulting RI distribution is shown in Figure 4-10. The two designs show the same qualitative features, and the small difference in D_4 is achieved by slightly changing the size and periodicity of the RI undulations. These subtle differences are difficult to be captured by traditional iterative solutions, but result naturally by the IS technique.

We have also extended even further the waveguide IS designs to rational reflection coefficients with seven poles, by adding two extra leaky poles $k_{5,6}$ = ±e_1+ie_2. In Figure 4-11 we plot the allowable (e_1,e_2) space and resulting dispersion map, using the existing five-pole design point

(c_1,c_2,d_1,d_2)=(1.7,1,3.18,0.22), denoted once again by the white cross in Figure 4-9 (b) and guided pole k_7=+i1μm^{-1}.

We see once again that the design with identical waveguide dispersion and slope to the five-pole design denoted by the red cross has a very similar curvature. It appears that in each case the addition of larger number of poles brings a small but measureable difference in the control of higher order dispersions about a three-pole design corresponding to the leaky pole pair with smallest modulus. This small change is represented by the higher complexity of the refractive index profiles.

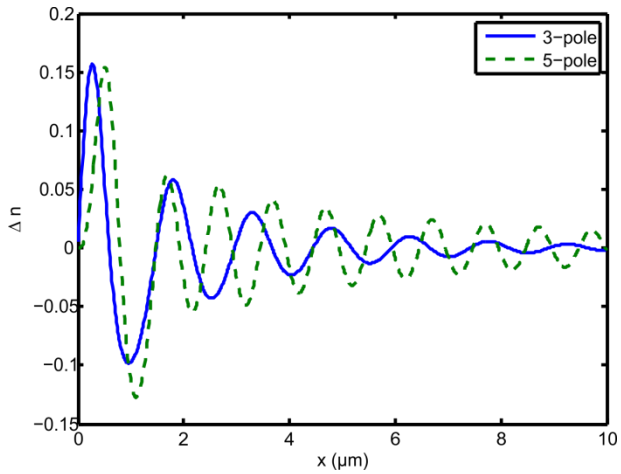

Figure 4-10: Three pole (c_1,c_2)=(2.2775,0.52692) and five-pole (c_1,c_2,d_1,d_2)=(1.7,1,3.18,0.22) designs with identical D_2=-261 ps/nm/km,D_3=0.130 ps/nm^2/km but differing D_4 (4.41x10^{-4} ps/nm^3/km & 4.29x10^{-4} ps/nm^3/km) (designs correspond to the 'white crosses' in Figure 5-4 & Figure 5-10 (b))

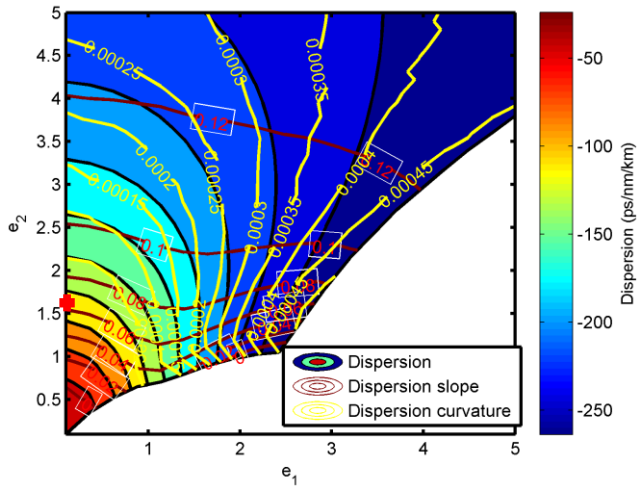

Figure 4-11: Seven-pole (e_1,e_2) allowable region and dispersion map, with fixed $(c_1, c_2, d_1, d_2) = (1.7,1,3.18,0.22)$.

4.3 Conclusions

In summary we have introduced a semi-analytical IS technique suitable for multipole, rational function reflection coefficients, and used it for the design of dispersion-engineered planar waveguides. The method is exact and stable and compared to other numerical methods it is shown not to introduce roundoff errors and instabilities [4.23]. Previous works [4.12], [4.13] have considered a three-pole reflection coefficient with a variable location of two conjugate symmetric leaky poles in the lower half of the k plane in order to obtain a waveguide design with a twofold larger core width than typically obtained by direct scattering techniques. However, the effect and relationship between the leaky pole positions and waveguide dispersion has not been considered to date. In addition, previous authors have not considered the inverse scattering of waveguides for rational reflection coefficients with more than three poles. We have shown that the addition of a larger number of poles, results in different 'pole allowable regions' and through the use of causality arguments in Appendix A we have developed a method to define these allowable regions. The technique is therefore used to derive extensive dispersion maps, including higher dispersion coefficients, corresponding to three-, five- and seven-pole reflection coefficients. The dispersion maps are obtained by varying systematically the pole positions within derived allowable regions. It is shown that common features of dispersion-controlled waveguides such as RI trenches, rings and oscillations come naturally from the IS theory when the magnitude of leaky poles in increased. In particular, while the leaky pole radius does lead to increased core size, trench size and dispersive properties, it is the magnitude of the c_1 parameter near the forbidden region that introduces and controls the period of oscillation in the RI profile. It is also shown that for the three-pole cases, the allowed Region B which has previously not been considered for waveguide designs provides the opportunity for increasingly dispersive designs.

The addition of further poles to the inverse scattering procedure, by which more general and not necessarily rational reflection coefficients can be approximated [4.21], has not been investigated previously and has been shown to offer a small but measureable change in higher order dispersion. It is important to note that the inverse scattering method employed in this work can be applied to an arbitrary number of poles and is therefore not limited. We have also shown that addition of larger number of poles, results in different "pole allowable regions". Using causality arguments, we have developed a method to define these allowable regions.

Although, a very large number of poles is needed to accurately describe general reflections coefficients, our work has shown the dispersion response is dominated primarily by the three pole design corresponding to the leaky pole pair with smallest modulus.

We believe that this initial study shows promise for the use of inverse scattering in the design of dispersion-engineered waveguides or fibres and we plan to consider these designs in future work. While we have yet to discover an analytic relationship between pole locations and waveguide

dispersion we shall in future work present 'engineering curves' relating the phase response of the rational reflection coefficient to the waveguide dispersion.

4.4 Appendix

Given a 5-pole reflection coefficient $r(k)$ of the form written in Eq. (14) and using the requirement of conservation of energy for all real k, it is straightforward to derive from $|r(k)|^2 \le 1$ the requirement that,

$$\frac{A}{B} \le 1 \tag{4.7}$$

where

$$A \equiv \left(c_1^{\,2} + c_2^{\,2}\right)^2 \left(d_1^{\,2} + d_2^{\,2}\right)^2 a^2 \tag{4.8}$$

and

$$\begin{aligned} B \equiv & \left(k^2 + 2kc_1 + c_1^{\,2} + c_2^{\,2}\right)\left(k^2 - 2kc_1^{\,2} + c_1^{\,2} + c_2^{\,2}\right)\left(k^2 + 2kd_1 + d_1^{\,2} + d_2^{\,2}\right) \\ & \times \left(k^2 - 2kd_1 + d_1^{\,2} + d_2^{\,2}\right)\left(k^2 + a^2\right). \end{aligned} \tag{4.9}$$

We observe that (4.16) is true whenever,

$$0 \le B - A \tag{4.10}$$

If we denote the polynomial in (4.18) by p(k) we observe that energy conservation is equivalent to requiring that for all real k,

$$0 \le p(k) \tag{4.11}$$

Sturm's theorem [4.26] states that given a polynomial of degree n, $p(k)$ and its derivative $p_1(k)$, there is an associated Sturm chain $S(k) = p(k), p_1(k), \ldots p_n(k)$, where $p_2(k)$ is the remainder of $p(k)$ divided by $p_1(k)$ with reverse sign, and $p_3(k)$ is the remainder of $p_1(k)$ divided by $p_2(k)$ with reverse sign, and so on until a constant is arrived at. Then the number of real roots in the open interval (a,b) is given by:

$$\rho = \nu_a - \nu_b \tag{4.12}$$

where ν_a and ν_b are the number of sign variations in the Sturm chain $S(a)$ and $S(b)$ respectively. For our case, we require that there are no real roots of $p(k)$ in the interval $(0,\infty)$ and make the necessary substitutions in the above. If we automate the process of determining whether $p(k)$ has real roots in the above interval for any combination of c_1, c_2, d_1, d_2 or as is required through the use

of a computer algebra package such as the MAPLE [4.28] function ‘sturm’, we obtain the domains illustrated in the contour plots of this paper.

4.5 References

[4.1] S. Ramachandran, “Dispersion-Tailored Few-Mode Fibers : A Versatile Platform for In-Fiber Photonic Devices,” *J. Light. Technol.*, vol. 23, no. 11, pp. 3426–3443, 2005.

[4.2] M. Wandel and P. Kristensen, “Fiber designs for high figure of merit and high slope dispersion compensating fibers,” *J. Opt. Fiber Commun.*, vol. 3, pp. 25–60, 2005.

[4.3] G. P. Agrawal, *Nonlinear Fiber Optics*. London, UK: Academic Press, 2001.

[4.4] J. M. Dudley and S. Coen, “Supercontinuum generation in photonic crystal fiber,” *Rev. Mod. Phys.*, vol. 78, no. 4, pp. 1135–1184, Oct. 2006.

[4.5] M. Takahashi, R. Sugizaki, J. Hiroishi, M. Tadakuma, Y. Taniguchi, and T. Yagi, “Low-Loss and Low-Dispersion-Slope Highly Nonlinear Fibers,” *J. Light. Technol.*, vol. 23, no. 11, pp. 3615–3624, 2005.

[4.6] M. Onishi, T. Okuno, and T. Kashiwada, “Highly nonlinear dispersion-shifted fibers and their application to broadband wavelength converter,” *Opt. Fiber Technol.*, vol. 4, no. 2, pp. 204–214, 1998.

[4.7] L. Grüner-Nielsen, S. Knudsen, and B. Edvold, “Dispersion-Compensating fibers,” *J. Light. Technol.*, vol. 23, no. 11, pp. 3566–3579, 2005.

[4.8] R. Feced, M. N. Zervas, and M. A. Muriel, “An Efficient Inverse Scattering Algorithm for the Design of Nonuniform Fiber Bragg Gratings,” *J. Quantum Electron.*, vol. 35, no. 8, pp. 1105–1115, 1999.

[4.9] J. Skaar and L. Wang, “On the synthesis of fiber Bragg gratings by layer peeling,” *J. Quantum Electron.*, vol. 37, no. 2, pp. 165–173, 2001.

[4.10] M. Ibsen, M. K. Durkin, M. N. Zervas, A. B. Grudinin, and R. I. Laming, “Custom design of long chirped Bragg gratings: application to gain-flattening filter with incorporated dispersion compensation,” *IEEE Photonics Technol. Lett.*, vol. 12, no. 5, pp. 498–500, 2000.

[4.11] M. N. Zervas and M. K. Durkin, “Physical insights into inverse-scattering profiles and symmetric dispersionless FBG designs,” *Opt. Express*, vol. 21, no. 15, pp. 17472–17483, 2013.

[4.12] S. Lakshmanasamy and A. K. Jordan, “Design of wide-core planar waveguides by an inverse scattering method.,” *Opt. Lett.*, vol. 14, no. 8, pp. 411–413, Apr. 1989.

[4.13] A. K. Jordan and S. Lakshmanasamy, “Inverse scattering theory applied to the design of single-mode planar optical waveguides,” *J. Opt. Soc. Am. A*, vol. 6, no. 8, pp. 1206–1212, 1989.

[4.14] C. Papachristos and P. Frangos, “Synthesis of single-and multi-mode planar optical waveguides by a direct numerical solution of the Gel’fand-Levitan-Marchenko integral equation,” *Opt. Commun.*, vol. 203, pp. 27–37, 2002.

[4.15] I. Hirsh, M. Horowitz, and A. Rosenthal, “Design of Planar Waveguides With Prescribed Mode-Profile Using Inverse Scattering Theory,” *J. Quantum Electron.*, vol. 45, no. 9, pp. 1133–1141, 2009.

[4.16] M. Cvijetic, “Dual-mode optical fibres with zero intermodal dispersion,” *Opt. Quantum Electron.*, vol. 16, no. 4, pp. 307–317, 1984.

[4.17] A. K. Jordan, D. Ph, and S. Ahn, “Inverse scattering theory and profile reconstruction,” *Proc. Inst. Electr. Eng.*, vol. 126, no. 10, pp. 945–950, 1979.

[4.18] S. Ahn and A. K. Jordan, “Profile inversion of simple plasmas and nonuniform regions: Three-pole reflection coefficient,” *IEEE Trans. Antennas Propag.*, vol. 24, no. 6, pp. 879–882, 1976.

[4.19] M. Reilly and A. K. Jordan, “The applicability of an inverse method for reconstruction of electron-density profiles,” *IEEE Trans. Antennas Propag.*, vol. 29, no. 2, pp. 245–252, 1981.

[4.20] I. Kay, “The Inverse Scattering Problem When the Reflection Coefficient is a Rational Function,” *Commun. Pure Appl. Math.*, vol. XIII, pp. 371–393, 1960.

[4.21] J. Xia and A. K. Jordan, “Inverse-scattering view of modal structures in inhomogeneous optical waveguides,” *JOSA A*, vol. 9, no. 5, pp. 740–748, 1992.

[4.22] P. Deift and E. Trubowitz, “Inverse scattering on the line,” *Commun. Pure Appl. Math.*, vol. 32, pp. 121–251, 1979.

[4.23] K. R. Pechenick, “Inverse scattering—exact solution of the Gel’fand-Levitan equation,” *J. Math. Phys.*, vol. 22, no. 7, pp. 1513–1516, 1981.

[4.24] D. B. Ge, A. K. Jordan, and L. S. Tamil, “Numerical inverse scattering theory for the design of planar optical waveguides,” *J. Opt. Soc. Am. A*, vol. 11, no. 11, p. 2809, 1994.

[4.25] K. R. Pechenick, “Exact solutions to the valley problem in inverse scattering,” *J. Math. Phys.*, vol. 24, no. 2, pp. 406–409, 1983.

[4.26] A. Akritas and P. Vigklas, “Counting the number of real roots in an interval with Vincent’s theorem,” *Bull. Math. Soc. Sci. Math. Roum.*, vol. 53, no. 3, pp. 201–211, 2010.

[4.27] K. Case, “On Wave Propagation In Inhomogeneous Media,” *J. Math. Phys.*, vol. 13, no. 3, p. 360, 1972.

[4.28] Maplesoft, "MAPLE," (2012).

Chapter 5: Inverse scattering designs of multimode planar waveguides with differential group delay equalisation

Part of the work in this chapter was presented at the Sixth International Conference on Optical, Optoelectronic and Photonic Materials (ICOOPMA 2014) as "Group velocity equalisation in multimode waveguides using inverse scattering designs" and published in Volume 619 of the Journal of Physics: Conference Series.

5.1 Introduction

There is currently great interest in spatial division multiplexing [5.1] in order to overcome the impending "capacity crunch" [5.2] of single-core, single-mode optical fibre transmission systems. In particular, mode-division multiplexing is of particular interest because of the large number of modes that can be used in a single fibre. However, in order to use such methods it is important to control the deleterious effect of differential group delay (DGD) as well as mode-coupling. Mode-coupling leads to crosstalk between multiplexed data streams which can in theory be addressed through MIMO signal processing. However, when both DGD and mode-coupling are present crosstalk between modes can spread across multiple bit periods making such MIMO hardware more complex [5.3]. As a result, work has been done to investigate the tailoring of optical fibre refractive index (RI) profiles to meet the needs of both low DGD and low mode-coupling through the use of graded-index cores and outer trenches [5.4]–[5.6]. While giving good performance in terms of minimisation of DGD and low mode coupling between the LP_{01} and LP_{11} modes, such designs rely upon a parametric design process. We were interested to know whether direct control of mode effective indices could be used to control both of these characteristics.

Here we extend our work on the inverse scattering (IS) design of single-mode planar waveguides in Chapter 4 to the case of multimode planar waveguides through the use of Darboux transformations as have been used previously by Mills and Tamil [5.7] in the design of optical interconnects. We show that through manipulation of the effective indices and thus phase velocities of the waveguide modes it is possible to manipulate the group velocities in such a way as to control the range of wavelengths over which they are equalised. It is clear that we have performed this investigation in planar waveguides rather than optical fibres, but we believe that the qualitative features of the designs will carry over, especially given the similarity between the mode fields of both low order TE and LP modes in planar waveguides and fibres respectively. More generally, fibres must be designed by calling upon the solution to the Gel'fand-Levitan-Marchenko integral equation in a cylindrical geometry such as is done in Chapter 9 of this thesis.

5.2 Theory

In the case of multiple guided modes, as discussed in Chapter 2, the RI profile $n(x)$ of the optical waveguide can be reconstructed by appropriate Darboux transformations. In addition, given that there exists Brown's identity [5.8] which connects the phase velocity v_p, group velocity v_g, refractive index n(x) and z-directed component of modal power density P_z in the waveguide regions,

$$v_p^{-1} v_g^{-1} = \frac{1}{c^2} \frac{\int n(x)^2 P_z dA}{\int P_z dA} \tag{5.1}$$

we proposed that control of dispersive properties would be possible through the manipulation of modal effective indices using the above method. With the propagation constants supplied a priori the potential is derived and its dispersive properties obtained through direct scattering. We applied this method to the design of planar waveguides with two, three and four modes. In all cases the design wavelength was chosen to be λ_d=1.55μm and a cladding index of n_2=1.444. The differential group delay (DGD) between two modes TE_m and TE_n is typically defined in terms of their effective indices as,

$$DGD = \frac{\left(n_{eff,m} - n_{eff,n}\right)}{c} - \frac{\lambda}{c}\left(\frac{\partial n_{eff,m}}{\partial \lambda} - \frac{\partial n_{eff,n}}{\partial \lambda}\right) \tag{5.2}$$

In addition, it was assumed in calculating the DGD that material dispersion is the same for all modes and profile dispersion is negligible.

5.3 Dual-mode designs

We first select the effective index of the TE_0 mode and vary the spacing of the TE_1 mode with respect to this and the cladding. In all cases the effective index values were chosen by trial and error and observing the DGD performance of the designs. This is performed in designs #1-#5 where the TE_0 mode effective index is fixed at 1.450000 and the increasing effective indices of the TE_1 modes are given in Table 5-1 and the refractive index profiles as well as differential delay curves are given in Figure 5-1 (a) and (b) respectively. We see in (a) that through an increase in the TE_1 mode effective index relative to that of the fixed TE_0 mode, there is an associated increase in the extent of the core depression with this seen clearest between design #1 (blue curve) and design #5 (pink curve). This behaviour is in fact to be expected from coupled-mode theory where two identical single-mode waveguides, here represented by the two halves of the designs mirrored about the origin, have supermodes whose effective index near-degeneracy gets closer with increased waveguide spacing. As such, bringing the TE_1 mode's effective index up to that of the TE_0 mode leads to the splitting of the initially single core (see design #1) into that of increasingly separate dual cores (see designs #4

and #5). In addition, in (b) we observe that the wavelength at which the group velocities of the TE_0 and TE_1 modes are equalised increases from ~1.2 to ~1.8 μm (design #1-design #5) with a decrease in TE_0-TE_1 mode effective index spacing and the associated splitting of the cores.

Table 5-1:Dual-mode waveguide designs with fixed TE_0=1.450000 and varying TE_1 at λ=1.55μm and $n_{cladding}$=1.444

Design	TE_1 n_{eff}
#1	1.446300
#2	1.446475
#3	1.446650
#4	1.446825
#5	1.447000

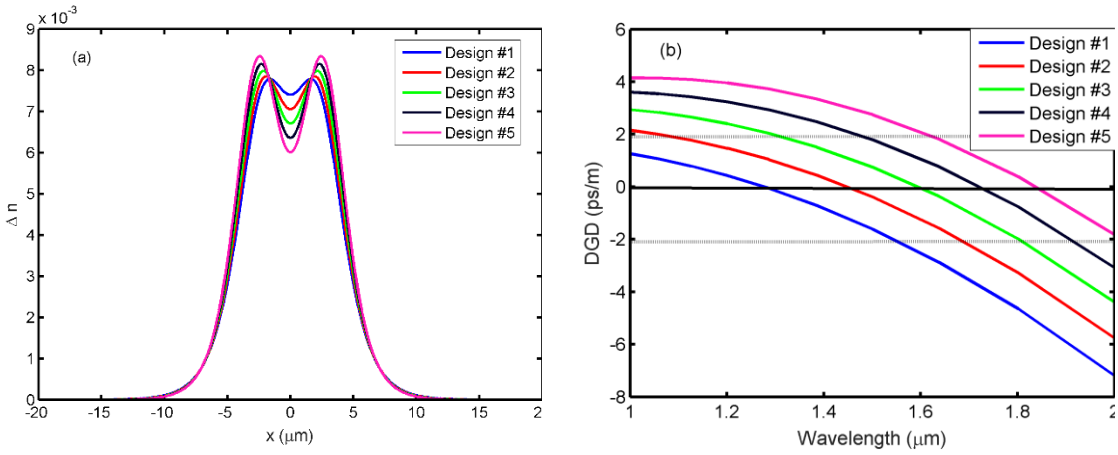

Figure 5-1: Dual mode waveguide designs with (a) varying TE_1 mode effective index for fixed TE_0=1.450000, and (b) associated differential group delay curves

This particular behaviour was initially observed by Stolen [5.9] in the context of ring-core optical fibres with improved group velocity equalisation for four-wave mixing interactions. Of particular interest is also the fact that, at a given wavelength, designs exist with opposite DGDs as can be seen, for example, at 1.55 μm where design #1 and design #4 have approximately ±2 ps/m DGD respectively. This could be used for equalisation in a similar way to dispersion compensation

approaches in the literature. In particular, design #3 has the DGD of the TE_1-TE_0 modes closest to zero.

5.4 Three and four-mode designs

We now investigate three-mode and four-mode waveguide designs where there is possible control over DGD. Once again, this is achieved by varying the relative effective indices of the propagating modes. In particular, we first consider the three-mode case where the TE_0 mode effective index is fixed at TE_0=1.450000, TE_1=1.447825 and the relative spacing of the TE_2 mode is varied. The value of TE_1 was guided by trial and error so that the TE_2 variation below led to the desired DGD performance. The effective indices of design #1-design #3 are shown in Table 5-2. In Figure 5-3 (a) we show how decreasing the spacing between the TE_1 and TE_2 modes in designs #1-#3 leads to a change in core behaviour from a small depression (blue line) to a mild peaked core (red line) to a more significant peak in core refractive index followed by outer ring depressions. It is interesting to see in Figure 5-2 (b) that at 1.55 μm design #1 leads to TE_1-TE_0 DGD of ~2.5 ps/m (solid blue) and TE_2-TE_0 DGD of ~-3ps/m (dashed blue) while design #3 leads to TE_1-TE_0 DGD of ~-2 ps/m (solid green) and TE_2-TE_0 DGD of ~2 ps/m (dashed green). As such, combining designs #1 and #3 could be concatenated to lead to minimisation of all DGDs in a three-mode design. In addition, design #2 depicted by the solid and dashed red curves has a low DGD (±0.4 ps/m) of both the TE_1-TE_0 and TE_2-TE_0 modes simultaneously at ~1.55 μm. This level of performance is typically achieved by graded-index designs such as those by OFS.

Table 5-2: Three-mode waveguide designs with fixed TE_0=1.450000, TE_1=1.447825 and varying TE_2 at λ=1.55μm and $n_{cladding}$=1.444

Design	$TE_2 n_{eff}$
#1	1.445000
#2	1.445500
#3	1.446000

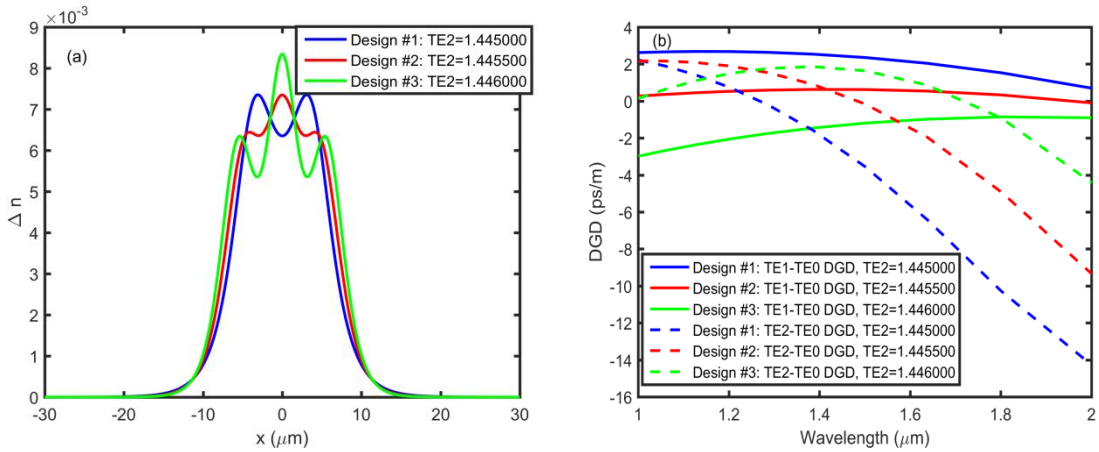

Figure 5-2: Three-mode waveguide designs with (a) varying TE_2 mode effective index for fixed TE_0=1.450000 and TE_1=1.447825, and (b) associated differential group delay curves

Decreasing the effective-index difference between the TE_1 and TE_2 modes with associated increase in pronounced central peak and outer ring also leads to DGD equalisation at ever larger wavelengths.

We now investigate the case of four-mode designs with DGD minimisation between all four modes. Here the effective indices of the TE_0, TE_1 and TE_2 modes are fixed at TE_0=1.450000, TE_1=1.448500, TE_2=1.446700 and the TE_3 mode effective index is moved relative to these. As before trial and error suggested these values. The effective indices of the TE modes for designs #1-designs #3 are given in Table 5-3, the refractive index profiles are shown in Figure 5-3 (a) and finally the DGD curves are shown in Figure 5-3 (b). It can be seen from design #1 (blue curve) – design #3 (green curve) that as in the previously considered cases, the increase of the TE_3 effective index towards that of the TE_2 mode and the associated decrease in spacing leads to the development of an increasingly large core depression and outer rings. For all designs the TE_1-TE_0 DGD is relatively flat across the range of wavelengths, while there is an increase in the gradient of the DGD curves from the TE_2-TE_0 to TE_3-TE_0 DGD values. In fact, as the TE_3 mode is increased from design #1 (blue) to design #3 (green) the DGD between TE_2-TE_0 becomes increasingly negative while the DGD between TE_3-TE_0 tends towards a small positive value ~1ps/m. In particular, design #2 is such that all three pairs of DGDs are within ~1 ps/m at a wavelength of 1.55 μm and the refractive index profile is qualitatively similar to that of a parabolic index profile.

Table 5-3: Four-mode waveguide designs with fixed TE_0=1.450000, TE_1=1.448500, TE_2=1.446700 and varying TE_3 at λ=1.55μm and $n_{cladding}$=1.444

Design	$TE_3 n_{eff}$
#1	1.445000
#2	1.445250
#3	1.445500

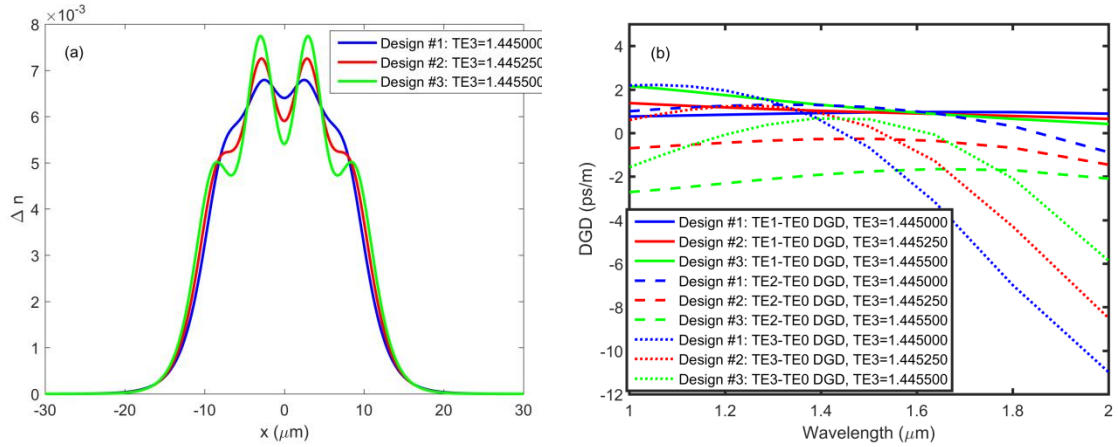

Figure 5-3: Four-mode waveguide designs with (a) varying TE_3 mode effective index for fixed TE_0=1.450000 and TE_1=1.448500, TE_2=1.446700, and (b) associated differential group delay curves

5.5 Interpretation of results

It should be noted that the infinitely extended parabolic refractive index profile considered by authors such as Adams [5.10] has modes for which the group velocity is approximately independent of the mode number and with the qualitative similarity seen above with increasing modality (2, 3 and 4-modes) it is interesting to consider how such designs compare with ours.

We now show in Figure 5-4 (a), (b) and (c) the inverse scattered designs of the 2, 3 and 4-moded cases which are approximately optimum for DGD equalisation and the closeness of fit with infinitely extended parabolic refractive index designs which have the same number of modes in each case.

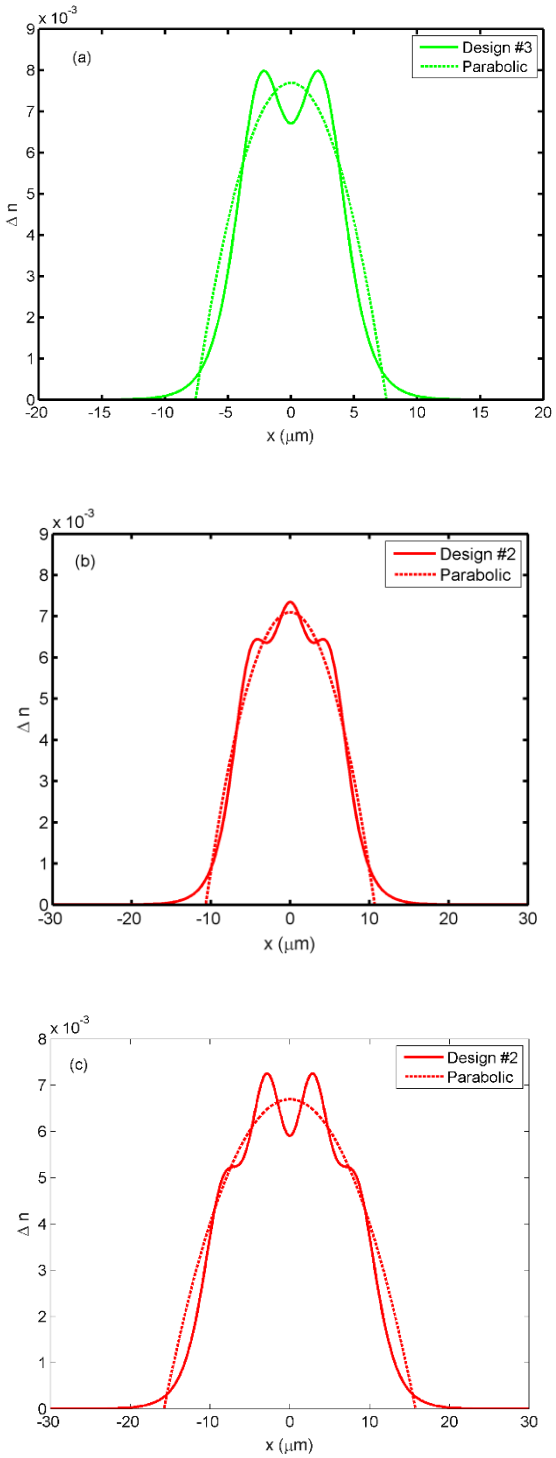

Figure 5-4: (a) two, (b) three and (c) four-moded inverse scattered designs leading to group velocity equalisation and their associated infinitely extended parabolic designs (dashed curves)

What we may learn from this is that the shape of the inverse scattering designs in these cases more closely resembles that of the idealised profile with increasing mode number as seen from Figure 5-4 (a) – (c).

Dual-mode design spectra

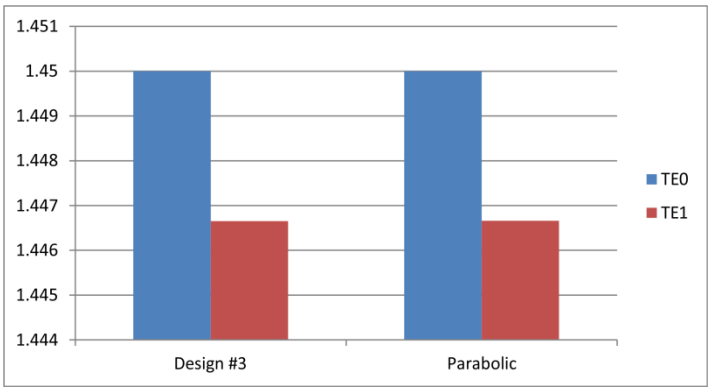

(a)

Three-mode design spectra

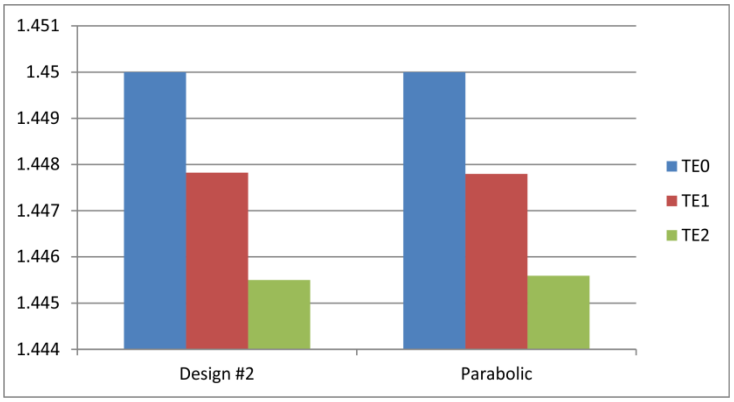

(b)

Four-mode design spectra

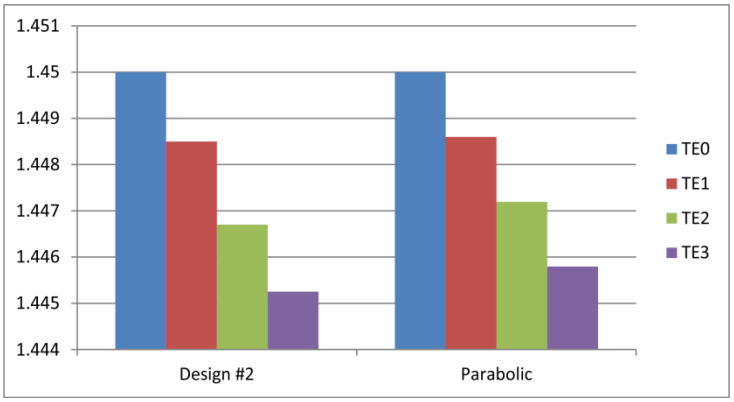

(c)

Figure 5-5: Comparison of inverse scattered and parabolic mode spectra for the (a) dual-mode, (b) three-mode and (c) four-mode designs with optimal DGD

In particular, in a sense the mode spacing in the 2, 3, and 4-moded IS cases with the best DGD equalisation follows that of the idealised parabolic cases as can be seen in Figure 5-5 where the effective indices of the inverse scattered and parabolic designs are compared.

We see in Figure 5-5 (a), as expected, that an extended parabolic design exists which has identical effective indices to that of the dual-mode inverse scattered case. Here given the low number of modes involved, the approximation of the inverse scattered design to that of the parabolic one is not very good as seen in Figure 5-4 (a). However, moving to Figures 5-4/5-5 (b) and then (c) we see that the approximation to the parabolic design improves and there is a similar pattern in effective index distribution. The original choice to place the effective indices by trial-and-error to optimise DGD now appears to be premature given that optimal designs suggest mode spectra should be chosen according to the extended parabolic design in the first place, which in fact is of the form of equally spaced effective indices [5.17]. This becomes more obvious when the number of modes is increased to six and then eight as seen in Figure 5-6 (a) and (b) below.

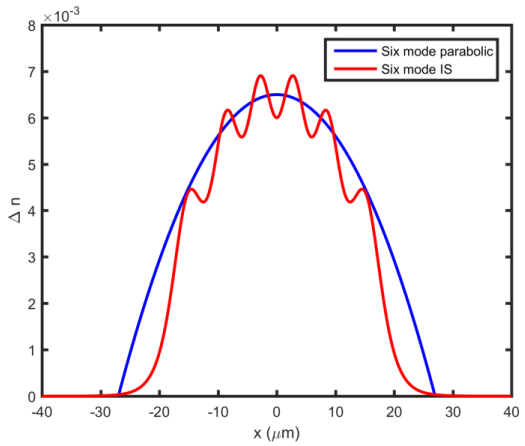

(a)

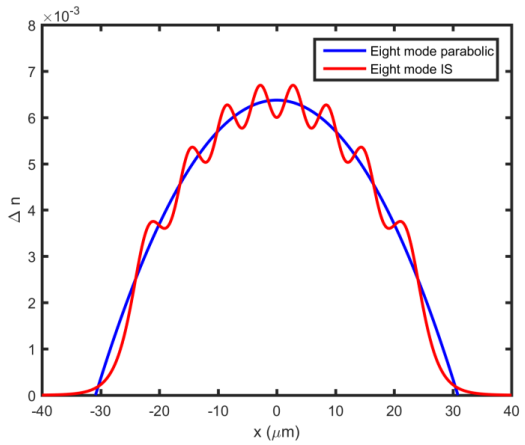

(b)

Figure 5-6: Comparison between IS and parabolic designs for (a) six modes, and (b) eight modes

As the number of modes is increased, the approximation to the parabolic profile improves considerably, and the effect can be likened to that of a Gibbs effect from Fourier analysis. As such, we see that equally spaced TE modes which lead to optimal DGD in our inverse scattering designs have refractive index designs which increasingly approximate the parabolic approach.

5.6 Conclusions

In this work we have shown that control of effective indices of modes through the use of the Darboux transformation can be used parametrically to minimise differential group delay over a range of wavelengths. This is possible by either designing the mode spectra to provide equalised group velocities directly, or by concatenating those designs with alternating positive and/or negative DGD. In addition, designs which result in peaked cores and outer rings when modes become nearly degenerate have also been explained away in terms of coupled-mode theory whereby two identical waveguides have super-modes whose effective index spacing is associated with an increase in waveguide core spacing. The result of this is the 'splitting' of the core observed.

We have also found that the parametrically obtained inverse scattered designs for minimisation of DGD have similar mode spectra to those of the extended parabolic design which is known in the literature to have modal group velocity independent of mode number. As the number of modes is increased, the inverse scattering designs increasingly approximate the extended parabolic designs in a way similar to that of the Gibbs effect of Fourier analysis.

While our investigation has been limited to planar waveguides there are similarities in intensity profiles between TE modes and LP modes and it is expected from Brown's identity that characteristics of these planar designs can be adapted for use in future optical fibres.

5.7 References

[5.1] D. J. Richardson, J. M. Fini, and L. E. Nelson, "Space-division multiplexing in optical fibres," *Nat. Photonics*, vol. 7, no. April, pp. 354–362, 2013.

[5.2] R. Essiambre and R. Tkach, "Capacity trends and limits of optical communication networks," *Proc. IEEE*, vol. 100, no. 5, pp. 1035–1055, 2012.

[5.3] D. Peckham, Y. Sun, A. McCurdy, and R. Lingle, "Few-Mode Fiber Technology for Spatial Multiplexing," in *Optical Fiber Telecommunications Volume VIA: Components and Subsystems*, 2013, pp. 283–316.

[5.4] F. Ferreira, D. Fonseca, and H. Silva, "Design of Few-Mode Fibers With Arbitrary and Flattened Differential Mode Delay," *IEEE Photonics Technol. Lett.*, vol. 25, no. 5, pp. 438–441, 2013.

[5.5] T. Sakamoto, T. Mori, T. Yamamoto, and S. Tomita, "Differential Mode Delay Managed Transmission Line for Wide-band WDM-MIMO System," *Opt. Fiber Commun. Conf.*, p. OM2D.1, 2012.

[5.6] L. Grüner-Nielsen and Y. Sun, "Few mode transmission fiber with low DGD, low mode coupling, and low loss," *J. Light. Technol.*, vol. 30, no. 23, pp. 3693–3698, 2012.

[5.7] D. W. Mills and L. S. Tamil, "Synthesis of Guided Wave Optical Interconnects," *IEEE J. Quantum Electron.*, vol. 29, no. 11, pp. 2825–2834, 1993.

[5.8] C.-L. Chen, *Foundations for Guided-Wave Optics* . Hoboken, New Jersey, USA: John Wiley & Sons, 2007.

[5.9] R. Stolen, "Modes in fiber optical waveguides with ring index profiles," *J. Appl. Opt.*, vol. 14, no. 7, pp. 1533–1537, 1975.

[5.10] M. Adams, *An Introduction to Optical Waveguides*. Chichester, UK: Wiley-Interscience, 1981.

Chapter 6: Inverse scattering designs of active multimode planar waveguides with differential modal loss and gain

The work in this chapter has been published in a Special Issue of the IEEE Journal of Selected Topics in Quantum Electronics as "Inverse Scattering Designs of Active Multimode Waveguides with Tailored Modal Gain"

6.1 Introduction

Spatial-division multiplexing (SDM) [6.1] is regarded as a potential solution to the forthcoming, previously mentioned optical communication "capacity crunch". SDM constitutes a drastic design departure from the currently used standard single-mode fibres (SMF) and relies on multicore and/or multimode fibres in order to increase the transmission degrees of freedom. Mode-division multiplexing (MDM), in particular, relies on specially designed multimode (MM) fibres and uses propagation optical modes as separate communication channels.

Recently this paradigm shift has been introduced into the field of integrated photonics technology in order to increase the bandwidth density of on-chip interconnects [6.2], [6.3] for computercom and data-center applications. The majority of the effort so far has been concentrated on the development of efficient multiplexers/de-multiplexers for high performance network-on-chip applications [6.2], [6.4]–[6.6]. However, in future highly integrated networking scenarios, on-chip amplification will be required in order to increase the reach of optical signals and support propagation over multiple modal add/drops and routing stages [6.7]. Thus far the design of effective waveguide amplifiers with individually prescribed modal gain has not been addressed. As has been discussed recently in the literature, uncorrected mode-dependent loss (MDL) has a deleterious effect on channel capacity [6.8], [6.9] and effective ways to mitigate this loss would be very useful.

Since the Darboux transformations are generally defined in the complex domain [6.10], [6.11] and can, in general, result in complex valued potentials [6.12]. here we extend the Darboux transformation algorithm to include complex propagation constants and apply it for the design of active multimode optical waveguides, with arbitrarily prescribed modal gains. In section 2, we first give examples of passive MM waveguides with prescribed real modal effective indices. In section 3 we give examples of active MM waveguides with arbitrary distribution of modal gains. It is shown that arbitrary modal gain distribution is achieved by complex potentials, which result in waveguide designs with distributed gain *and* loss core regions. To the best of our knowledge, such active

waveguide designs are presented for the first time. In section 6.4, finally, we discuss the connection of the current work with recently published MM fibre amplifier results in the context of MDM optical communication systems.

6.2 Design of passive multimode waveguides

In the case of passive MM waveguides, we consider real β_m associated with each mode with propagation constant β_m where $n_{eff,m} = \beta_m/k_0$, m=1,2,…,N. We begin the design process by applying the DT IS algorithm outlined above to design a passive four-mode waveguide with mode effective indices which match those of equivalent step-index (SI) waveguides. Throughout this chapter we assume cladding RI n_2=1.444 and a wavelength λ_0 = 1.55μm. The SI waveguide width is 15μm and the core RI is 1.458. The effective indices of the first four TE modes of the SI waveguide are 1.457773, 1.455789, 1.452551 and 1.448244, respectively. We progressively add the TE_0, TE_1, TE_2 and TE_3 modes one-by-one and the reconstructed waveguide RI distributions are shown in Figure 6-1. It is shown that when all four modes have been taken into account the DT IS designs closely follows that of the original SI RI distribution. Progressively smaller residual ripples, resembling those observed in the "Gibbs phenomenon" when a Fourier series overshoots at a jump discontinuity, are seen with increasing number of added modes.

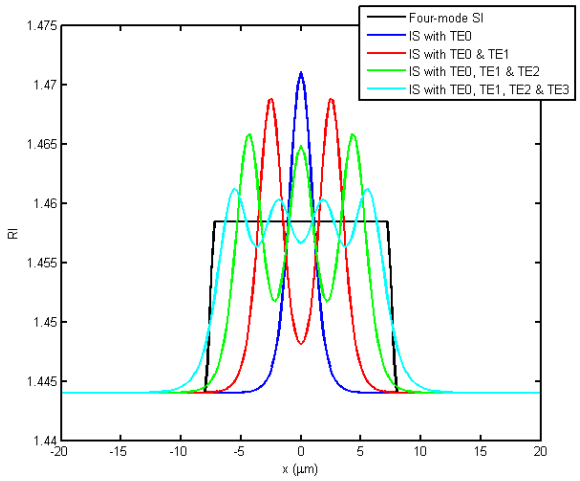

Figure 6-1: Refractive index distribution of a four mode SI waveguide and synthesized IS designs with increasing numbers of modes with effective indices equal to those of the original SI design, showing an increasing frequency "Gibbs like" ripple effect.

To confirm that the DT IS waveguide supports four modes with the prescribed effective indices, we use a commercial mode-solver software Lumerical MODE Solutions with the RI profile shown in Figure 6-1. The reconstructed effective indices are in excellent agreement with the original ones. Figure 6-2 (a)-(d) compare also the field profiles for the equi-spectral modes TE0 to TE3 supported

by the original SI and the DT IS waveguides. It is observed that despite the RI ripples, the mode profiles follow each other very closely.

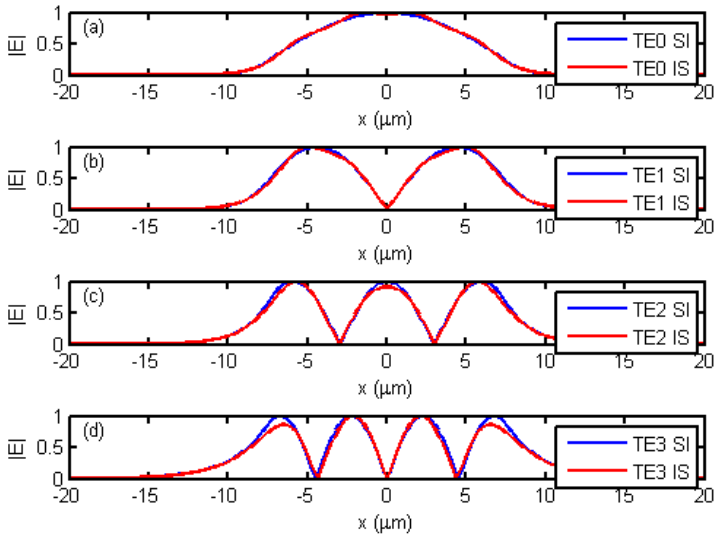

Figure 6-2: Mode field profiles for the four-mode SI (blue) and IS (red) (a) TE0 mode; (b) TE1 mode; (c) TE2 mode and (d) TE3 mode

6.3 Design of waveguides with tailored modal gain

Active waveguides with tailored modal gain or loss can be designed using the DT IS procedure outlined above by adding an imaginary component to the mode effective indices of the passive design shown in Figure 6-2 as, in general, This way, we can design active waveguides with pre-defined modal propagation gains in addition to pre-defined propagation constants. To demonstrate the technique we choose to arbitrarily add $\gamma_m \approx 3.5$ dB/cm gain selectively to each of the four TE modes of the original waveguide. This corresponds to the imaginary component of the effective index being $n_{effI,m} = 10^{-5}$.

6.3.1 Four-moded waveguide with gain in one mode only

Figure 6-3 plots the real and imaginary parts of the reconstructed RI for the case where only the TE_0 mode experiences γ_1 =3.5 dB/cm gain while the other mode remains gain-less. As can be seen in Figure. 6-3(a), the introduction of a complex effective index for the TE_0 mode results in a complex waveguide RI distribution. It is also shown that the real part (black line) is identical to the one of the original passive waveguide (c.f. Figure 6-1) while the imaginary part (green line) on the other hand shows both negative (blue shade-corresponding to gain) and positive (red shade corresponding to loss) variation over the waveguide width.

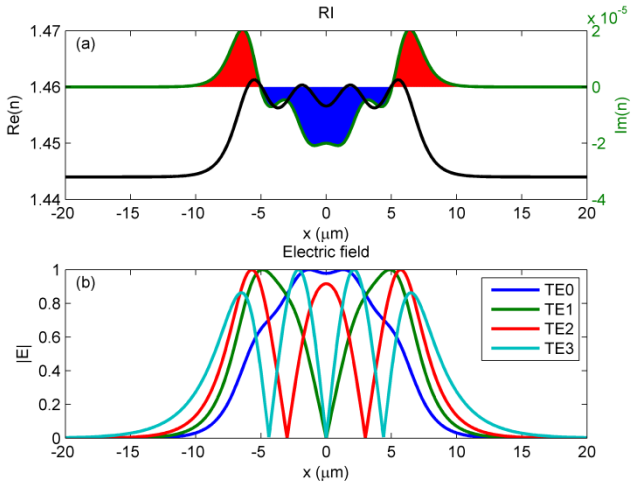

Figure 6-3: (a) Real and imaginary part of waveguide RI profile (red shade: loss, blue shade: gain) required to obtain selective gain of γ_1 =3.5 dB/cm for only the TE_0 mode, and (b) the associated modal fields.

It is observed that the TE_0 mode strongly overlaps with the waveguide gain region (blue shade), which results in the desired TE_0 mode propagation gain. The rest of the gain-less modes overlap with the waveguide gain region (blue) in such a way that this overlap is exactly balanced by their overlap with the loss region (red) and results in zero overall gain/loss.

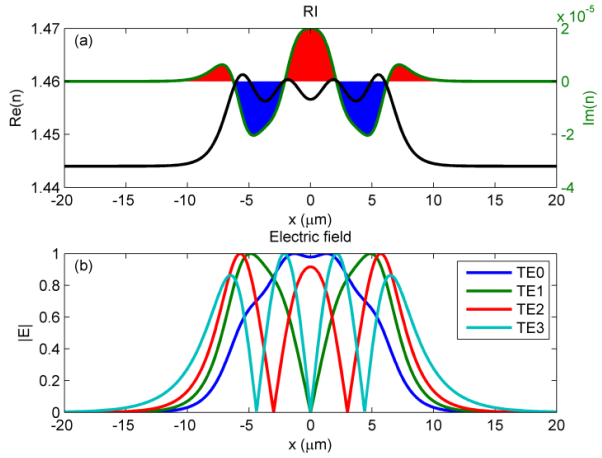

Figure 6-4: (a) Real and imaginary part of waveguide RI profile (red shade: loss, blue shade: gain) required to obtain selective gain of γ_2 =3.5 dB/cm for only the TE_1 mode, and (b) the associated modal fields

Figure 6-3, Figure 6-4 and Figure 6-5(a) show the real and imaginary parts of the reconstructed RI for the case where only the TE_1, TE_2, and TE_3 modes, respectively, experience 3.5 dB/cm gain while the rest of the modes remain gain-less. Again, it is observed that in all cases the real part of the RI (black line) and the modal profiles are identical to that of the original passive waveguide (c.f.Figure

6-1) However, the imaginary part of the RI changes shape dramatically depending upon which mode is to be amplified.

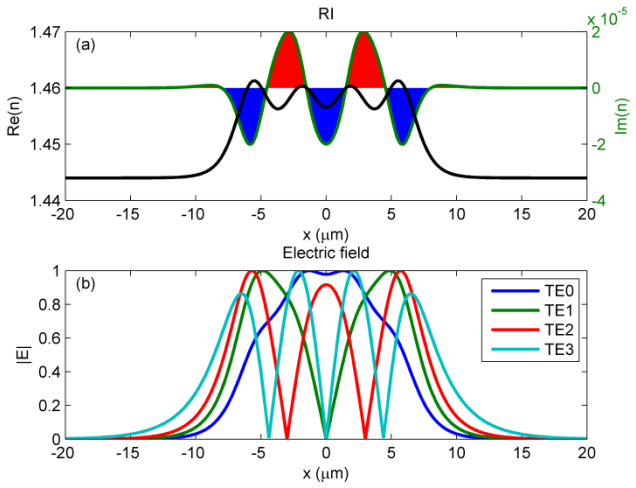

Figure 6-5: (a) Real and imaginary part of waveguide RI profile (red shade: loss, blue shade: gain) required to obtain selective gain of γ_3 =3.5 dB/cm for only the TE_2 mode, and (b) the associated modal fields

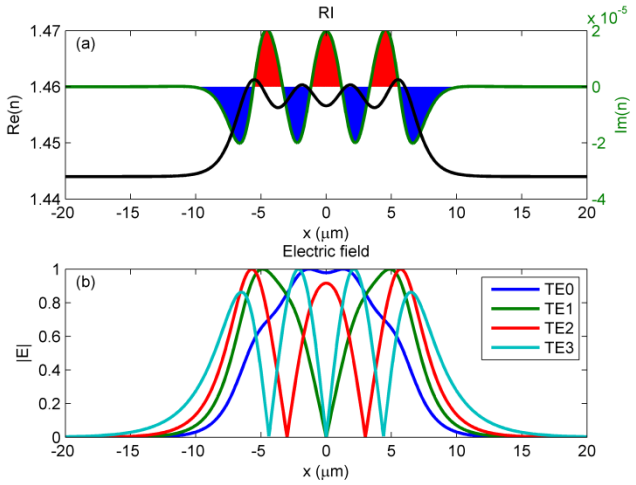

Figure 6-6: (a) Real and imaginary part of waveguide RI profile (red shade: loss, blue shade: gain) required to obtain selective gain of γ_4 =3.5 dB/cm for only the TE_3 mode, and (b) the associated modal fields

As before, in all cases the desired mode overlaps strongly with the gain region (blue shade), while the loss (red shade) is placed around the areas of zero field, and as a result the pre-defined mode experiences gain. The rest of the gain-less modes again overlap optimally with the gain and loss areas, which results in a final net-zero overall gain/loss.

6.3.2 Four-moded waveguide with equal modal gains

If the same imaginary part is added to the effective index of all guided modes, we obtain a waveguide for which all the guided modes experience identical gains. This is shown in Figure 6-7 (a) where *all* modes experience identical $\gamma_m \approx 3.5$ dB/cm gain (m=1,2,3,4). In this case the gain region (blue) is modulated periodically mirroring the real part of the RI variation. The loss region now extends only at the waveguide edges and cladding area and affects predominantly the evanescent fields of all the modes. Here, all modes overlap optimally with the gain and loss regions and result in equal propagation gains.

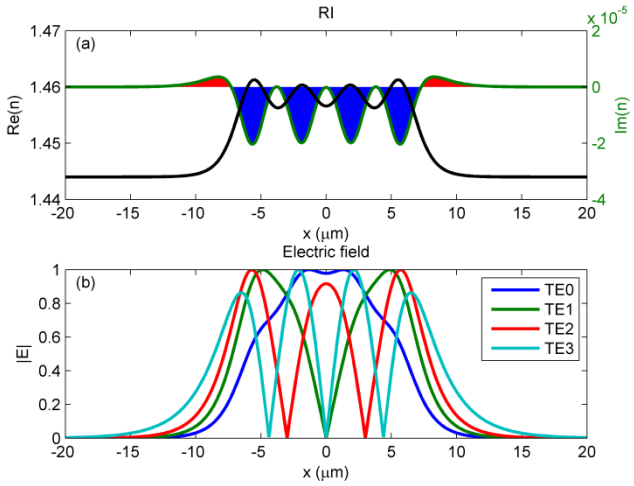

Figure 6-7: (a) Real and imaginary part of waveguide RI profile (red shade: loss, blue shade: gain) required to obtain selective gain of $\gamma_1 = \gamma_2 = \gamma_3 = \gamma_4 = 3.5$ dB/cm for *all* the guided modes, and (b) the associated modal fields.

6.3.3 Four-moded waveguide with biased modal gains

From the point of view of the mitigation of mode-dependent losses (e.g. bend-induced losses), it is useful to also consider the case where there is an increase in modal gain with mode number. If an increasingly larger imaginary component is added to the effective index of the guided modes, it becomes possible to potentially increase the modal gain and compensate for MDL. An example of such a design is shown in Figure 6-8 (a), where selective modal gains of $\gamma_1 = 2.5$ dB/cm for TE_0, $\gamma_2 = 3.5$ dB/cm for TE_1, $\gamma_3 = 4.5$ dB/cm for TE_2 and $\gamma_4 = 5.5$ dB/cm for TE_3 have been assumed. In contrast with the case of gain-equalized modes (see Figure 6-6(a)), it is observed that the gain regions (blue shade) increase away from the waveguide center. In addition, loss regions (red shade) are re-introduced between the gain regions.

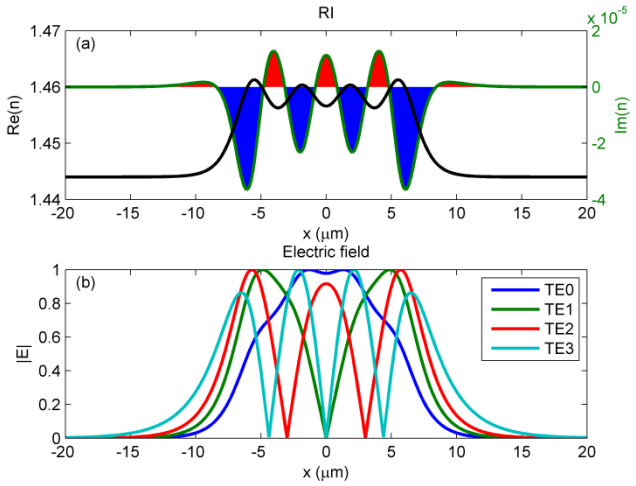

Figure 6-8: (a) Real and imaginary part of waveguide RI profile (red shade: loss, blue shade: gain) required to obtain selective gain of γ_1 =2.5 dB/cm for TE_0, γ_2 =3.5 dB/cm for TE_1, γ_3 =4.5 dB/cm for TE_2 and γ_4 =5.5 dB/cm for TE_3, and (b) the associated modal fields.

6.3.4 Three- & two-moded waveguide with equal modal gains

For completeness, in Figure 6-9 and Figure 6-10 (a) we present the cases of three- and two-moded waveguides, respectively, with equal modal gains of γ_m =3.5 dB/cm. Figures 6-9(b) and 6-10(b) show the corresponding modal field distributions.

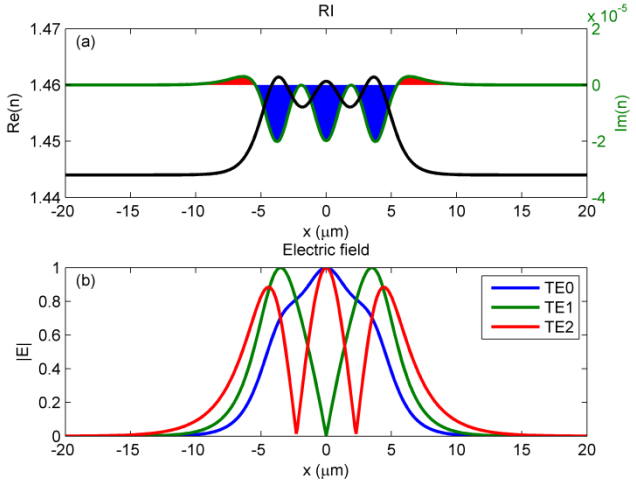

Figure 6-9: (a) Real and imaginary part of waveguide RI profile (red shade: loss, blue shade: gain) required to obtain selective gain of $\gamma_1 = \gamma_2 = \gamma_3$ =3.5 dB/cm for TE_0 TE_1 and TE_2 modes, and (b) the associated modal fields.

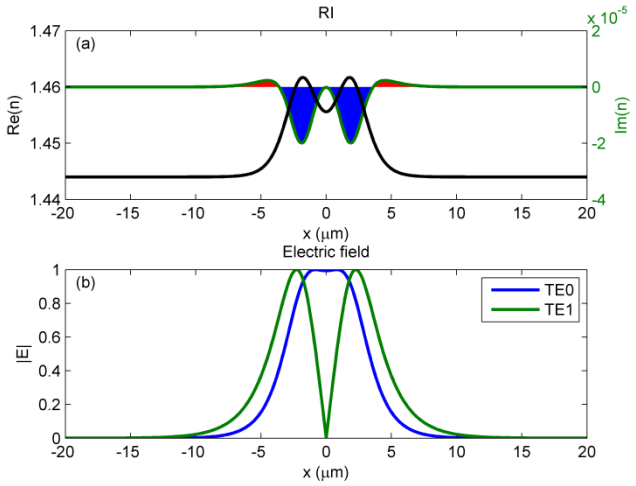

Figure 6-10: (a) Real and imaginary part of waveguide RI profile (red shade: loss, blue shade: gain) required to obtain selective gain of $\gamma_1 = \gamma_2 = 3.5$ dB/cm for TE_0 and TE_1 modes, and (b the associated modal fields

From Figure 6-7 (a), Figure 6-9 (a) and Figure 6-10 (a) it is observed that MM waveguides with equalized modal gain share similar gain/loss distribution features. The gain region is periodically modulated and aligned with the field maxima of the highest-order mode, while the lossy areas lie on the edges of the waveguide and extend mostly in the cladding.

In all the examples presented in section 6.4, we used the commercial mode-solver software Lumerical MODE Solutions to calculate the direct problem with the complex RI profile shown in Figure 6-3 (a) - Figure 6-10 (a). In all cases, the reconstructed complex-mode effective indices are in excellent agreement with the starting ones. We notice that the associated electric field distributions plotted in Figure 6-3 (b) - Figure 6-10 (b) dependent on the choice of the real part of the effective RIs only and do not change with the variation of the imaginary parts. They are also in excellent agreement with the distributions of the corresponding passive waveguides (with just the real part of the RI).

6.3.5 Four-moded waveguide without equalizing lossy areas

The DT IS scattering technique, adopted in this work, demonstrates that *exact* equalization of modal gain in MM waveguides requires the existence of both gain and loss in the RI distribution. To illustrate this more clearly, we show in Table I the DMG with respect to the TE_0 mode when the outer lossy layer (shaded red) is removed from the designs in Figure 6-7(a), Figure 6-9 (a) and Figure 6-10 (a).

Table 6-1: 2, 3 and 4-mode designs without the lossy (red shade) layer

Design	Mode	Effective Index (n_{eff})	DMG (w.r.t TE_0)
2-mode	TE_0	$1.456396 - i\ 1.006815\text{x}10^{-5}$	-
	TE_1	$1.450625 - i\ 1.031072\text{x}10^{-5}$	0.085 dB/cm
3-mode	TE_0	$1.457358 - i\ 1.003593\text{x}10^{-5}$	-
	TE_1	$1.454175 - i\ 1.015464\text{x}10^{-5}$	0.045 dB/cm
	TE_2	$1.449136 - i\ 1.040546\text{x}10^{-5}$	0.13 dB/cm
4-mode	TE_0	$1.457773 - i\ 1.002184\text{x}10^{-5}$	-
	TE_1	$1.455789 - i\ 1.009137\text{x}10^{-5}$	0.024 dB/cm
	TE_2	$1.452552 - i\ 1.022446\text{x}10^{-5}$	0.071 dB/cm
	TE_3	$1.448247 - i\ 1.047083\text{x}10^{-5}$	0.16 dB/cm

As expected, the higher-order modes have larger DMGs due to their larger mode field overlaps with the gain-doping (shaded blue) and the lack of compensation through the addition of the loss specified by the IS design technique. We see that without the addition of the lossy layer in the waveguide cladding, exact modal gain equalization is not possible. To the best of our knowledge, the proposal of the addition of judiciously distributed gain (blue shade) *and* loss (red shade) to the waveguide RI for *exact* modal gain equalization is presented for the first time.

6.4 Conclusions

We have proposed a powerful inverse-scattering technique, based upon complex Darboux transformations, for the design of multimode optical waveguides with arbitrarily prescribed modal gains. We have shown examples of optical waveguides for which only one (arbitrarily chosen) mode is amplified, as well as designs for which all modes exhibit equal gain. In addition we have shown designs where there is an increase in modal gain associated with increasing mode number and proposed it as an approach to mitigate for mode-dependent losses in optical waveguides and waveguide circuits. To achieve such unique modal gain combinations both gain *and* loss regions are optimally introduced into the waveguide. Such modal gain characteristics cannot be achieved by gain regions alone, no matter how it is distributed and optimised.

Recent works studying the equalization of modal gain in multimode fibre amplifiers based upon few-mode fibres have considered various forms Erbium doped ring-core designs [6.13]–[6.16]. Initially in the literature a 20 dB gain with differential modal gain (DMG) of less than 3dB was demonstrated between the LP_{01} and LP_{11} modes [6.17] and this was further expanded upon to include LP_{11} and LP_{21} modes [6.13] through such a ring-doping design approach. Superior control over DMG was then realised by incorporating further rings resulting in multiple-doped ring designs [6.14] with a DMG of less than 1 dB. However, in contrast with the designs presented here, these demonstrations rely on modulated gain regions only.

Finally we have demonstrated that the commonly used approach of ring-doping Erbium to equalize modal gain in fibres is a subset of the approach that comes out of inverse scattering theory for the exact equalization of modal gain whereby both gain *and* loss are required. As such this IS design approach can be modified to address differential modal gain in cylindrical waveguides, such as multimode optical fibre amplifiers. However, the current approach and designs are directly applicable to the design of special ribbon cores [6.18], [6.19] and high-aspect ratio rectangular core fibres [6.20].

6.5 References

[6.1] D. J. Richardson, J. M. Fini, and L. E. Nelson, "Space-division multiplexing in optical fibres," *Nat. Photonics*, vol. 7, no. April, pp. 354–362, 2013.

[6.2] L.-W. Luo, N. Ophir, C. P. Chen, L. H. Gabrielli, C. B. Poitras, K. Bergmen, and M. Lipson, "WDM-compatible mode-division multiplexing on a silicon chip.," *Nat. Commun.*, vol. 5, 3069, pp. 1-7, 2014.

[6.3] D. Dai, J. Wang, and S. He, "Silicon multimode photonic integrated devices for on-chip mode-division-multiplexed optical interconnects," *Prog. Electromagn. Res.*, vol. 143, no. November, pp. 773–819, 2013.

[6.4] Y.-D. Yang, Y. Li, Y.-Z. Huang, and A. W. Poon, "Silicon nitride three-mode division multiplexing and wavelength-division multiplexing using asymmetrical directional couplers and microring resonators," *Opt. Express*, vol. 22, no. 18, p. 22172, 2014.

[6.5] J. Wang, S. Chen, and D. Dai, "Silicon hybrid demultiplexer with 64 channels for wavelength / mode-division multiplexed on-chip optical interconnects," *Opt. Lett.*, vol. 39, no. 24, pp. 6993–6996, 2014.

[6.6] D. Dang, B. Patra, R. Mahapatra, and M. Fiers, "Mode-Division-Multiplexed Photonic Router for High Performance Network-on-Chip," *2015 28th Int. Conf. VLSI Des.*, pp. 111–116, 2015.

[6.7] D. Nikolova, R. Hendry, Q. Li, S. Member, D. Calhoun, and K. Bergman, "Silicon Photonics for Exascale Systems," *J. Light. Technol.*, vol. 33, no. 3, pp. 547–562, 2015.

[6.8] A. Lobato, F. Ferreira, J. Rabe, B. Inan, and S. Adhikari, "Mode-Dependent-Loss Mitigation for Mode-Division Multiplexed Systems," in *Transparent Optical Networks (ICTON), 2013 15th International Conference on*, 2013, no. 1, pp. 3–5.

[6.9] K.-P. Ho and J. M. Kahn, "Mode-Dependent Loss and Gain: Statistics and Effect on Mode-Division Multiplexing," *Opt. Express*, vol. 19, no. 17, pp. 16612–16635, 2011.

[6.10] H. Feshbashh, C.E. Porter and V. F. Weisskoff, "Model for Nuclear Reactions with Neutrons," *Phys. Rev.*, vol. 96, no. 2, pp. 448 – 464, 1954.

[6.11] D. Baye, G. Lévai, and J.-M. Sparenberg, "Phase-equivalent complex potentials," *Nucl. Phys. A*, vol. 599, no. 3–4, pp. 435–456, 1996.

[6.12] N. Fernández-García and O. Rosas-Ortiz, "Gamow-Siegert functions and Darboux-deformed short range potentials," *Ann. Phys. (N. Y).*, vol. 323, no. 6, pp. 1397–1414, 2008.

6.13] Q. Kang, E.-L. Lim, F. P. Y. Jung, C. Baskiotis, S. Alam, and D. J. Richardson, "Minimizing differential modal gain in cladding-pumped EDFAs supporting four and six mode groups," *Opt. Express*, vol. 22, no. 18, p. 21499, 2014.

[6.14] C. Jin, B. Ung, Y. Messaddeq, and S. LaRochelle, "Tailored modal gain in a multi-mode erbium-doped fiber amplifier based on engineered ring doping profiles," in *Photonics North*, 2013, vol. 8915, p. 89150A.

[6.15] F. Ferreira, D. Fonseca, and H. Silva, "Design of Few-Mode Fibers With Arbitrary and Flattened Differential Mode Delay," *IEEE Photonics Technol. Lett.*, vol. 25, no. 5, pp. 438–441, Mar. 2013.

[6.16] G. Le Cocq, Y. Quiquempois, A. Le Rouge, G. Bouwmans, H. El Hamzaoui, K. Delplace, M. Bouazaoui, and L. Bigot, "Few mode Er^3+-doped fiber with micro-structured core for mode division multiplexing in the C-band," *Opt. Express*, vol. 21, no. 25, p. 31646, 2013.

[6.17] Y. Yung, S. Alam, Z. Li, a. Dhar, D. Giles, I. Giles, J. Sahu, L. Gruner-Nielsen, F. Poletti, and D. J. Richardson, "First demonstration of multimode amplifier for spatial division multiplexed transmission systems," *2011 37th Eur. Conf. Exhib. Opt. Commun.*, vol. 1, pp. 1–3, 2011.

[6.18] D. R. Drachenberg, M. J. Messerly, P. H. Pax, A. Sridharan, J. Tassano, and J. Dawson, "First selective mode excitation and amplification in a ribbon core optical fiber," *Opt. Express*, vol. 21, no. 9, p. 11257, 2013.

[6.19] D. Drachenberg, M. Messerly, P. Pax, A. Sridharan, J. Tassano, and J. Dawson, "First multi-watt ribbon fiber oscillator in a high order mode," *Opt. Express*, vol. 21, no. 15, pp. 18089–18096, 2013.

[6.20] J. R. Marciante, V. V. Shkunov, and D. a. Rockwell, "Semi-guiding high-aspect-ratio core (SHARC) fiber amplifiers with ultra-large core area for single-mode kW operation in a compact coilable package," *Opt. Express*, vol. 20, no. 18, p. 20238, 2012.

Chapter 7: Inverse scattering designs of mode-selective waveguide couplers

7.1 Introduction

In recent times, spatial-division multiplexing [7.SDM] has been concentrated on the development of efficient multiplexers/de-multiplexers (MUX/DEMUX) for high-performance network-on-chip applications [7.1]–[7.4] and recently approaches to waveguide design based upon supersymmetry (SUSY) such as that by the Christodoulides group [7.5] have been developed whereby multimode trunk waveguides are coupled to single or few-mode partner waveguides, hereafter referred to as trunk-partner pairs, and designed to be perfectly phase-matched. However, this approach is limited in that it can only add/drop one mode at a time and therefore requires a cascade or ladder of partners. We, by contrast, propose the development of mode-selective couplers designed through the Darboux transformation (DT) of inverse scattering theory (IS) as has been described earlier in Chapter 2 of this thesis and by Mills and Tamil [7.6], but with the additional judicious but straightforward addition of material loss/gain to the refractive index (RI) profile as suggested by Chen et al. [7.7] so that arbitrary combinations of modes can be add/dropped simultaneously.

7.2 Phase-matched trunk-partner pairs

As discussed in our previous works [7.8], it is possible using the Darboux transformation to create trunk-partner pairs where any combination of modes can be phase-matched at will. To demonstrate this, a step-index waveguide is created in Figure 7-1 (a) which supports eight TE modes and this is then paired with (b) where the four lowest-order TE_0, TE_1, TE_2 and TE_3 modes of the partner are phase matched to those of the trunk, (c) where the alternate order TE_0, TE_2, TE_4 and TE_6 trunk modes are phase-matched to the TE_0, TE_1, TE_2 and TE_3 modes of the partner and finally (c) where the four highest-order trunk modes TE_4, TE_5, TE_6 and TE_7 are phase-matched to the TE_0, TE_1, TE_2 and TE_3 modes of the partner. In each case the refractive index contrast Δn relative to the cladding of the waveguide is drawn in blue and the associated effective index and mode field profiles are also shown to demonstrate not only the phase-matching but also mode conversion, which has been discussed in the literature [7.9] in the context of the SUSY ladders/cascades. However, to date the associated coupling lengths of each phase-matched mode have not been discussed in detail and it is important to note that even if the trunk-partner pairs are phase-matched, their coupling lengths differ due to the differing mode pair coupling coefficients. This presents a difficulty as in order to ‘drop’ modes simultaneously from a trunk, the coupling lengths must be equalized. Fortunately, earlier work by Chen et al. [7.7] suggests a solution to this problem through the equalization of coupling lengths

using the addition of gain/loss to the refractive index profile. This is now discussed further first by introducing waveguide coupler theory, and then the determination of the required gain/loss.

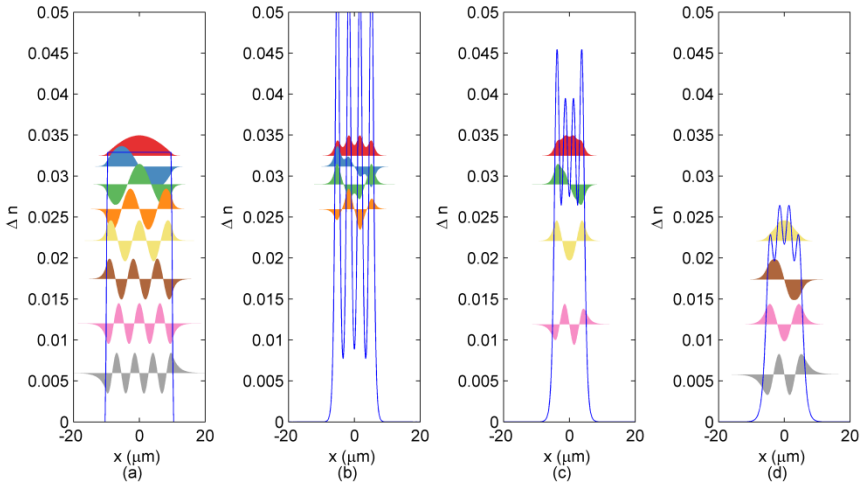

Figure 7-1: RI profile contrast Δn relative to the cladding of (a) multimode step-index trunk waveguide, and partner waveguides for (b) four lowest- order, (c) four alternate-order and (d) four highest-order modes @ λ=1.55μm, $n_{cladding}$ =1.444

7.3 Waveguide coupler theory

Waveguide couplers are well described by coupled-mode theory [7.10], [7.11] and as has been discussed by Chen et al. [7.7] total transfer of power is possible between a trunk waveguide and a parallel partner waveguide if gain and/or loss is considered in the design process. In this section we describe how the appropriate amount of gain or loss can be added to the partner to achieve complete transfer of power from the trunk of *any* selected set of modes at a *single* coupling length.

The transfer of power between the system of coupled waveguides is found as a solution to the system of coupled differential equations [7.11],

$$\begin{aligned} \frac{da_1}{dz} &= i\beta_1 a_1 + iC_{12}a_2 \\ \frac{da_2}{dz} &= i\beta_2 a_2 + iC_{21}a_1 \end{aligned} \tag{7.1}$$

where, as discussed previously, $\beta_m = \beta_{mR} + i\,\beta_{mI}$, is the complex propagation constant, with $\beta_{mI}>0$ corresponding to loss and $\beta_{mI}<0$ corresponds to gain and C_{12} and C_{21} are the coupling coefficients. The solution to this system, assuming that all the power is initially in the trunk ($a_1(0)=1$ and $a_2(0)=0$) may be written,

$$a_1(z) = \left[\cos(\beta_0 z) + i\frac{\beta_1 - \beta_2}{2\beta_0}\sin(\beta_0 z)\right] \times \exp\left[i\frac{\beta_1 + \beta_2}{2}z\right] \tag{7.2}$$

$$a_2(z) = \frac{iC_{21}}{\beta_0}\sin(\beta_0 z)\exp\left[i\frac{\beta_1+\beta_2}{2}z\right] \tag{7.3}$$

with,

$$\beta_0 = \sqrt{\left(\frac{\beta_1-\beta_2}{2}\right)^2 + C_{12}C_{21}} \tag{7.4}$$

It may be seen following some manipulation that (7.2) can be rewritten in the form,

$$a_1(z) = C\cos(\beta_0 z - D)\exp\left[i\frac{\beta_1+\beta_2}{2}z\right] \tag{7.5}$$

with,

$$C = \sqrt{1-\left(\frac{\beta_1-\beta_2}{2\beta_0}\right)^2} \tag{7.6}$$

and,

$$D = \tan^{-1}\left[\frac{i(\beta_1-\beta_2)}{2\beta_0}\right] \tag{7.7}$$

If we introduce a mismatch in the imaginary components of the propagation constants of the m'th pair of coupled modes, following [7.7] while assuming the real components are phase-matched,

$$M_m = \frac{\beta_{2I,m}-\beta_{1I,m}}{2\sqrt{C_{12,m}C_{21,m}}} \tag{7.8}$$

and then assume that any gain or loss is entirely in the partner waveguide, we rewrite in terms of the complex mismatch, giving,

$$\beta_{0,m} = \sqrt{C_{12,m}C_{21,m}\left(1-M_m{}^2\right)} \tag{7.9}$$

$$\beta_{1,m}-\beta_{2,m} = -i\beta_{2I,m} = -2iM_m\sqrt{C_{12,m}C_{21,m}} \tag{7.10}$$

and finally (7.7) becomes,

$$D_m = \sin^{-1}(M_m) \tag{7.11}$$

Now, the n'th coupling length of the m'th pair of modes ($L_{m,n}$) when involving a mismatch M_m may be written,

$$\beta_{0,m}L - D_m \equiv \beta_{0,m}L_{m,n} - \sin^{-1}\left(M_m\right) = \frac{\left(2n+1\right)\pi}{2} \tag{7.12}$$

As such, all power associated with the m'th given mode will have left the trunk at the n'th coupling length and $L_{m,n}$ may be obtained as,

$$L_{m,n} = \frac{\frac{\left(2n+1\right)\pi}{2} + \sin^{-1}\left(M_m\right)}{\beta_{0,m}} \equiv \frac{\frac{\left(2n+1\right)\pi}{2} + \sin^{-1}\left(M_m\right)}{\sqrt{C_{12,m}C_{21,m}\left(1-M_m{}^2\right)}} \tag{7.13}$$

It should be stressed at this point that as (7.13) implies, introduction of differential loss/gain in a coupled waveguide system (i.e finite $M_{m,n}$) can be used to alter the coupling length between different mode pairs. This unique property of couplers with differential modal gain/loss will be used to fine tune and equalise the coupling lengths of different mode groups in modal add/drop multiplexers/demultiplexers.

Now, if in general we wish that the n'th order coupling length of the m'th phase-mismatched mode pair has identical coupling length to that of the q'th order coupling length of the p'th phase-matched mode pair involving no gain/loss, we may then obtain the generalised mismatch $M_{m,n}$ by solving,

$$\frac{\frac{\left(2n+1\right)\pi}{2} + \sin^{-1}\left(M_{m,n}\right)}{\sqrt{C_{12,m}C_{21,m}\left(1-M_{m,n}{}^2\right)}} = \frac{\left(2q+1\right)\pi}{2\sqrt{C_{12,p}C_{21,p}}} \tag{7.14}$$

The choice of integers (n, q) for modes (m,p) is motivated by the requirement that the imaginary correction to the partner waveguide mode effective index should be as small as possible. In the next section we have investigated the mode losses at the chosen coupling lengths in the (n,q) space. It is interesting to note that this use of loss in a partner fibre/waveguide coupled to a lossless one, is also discussed in the context of quantum mechanical PT-symmetry breaking where the overall transmission behaviour of the coupled system counter-intuitively increases with increasing partner waveguide loss past a transition point. This is discussed further in [7.12] and is very much at the forefront of research.

7.4 Designs with identical coupling lengths

In the above we have derived a method by which modes can be 'dropped' from a trunk waveguide at identical coupling lengths. This motivates a method by which arbitrary selected modes can be removed from the trunk waveguide simultaneously. From the start we note from (7.10) that the correction is proportional to the coupling coefficient of the trunk-partner mode pair to be corrected and so it makes sense that the lower order partner mode should always be corrected since the

associated coupling coefficient will be smaller. It is also necessary to take into account the overall loss of the coupled mode in the partner at the (to be determined) associated coupling length as we may wish to then manipulate this mode further. The expression for the total loss at the n'th coupling length of the m'th corrected mode pair in terms of the calculated mismatch $M_{m,n}$ at the determined q'th order coupling length of the p'th higher-order mode pair is,

$$\alpha_{m,n,p,q} \approx 4.34\Delta_{m,n}k_0L_{p,q} \tag{7.15}$$

where,

$$\Delta_{m,n} = \frac{2M_{m,n}\sqrt{C_{12,m}C_{21,m}}}{k_0} \tag{7.16}$$

$$L_{p,q} = \frac{(2q+1)\pi}{2\sqrt{C_{12,p}C_{21,p}}} \tag{7.17}$$

We calculate the mismatches $M_{m,n}$ and thereby effective index corrections $\Delta_{m,n}$ and substitute these into (7.15) to obtain the optimum choice of (n,q). Now we begin the process as follows: (1) we start with a trunk waveguide that supports a set of guided modes. (2) We choose the particular modes from that set we wish to remove and IS design a partner waveguide that is phase-matched to these modes. (3) We calculate the coupling coefficients $C_{12,m}$ and $C_{21,m}$ for each phase-matched set of modes. (4) We now solve (7.14) and use (7.15) to determine the optimum combination of (n,q). From this we then determine the optimum mode effective index correction $\Delta_{m,n.}$

Following step (1) we calculate the coupling coefficients in terms of the RI profile, angular frequency ($\omega=2\pi c/\lambda$), permeability of free space μ_0, permittivity of free space ε_0 and the normalized electric fields $E_{yi}(x)$ and $E_{yj}(x)$ where W_i indicates that the integral should be performed over waveguide i,

$$C_{ij} = \omega\varepsilon_0 \int_{W_i} \left(n^2 - n^2{}_j\right) E_{yi}{}^*(x)E_{yj}(x)dx \tag{7.18}$$

We note that the normalization of the electric fields here follows that of [7.13] such that, for i=1,2

$$4\times\left[\frac{\beta}{2\omega\mu_0}\int_{W_i}\left|E_{yi}(x)\right|^2 dx\right] = 1 \tag{7.19}$$

7.4.1 Two-mode-drop couplers

As an example, we now calculate the coupling coefficients in Table 7-1 & 7-3 respectively for the cases of the eight-mode SI trunk waveguide and dual-mode IS waveguide partners (Cases #1 & #2) where we have arbitrarily chosen first the phase-matching of the two lowest-order trunk-partner modes TE_0 –TE_0 and TE_1-TE_1 (Case #1) followed next by the TE_2-TE_0 and TE_4-TE_1 trunk-partner

modes (Case #2). The optical power transfer between the trunk and partner waveguides are shown for coupling between the TE_0-TE_0 and TE_1-TE_1 mode pairs in Figures 7-2 & 7-3 respectively. We observe that all the power is removed from the TE_1 mode in the trunk waveguide in Figure 7-3 after odd numbers of TE_1 –TE_1 coupling lengths, and in Figure 7-2 the TE_0-TE_0 power transfer occurs with a differing periodicity.

Table 7-1: Coupling coefficients for Case #1 with two phase-matched modes with trunk-partner spacing 16.25 μm apart

Modes (Trunk-Partner)	C_{12} / C_{21} (m^{-1})
TE_0-TE_0	46.7 / 46.7
TE_1-TE_1	106 / 106

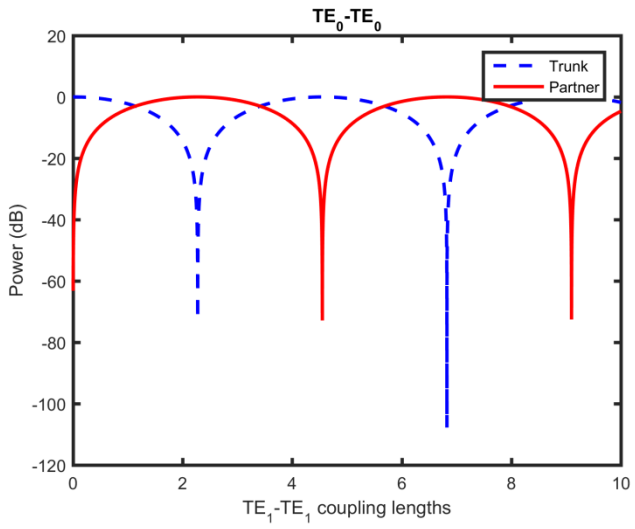

Figure 7-2: Variation in optical power between the case #1 trunk SI and partner IS waveguide (TE_0-TE_0) mode pairs as a function of TE_1 –TE_1 coupling lengths, before correction

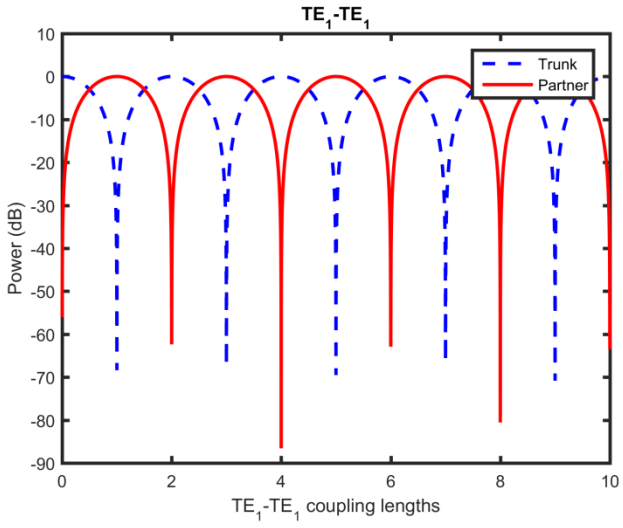

Figure 7-3:Variation in optical power between the case #1 trunk SI and partner IS waveguide (TE_1 –TE_1) modes as a function of TE_1 –TE_1 coupling lengths

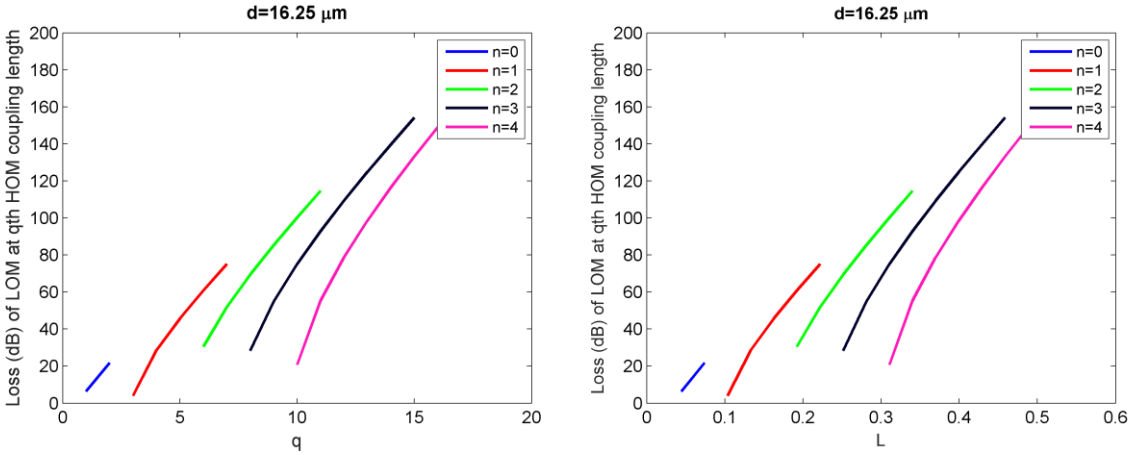

(a) (b)

Figure 7-4: Loss curves for determining the case #1 design - (a) the (n,q) loss curve showing the loss (dB) at the q'th order coupling length of the TE_1-TE_1 pair for various corrected n'th order TE_0 TE_0 coupling lengths, (b) the same but with length of device in metres

In order to use our coupling length equalization method, using the coupling coefficients for Case #1 in Table 7-1 and by solving (7.13) we now determine the optimum (n,q) pair and thus correction to the partner TE_0 mode effective index. In Figure 7-4 we plot the loss (dB) at the q'th order coupling length of the TE_1-TE_1 pair for the n'th order corrected TE_0-TE_0 pair. From this we determine that the correction resulting in a loss of ~6.4 dB power in the transferred TE_0 mode of partner waveguide is when we have (n,q)=(0,1). This corresponds to a value of $M_{1,0}$= 0.3891 or a correction to the effective index of the TE_0 partner mode effective index of $\Delta_{1,0}=i8.96\times10^{-6}$ and a device length of ~44mm.

Table 7-2: Corrected (IS) partner effective indices for Case #1 with equalised coupling lengths

Modes	n_{eff}
TE_0	$1.476464+i8.96x10^{-6}$
TE_1	1.475157

The result of this correction on the effective indices of the partner waveguide is given in Table 7-2 and the resulting coupler design in shown in Figure 7-5.

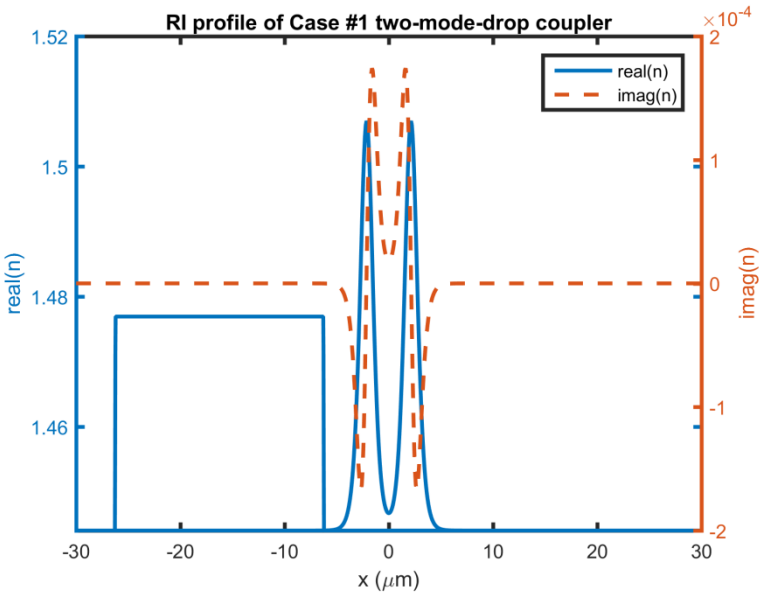

Figure 7-5: RI profile of IS designed trunk-partner coupler with partner mode effective indices as indicated in Table 7-2

With the correction made to the partner waveguide the power transfer in the coupler between the TE_0-TE_0 pair is shown in Figure 7-6 where it can be seen that the coupling length of the 0^{th}-order TE_0-TE_0 coupling length has been successfully equalised to [7.(2x1)+1=3] TE_1-TE_1 coupling lengths or ~44mm with <-80 dB of the TE_0 mode power left in the trunk and ~-6.4 dB of the original power of the trunk TE_0 mode now in the partner TE_0 mode. This contrasts considerably with the pre-corrected case where there was still ~-6.4 dB of the TE_0 power in the trunk at this length.

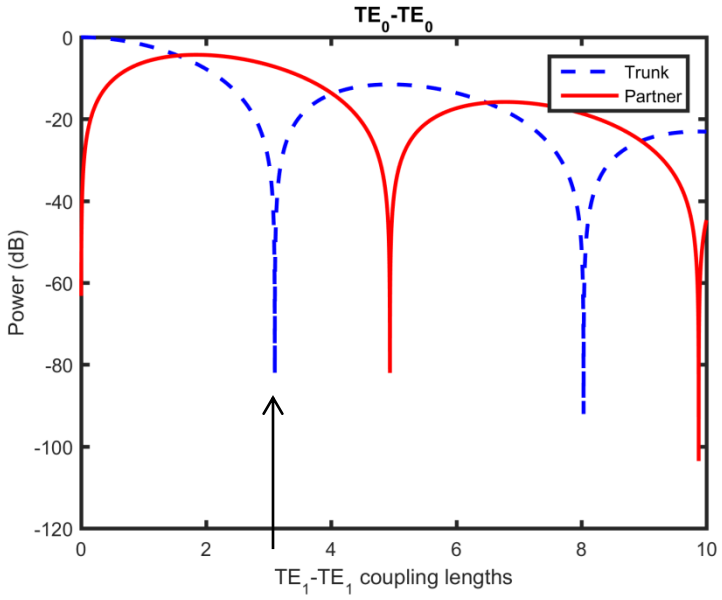

Figure 7-6: Variation in optical power for the case #1 dual-mode coupler between the trunk SI and partner IS waveguide TE_1 modes as a function of TE_2 –TE_2 coupling lengths after correction

We now proceed to Case #2 where we investigate the phase-matching and mode conversion between the trunk and partner TE_2-TE_0 and TE_4-TE_1 pairs. Referring to Table 7-3 for the coupling coefficients it is again possible to calculate the power transfer between the waveguides and this is shown in Figure 7-7 for the TE_2-TE_0 pair in terms of the TE_4-TE_1 coupling length where again the 0^{th}-order coupling length is just under 3 TE_4-TE_1 coupling lengths.

Table 7-3: Coupling coefficients for Case #2 with two phase-matched modes with trunk-partner spacing 15 μm apart

Modes (Trunk-Partner)	C_{12} / C_{21} (m^{-1})
TE_2-TE_0	336.2 / 336.2
TE_4-TE_1	968.1 / 968.1

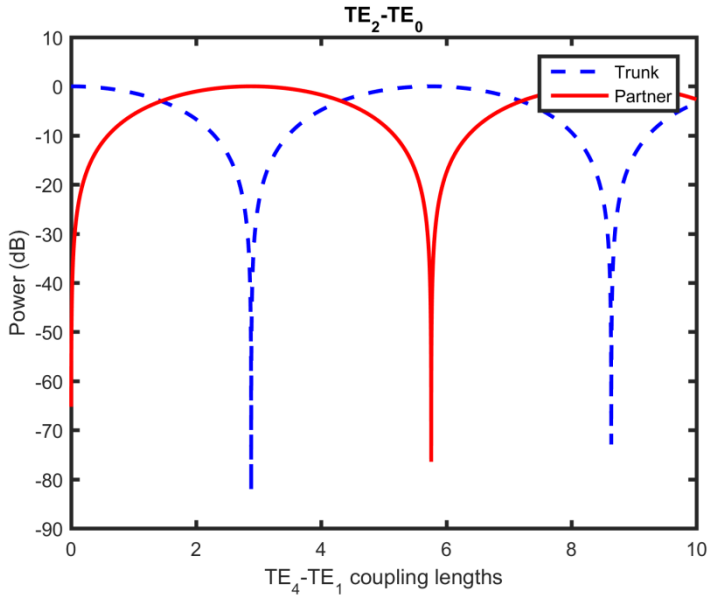

Figure 7-7: Variation in optical power between the case #2 trunk SI and partner IS waveguide (TE_2-TE_0) modes as a function of TE_4 –TE_1 coupling lengths

Again we calculate the optimum (n,q) pair and thus correction to the partner TE_0 mode effective index using Figure 7-8 and find it to be (1,4). This pair is chosen so that the loss of power transferred to the TE_0 partner mode at the coupling length is not too high and the device is not too short. It can be seen that an appropriate loss/device length in the TE_2-TE_0 coupling occurs for the equalisation of the 1st-order TE_2-TE_0 pair coupling length to the 4th-order TE_4-TE_1 pair [7.2x4+1=9] coupling length with ~-6.2 dB TE_0 power in the partner.

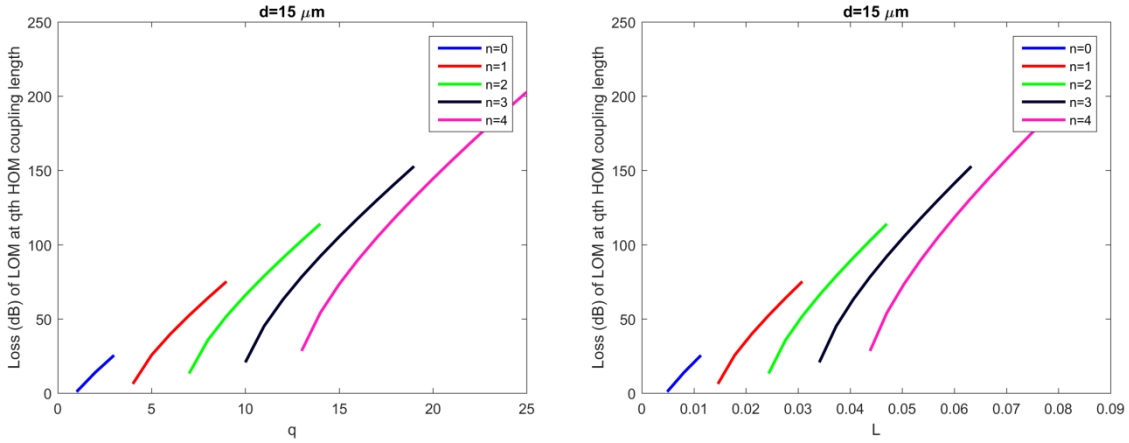

(a) (b)

Figure 7-8: Loss curves for determining the case #2 design - (a) the (n,q) loss curve showing the loss (dB) at the q'th order coupling length of the TE_4-TE_1 pair for various corrected n'th order TE_2 TE_0 coupling lengths, (b) the same but with length of device in metres

This above choice corresponds to a value of $M_{1,1}$ =0.1448 or a correction to the effective index of the TE_0 partner mode effective index of $\Delta_{1,1}$=i2.40×10^{-5} and the effective indices of the partner waveguide are given in Table 7-4 and the refractive index profile of the coupler design is shown in Figure 7-9.

Table 7-4: Corrected (IS) partner effective indices for Case #2 with equalised coupling lengths

Modes	n_{eff}
TE_0	1.472982+i2.40x10^{-5}
TE_1	1.466061

In Figure 7-10 the power transfer between the trunk TE_2 and partner TE_0 modes is shown where it can be seen that the correction has, as required, led to the 1th-order TE_2-TE_0 pair coupling length being moved to the 4th–order TE_4-TE_1 pair [7.2x4+1=9] coupling length with <-90 dB of the TE_2 mode power left in the trunk and therefore the lengths of the pairs and now effectively equalised. This again contrasts considerably with the initial uncorrected TE_2 power left in the trunk at the 4th-order TE_4-TE_1 coupling length of ~-10 dB. We also note, as predicted, that the power in the partner TE_0 mode is now ~-6.2 dB.

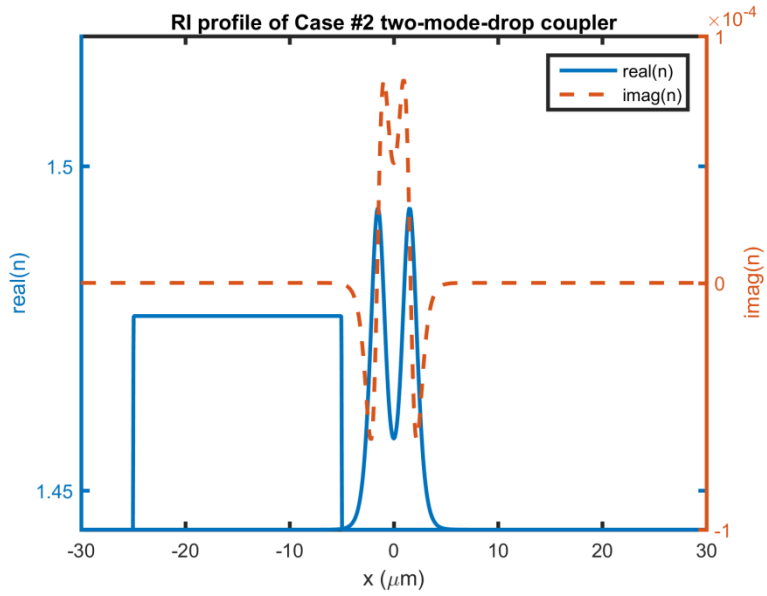

Figure 7-9: RI profile of IS designed case #2 trunk-partner coupler with partner mode effective indices as indicated in Table 7-4

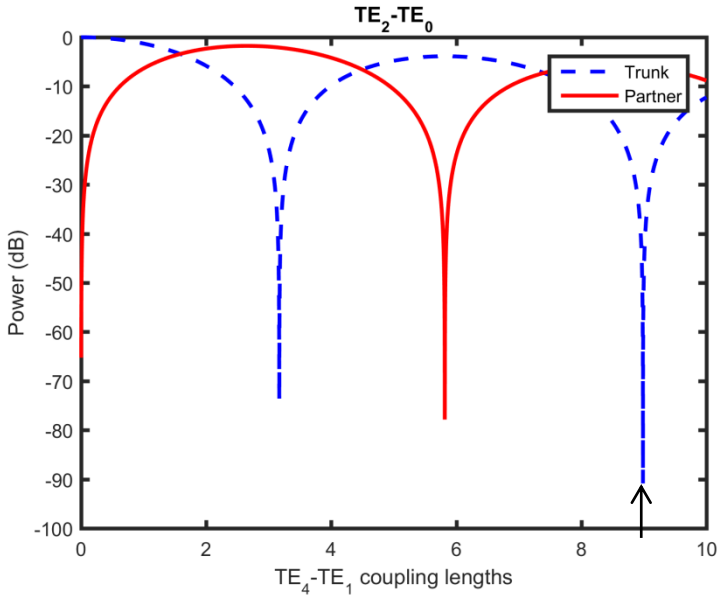

Figure 7-10: Variation in optical power for the three-mode design, between the trunk SI and partner IS waveguide TE_2 and TE_0 modes as a function of TE_2 –TE_2 coupling lengths after correction

7.4.2 Three-mode-drop couplers

We now investigate a step further in the equalized 'drop' of three modes at once from a trunk waveguide (Case #3). In this case the (TE_1, TE_3, TE_5) modes of the trunk are phase-matched to the (TE_0, TE_1, TE_2) partner modes. The coupling coefficients are given in Table 7-5 and are used in the calculation of the power transfer of the TE_1-TE_0 and TE_3-TE_1 pairs in Figures 7-11 & 7-12. In Figure 7-11 it can be seen that the 0^{th}-order coupling length of the TE_1-TE_0 pair occurs at ~9 TE_5-TE_2 coupling lengths while that of the TE_3-TE_1 pair occurs at ~2 TE_5-TE_2 coupling lengths. As before, we may calculate the 'correction curves' for this case where correction will be applied to both the TE_0 and TE_1 partner waveguide modes and these are shown in Figure 7-13.

Table 7-5: Coupling coefficients for Case #3 with three phase-matched modes with trunk-partner spacing 16.25 μm apart

Modes (Trunk-Partner)	C_{12} / C_{21}
TE_1-TE_0	131.6 / 131.6
TE_3-TE_1	540.3 / 540.3
TE_5-TE_2	1194 / 1194

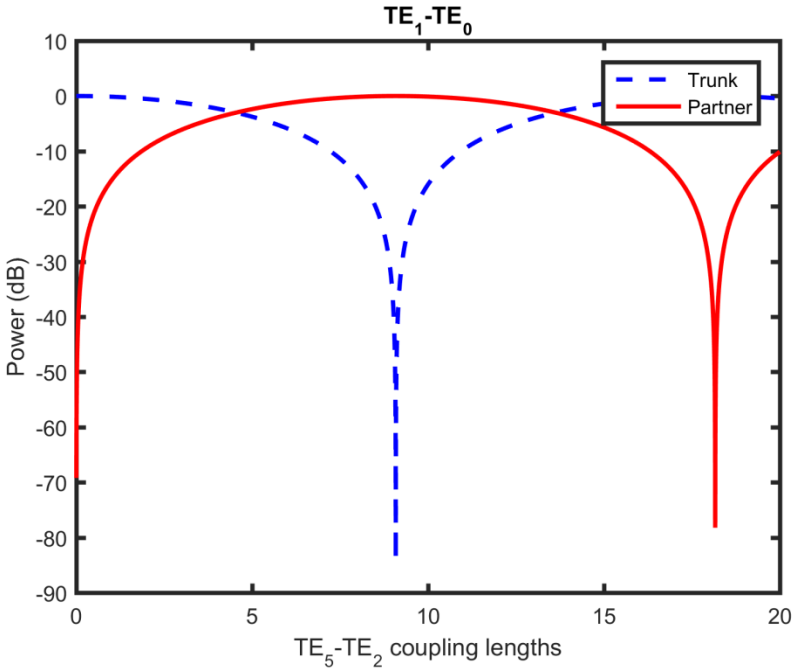

Figure 7-11: Variation in optical power for case #3 between the trunk SI and partner IS waveguide (TE_1-TE_0) modes as a function of TE_5 –TE_2 coupling lengths before correction

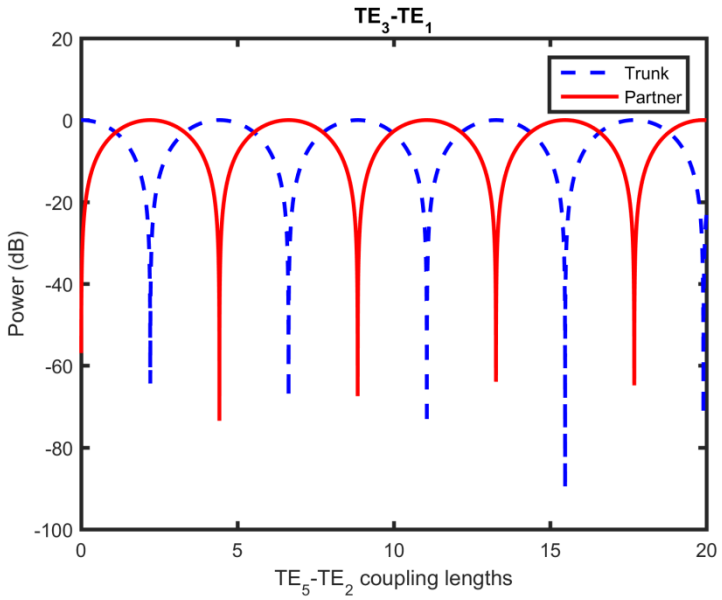

Figure 7-12: Variation in optical power between the case #3 trunk SI and partner IS waveguide (TE_3-TE_1) modes as a function of TE_5 –TE_2 coupling lengths

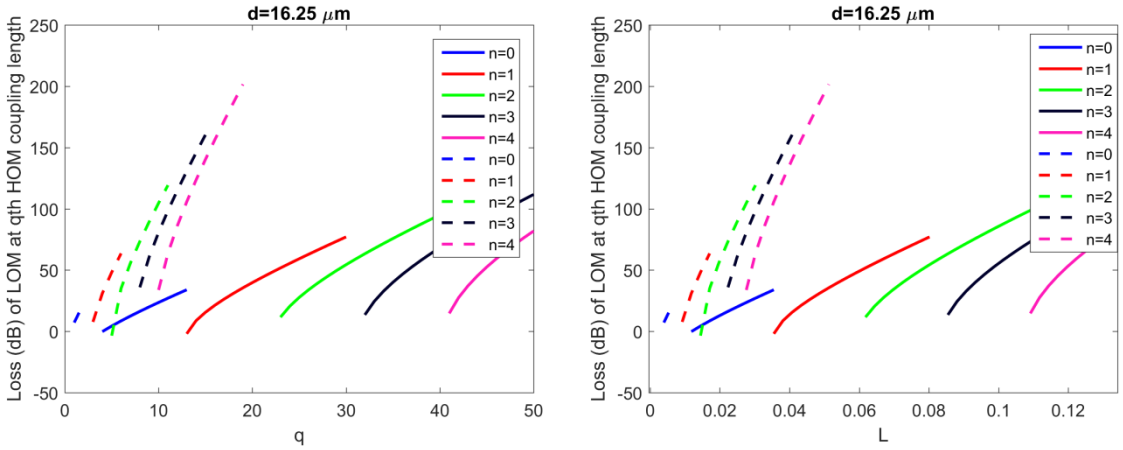

(a) (b)

Figure 7-13: Loss curves for determining the case #3 design - (a) the (n,q) loss curve showing the loss (dB) at the q'th order coupling length of the TE_5-TE_2 pair for various corrected n'th order TE_1 TE_0 pair (solid lines) and n'th order TE_3-TE_1 pair coupling lengths (dashed lines), (b) the same but with length of device in metres

The correction leading to the an optimum combination of mode losses and gains in coupling power between both pairs of modes is identified as being (0, 5) and (3,5) corresponding to the 0th-order TE_1-TE_0 and 3rd-order TE_3-TE_1 coupling lengths being equalized with the [7.2x5+1]=11th-order TE_5-TE_2 coupling length with a loss of ~4.3 dB and a gain of ~3.6dB respectively. This corresponds to a value of $M_{1,0}$ =0.2620 or a correction to the effective index of the TE_0 partner mode effective index of $\Delta_{1,0}=i1.70\times10^{-5}$ and $M_{2,3}$ =-0.0525 or a correction to the effective index of the TE_1 partner mode effective index of $\Delta_{2,3}=-i1.40\times10^{-5}$ and the effective indices of the corrected partner waveguide are given in Table 7-6 and the refractive index profile of the coupler design is shown in Figure 7-14.

Table 7-6:Corrected (IS) partner effective indices for Case #3 with equalised coupling lengths

Modes	n_{eff}
TE_0	1.475157+i1.70x10^{-5}
TE_1	1.469945-i1.40x10^{-5}
TE_2	1.461353

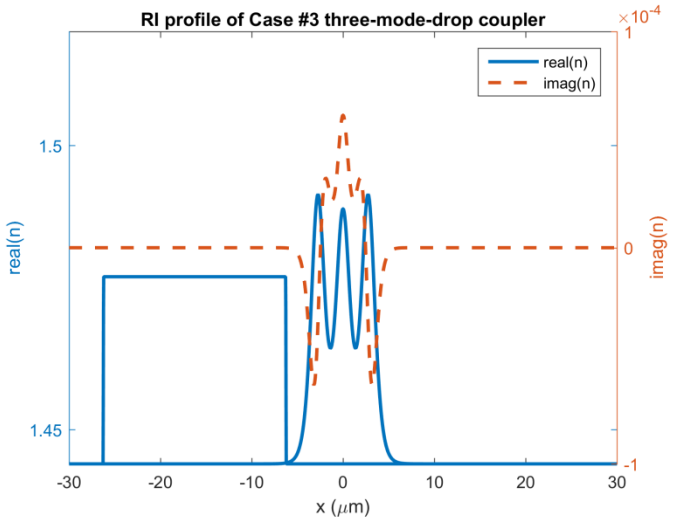

Figure 7-14: RI profile of IS designed trunk-partner coupler with partner mode effective indices as indicated in Table 8-6

In Figure 7-15 the power transfer between the trunk TE_1 and partner TE_0 modes is shown where it can be seen that the correction has led the 0th-order TE_1-TE_0 pair coupling lengths being equalized with the 5th –order TE_5-TE_2 pair coupling length. Here the power remaining in the trunk TE_1 mode is <-90 dB which compares very favourably with that of ~-10 dB before correction. Figure 7-16 also shows that the 2nd- order TE_3-TE_1 pair coupling length has been equalized once again to the 5th-order TE_5-TE_2 coupling length with <-60 dB power remaining in the trunk TE_3 mode at this length. This compares very favourably, again, with that of ~-15 dB before correction. Once again we also note that the power in the TE_0 partner mode is now ~-4.3 dB and that of the TE_1 mode is ~3.6 dB, as expected.

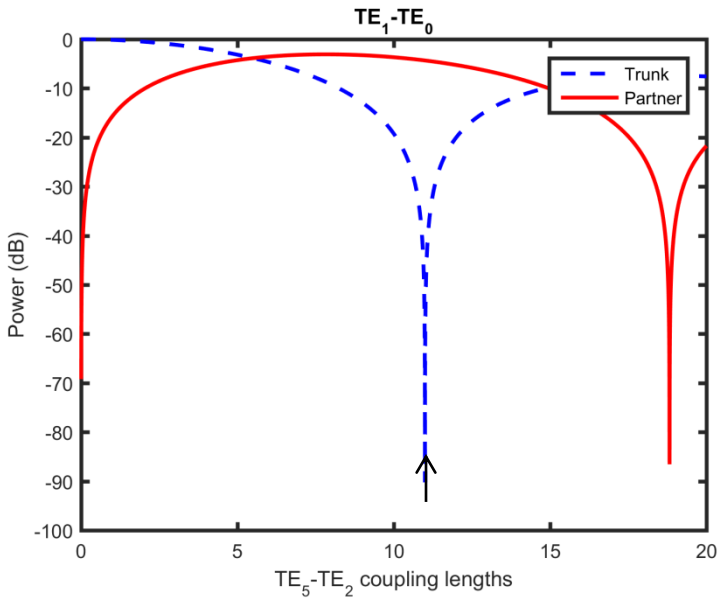

Figure 7-15: Variation in optical power for case #3 between the trunk SI and partner IS waveguide (TE_1-TE_0) modes as a function of TE_5 –TE_2 coupling lengths after correction

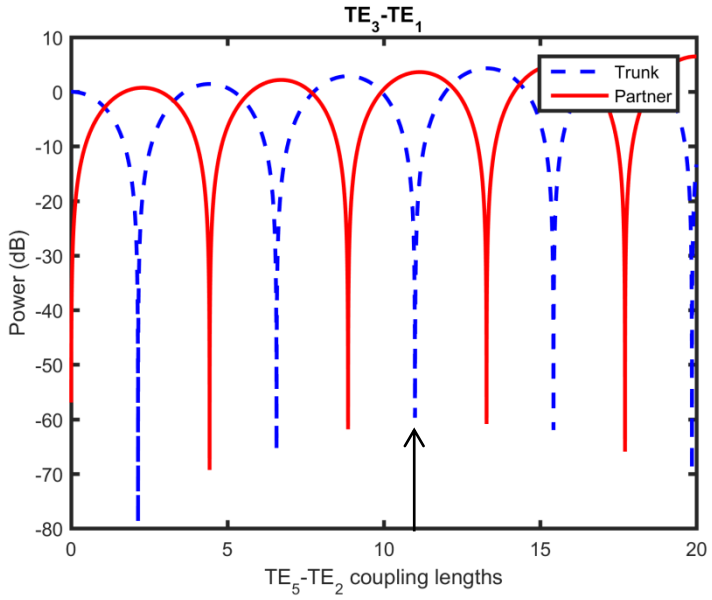

Figure 7-16: Variation in optical power for case #3, between the trunk SI and partner IS waveguide (TE_3- TE_1) modes as a function of TE_5 –TE_2 coupling lengths after correction

7.5 Discussion

In this chapter we have demonstrated that it is possible to remove or 'drop' modes simultaneously from a trunk waveguide using a coupled partner waveguide which has a calculated imaginary phase-mismatch which was first proposed by Chen et al [7.7]. In the dual-mode-drop cases #2 & #3, loss has been used in partner waveguides, the value of which is calculated using coupled-mode theory, and then implemented using inverse-scattering theory. In addition, in case #3 both loss in the partner TE_0 mode and gain in the TE_1 mode are used to equalise all three coupling lengths. We also note that in cases #2 & #3 there is also mode conversion being performed at will. In each design the combination of waveguide spacing and partner mode gain or loss is determined by considering a balance between the power transfer difference between the trunk and the partner due to the coupling as well as the length of the point of coupling length equalization, and this is performed using trial-and-error optimisation of the results of (7.14)-(7.17) and the use of 'correction curves'. It should be noted at this point that the aforementioned method always results in either gain or loss in the coupling process, and is therefore not ideal. However, we have performed this work with the aim of showing that at least in theory the previously undiscussed equalisation of coupling lengths in the context of SUSY transformations can be avoided through the use of the Darboux transformation whereby the required corrections to phase-matched modes can be realised.

We believe that this technique shows great potential in arbitrary mode multiplexing/de-multiplexing and is a more flexible alternative to the SUSY approach where for the first time the equalisation of coupling lengths has also been explicitly considered.

7.6 References

[7.1] D. Dai, J. Wang, and S. He, "Silicon multimode photonic integrated devices for on-chip mode-division-multiplexed optical interconnects," *Prog. Electromagn. Res.*, vol. 143, no. November, pp. 773–819, 2013.

[7.2] L.-W. Luo, N. Ophir, C. P. Chen, L. H. Gabrielli, C. B. Poitras, K. Bergmen, and M. Lipson, "WDM-compatible mode-division multiplexing on a silicon chip.," *Nat. Commun.*, vol. 5, p. 3069, 2014.

[7.3] J. Wang, S. Chen, and D. Dai, "Silicon hybrid demultiplexer with 64 channels for wavelength / mode-division multiplexed on-chip optical interconnects," *Opt. Lett.*, vol. 39, no. 24, pp. 6993–6996, 2014.

[7.4] D. Dang, B. Patra, R. Mahapatra, and M. Fiers, "Mode-Division-Multiplexed Photonic Router for High Performance Network-on-Chip," *2015 28th Int. Conf. VLSI Des.*, pp. 111–116, 2015.

[7.5] M.-A. Miri, M. Heinrich, and D. N. Christodoulides, "Supersymmetric optical waveguides," in *SPIE Photonics West 2014-OPTO: Optoelectronic Devices and Materials*, 2014, vol. 8980, p. 89801F.

[7.6] D. W. Mills and L. S. Tamil, "Synthesis of Guided Wave Optical Interconnects," *IEEE J. Quantum Electron.*, vol. 29, no. 11, pp. 2825–2834, 1993.

[7.7] Y. Chen, A. W. Snyder, and D. N. Payne, "Twin core nonlinear couplers with gain and loss," *IEEE J. Quantum Electron.*, vol. 28, no. 1, pp. 239–245, 1992.

[7.8] A. R. May and M. N. Zervas, "IS designs for mode selective waveguide couplers," in *23rd Int. Workshop OWTNM*, 2015.

[7.9] M. Heinrich, M.-A. Miri, S. Stützer, R. El-Ganainy, S. Nolte, A. Szameit, and D. N. Christodoulides, "Supersymmetric mode converters.," *Nat. Commun.*, vol. 5, p. 3698, 2014.

[7.10] A. Yariv, "Coupled-mode theory for guided-wave optics," *IEEE J. Quantum Electron.*, vol. 9, no. 9, 1973.

[7.11] H. Haus and L. Molter-Orr, "Coupled multiple waveguide systems," *IEEE J. Quantum Electron.*, vol. 19, no. 5, pp. 840–844, 1983.

[7.12] A. Guo, G. J. Salamo, D. Duchesne, R. Morandotti, M. Volatier-Ravat, V. Aimez, G. A. Siviloglou, and D. N. Christodoulides, "Observation of PT-symmetry breaking in complex optical potentials," *Phys. Rev. Lett.*, vol. 103, no. 9, pp. 1–4, 2009.

[7.13] K. Okamoto, *Fundamentals of Optical Waveguides*. London, UK, 2006.

Chapter 8: Few-mode fibres with intuitively improved mode spacings

The work in this brief chapter is based upon that presented as "Few-Mode Fibers with Improved Mode Spacing" at ECOC 2015, Valencia, Spain, and was the first time we had considered the design of optical fibres using the intuition gained from the inverse scattering design of waveguides. In particular, previous chapters showed that selective control over modes came about through the regions of overlap between the modal fields and the refractive index profile. It is from this basis that we used intuition to improve LP mode spacing through step-index design perturbations for both four and six mode groups.

8.1 Introduction

Multimode-division multiplexing (MDM) [8.1] relies on specially designed multimode fibres (MMFs) and uses propagating optical modes as separate communication "channels". High capacity MDM has been implemented by using MMFs supporting highly-coupled, low differential mode delay (DMD) and extensive, energy-hungry digital signal processing (DSP) such as by Bigot-Astruc et al. [8.2] Alternatively, high performance MDM systems have also been demonstrated using MMFs with virtually uncoupled, high differential mode delay (DMD) modes, with minimum DSP requirements such as by Boivin et al. [8.3] and Sillard et al. [8.4].

The major consideration in designing un-coupled MDM (UC-DMD) systems is the degree of modal cross-coupling. It is known that cross-coupling is inversely-proportional to the effective index difference as discussed by Olshansky [8.5] and it is, therefore, more severe between adjacent modes. So far, UC-DMD is based primarily on optimised step-index fibres. Step-index designs offer simplicity in terms of their design and fabrication and previous authors such as Bigot-Astruc et al. [8.2], Boivin et al. [8.3] and Sillard et al. [8.6] have investigated their use in up to six-LP-mode fibres. Also, it is important for improved designs to have large mode effective areas and differential group delays (DGD) (>0.5ps/m) to limit inter-mode non-linearity as well as meeting the optimum trade-off between micro- and macro-bend losses.

It has been shown that step-index fibres, despite the parameter optimisation, still support modes with non-equally spaced effective indices. Due to cylindrical symmetry, this is particularly severe between LP_{21} and LP_{02} modes. As a result, strong mode cross-coupling has been measured in relatively short MMF lengths using the S2 method such as by Jespersen & Li [8.7].

In this chapter we investigate an alternative MMF refractive index (RI) design showing substantially equalized mode effective indices, compared with state-of-the-art step-index fibres. Since large DGDs

follow naturally from step-index designs and those without a graded-index core, the particular design focus is on mode index equalisation improvements which are achieved by introducing optimum 1) rotationally-symmetric RI perturbations inside the core, affecting primarily one sub-group of modes, and 2) rotationally-non-symmetric RI perturbations in the cladding, affecting primarily the rest of the supported modes. The design optimisation strategy is based on simple, physically-intuitive arguments.

8.2 Design strategy for fibres with optimally distributed mode spacing

Given that what we try to achieve is the effective index manipulation, where targeted RI perturbations (Δn) could be introduced in a known starting profile $\bar{n}$ (e.g. standard step-index) in order to selectively affect the propagation constant of individual modes (β), an excellent, intuitive guiding principle is the following well known perturbation formula derived by Snyder & Love [8.8],

$$\beta \approx \bar{\beta} + k \frac{\int_A \Delta n \left|\bar{e}\right|^2 dA}{\int_A \left|\bar{e}\right|^2 dA} \tag{8.1}$$

where k is the free-space wavenumber, $\bar{\beta}$ the mode propagation constant and $\bar{e}$ the electric field of the known profile $\bar{n}$. As already mentioned, the main issue with the mode effective index distribution in step-index fibres stems from the small separation between LP_{21} and LP_{02} modes.

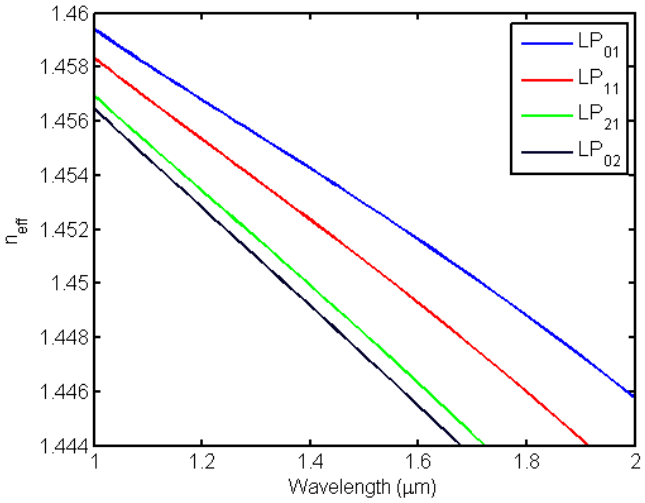

Figure 8-1: Effective index distribution for the Sillard [8.4] four mode-group step index design

In Figure 8-1 this main limitation of the Sillard [8.4] four mode-group design at 1.55 μm is shown more clearly where it can be seen that the LP_{21}-LP_{02} mode spacing (black vs green curves) is significantly limited ($<1x10^{-3}$) which could lead to a larger degree of modal cross-coupling than between the other mode-groups. We address this issue by first considering refractive index perturbations as illustrated in Figure 8-2 where firstly an inner core depression was added which has

the effect of increasing the LP_{21} - LP_{02} index difference, mainly achieved by lowering the LP_{02} index closer to the cladding refractive index since the inner core depression overlaps mostly with the cylindrically-symmetric LP_{01} and LP_{02} modes and as expected from Equation (8.1) their effective index is reduced. LP_{11} and LP_{21} on the other hand have intensity minima in the core centre and therefore the index depression leaves them almost unaffected. The optimum value of the core depression was achieved by considering the minimisation of the objective function,

$$f(b,n_3) = \left|LP_{11}(b,n_3) - 3\Delta\right| + \left|LP_{21}(b,n_3) - 2\Delta\right| + \left|LP_{02}(b,n_3) - \Delta\right|; \\ \Delta(b,n_3) = [LP_{01}(b,n_3) - n_2]/4 \tag{8.2}$$

In the objective function, the effective index of each LP mode is referred to as well as the optimum spacing, Δ, between modes defined in terms of the difference between the effective index of the LP_{01} mode and the cladding n_2. However, the lowering of the LP_{02} mode effective index increases the macro- and micro-bending sensitivity of the design. Fibres with depressed inner core have been discussed in the context of MM fibres with maximum four-wave mixing by Stolen [8.9].

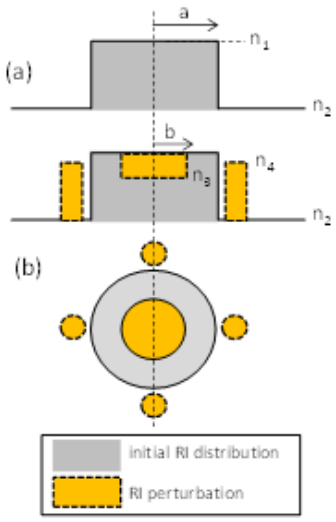

Figure 8-2: Refractive index distribution schematics of (a) standard SI fibre and (b) an optimally perturbed proposed design

In order to improve the LP_{02} micro- and macro-bending performance and maintain the improved LP_{21} – LP_{02} effective index separation we consider the addition of localized RI perturbations in the cladding overlapping optimally with the four intensity lobes of the LP_{21} mode. We have added 1 μm radius high-index rods at the edge of the outer core. Such cylindrically non-symmetric perturbation increases the effective indices of LP_{21} and LP_{02} by amounts given by (8.1). As expected, modes LP_{01} and LP_{11} are affected by small amounts due to negligible overlaps with the additional perturbations. Representative LP-mode field distributions of the fully optimised (ring+rods) profiles are shown in Figure 8-3. It is shown that the cylindrically non-symmetric modes LP_{11} and LP_{21} are aligned with the added cladding rods. At this point, we should mention that the addition of RI perturbing rods in the fibre cladding breaks the rotational degeneracy of the LP_{11} and LP_{21} modes. The mode profiles

with maxima falling between the RI modifying rods have effective indices close to the unperturbed case. In addition to shifting the mode effective index, the RI modifying rods "lock" the optimum separation modes spatially inside the fibre.

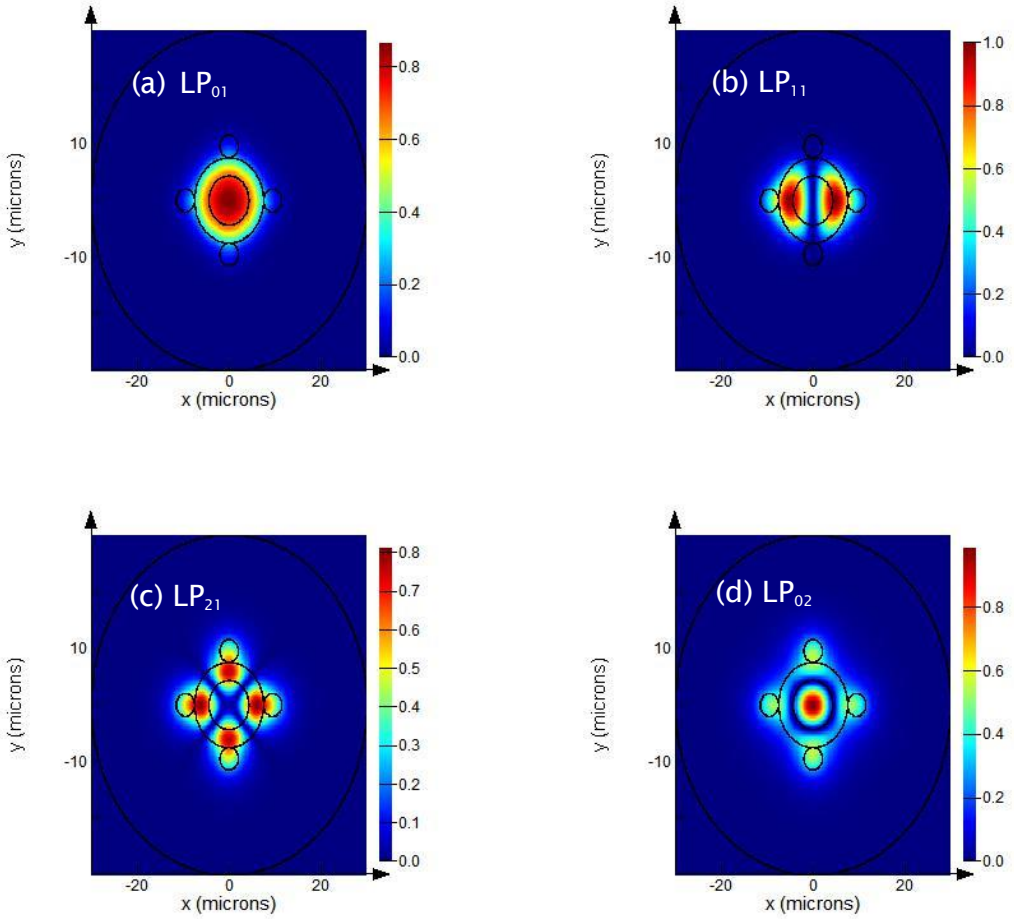

Figure 8-3: Orientation of equalized effective-index modes with respect to index modifying rods (a) LP_{01} , (b) LP_{11}, (c) LP_{21} and (d) LP_{02}

This 'locking' avoids unwanted modal rotation which complicates enormously the efficient mode demultiplexing and detection at the end of the optical link. The benefits of such spatial mode "locking" in the case of dual-moded fibre have been achieved by using elliptical core fibres. In the case of single-mode fibre, this is equivalent to "fixing" mode polarization by using high-bi fibres. The performance of the new four mode-group fibre designs, with optimally spaced mode effective indices, and the comparison with state-of-the-art SI fibres are summarized in and Table 8-1.

We also show the result of the perturbation calculation using (8.1) which verifies that the approach is valid. In addition to the discussed mode spacings, we compare the differential group delays (DGD) and mode effective areas. The last two parameters define the nonlinear performance of the fibres. It is shown that in addition to improved mode effective-index distribution the new designs provide substantially larger mode effective areas. The DGDs are in excess of 4ns/km for all the supported

modes. It is therefore expected to have superior non-linear performance in comparison with standard SI fibres.

Table 8-1: Performance comparison of new designs with state-of-the-art four mode-group step index fibres (@ λ=1550nm)

Mode	**LP_{01}**	**LP_{11}**	**LP_{21}**	**LP_{02}**
n_{eff}-n_{cl} (ring - step 1)	$7.7x10^{-3}$	$5.7x10^{-3}$	$3.0x10^{-3}$	$1.9x10^{-3}$
n_{eff}-n_{cl} (rods – step1+step 2)	$7.7x10^{-3}$	$6.0x10^{-3}$	$3.9x10^{-3}$	$2.7x10^{-3}$
n_{eff}-n_{cl} (rods – step1+step 2) using (8.1)	$7.8x10^{-3}$	$5.9x10^{-3}$	$4.3x10^{-3}$	$2.8x10^{-3}$
n_{eff}-n_{cl} – ref Sillard et al. [8.4]	$8.3x10^{-3}$	$6.0x10^{-3}$	$3.2x10^{-3}$	$2.4x10^{-3}$
DGD w.r.t LP_{01} (ns/km) – (step1+step2)	-	4.4	6.2	3.9
DGD w.r.t LP_{01} (ns/km) [8.4]	-	4.4	8.5	7.2
Aeff (μm^2) – (step1+step2)	151	203	172	171
Aeff (μm^2) – ref [8.4]	124	118	133	127

Table 8-2: Mode spacing comparison of new designs with state-of-the-art four mode-group step-index fibres (@ λ=1550nm)

Mode Spacing	**LP_{01}-LP_{11}**	**LP_{11}-LP_{21}**	**LP_{21}-LP_{02}**
Ring (step1)	$2.0x10^{-3}$	$2.7x10^{-3}$	$1.1x10^{-3}$
Rods (step1+step 2)	$1.7x10^{-3}$	$2.1x10^{-3}$	$1.2x10^{-3}$
Ref [8.4]	$2.3x10^{-3}$	$2.8x10^{-3}$	$0.8x10^{-3}$

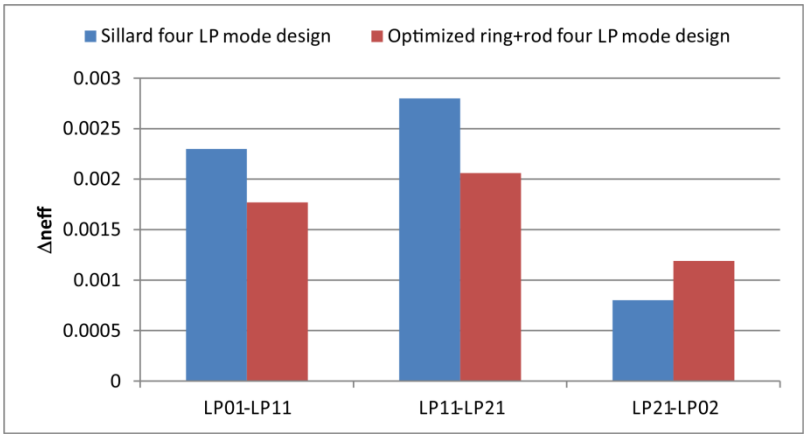

Figure 8-4: Comparison between mode spacing of Sillard four LP mode step-index design and optimised ring+rod design @ 1550nm

For ease of interpretation, we also show the data of Table 8-2 in Figure 8-4. We see that the addition of the ring and rods has achieved closer equalisation of mode spacings for the four mode-group case and quite significantly increased the LP_{21}-LP_{02} spacing when compared with the original Sillard et al. [8.4] design ($0.8x10^{3}$ vs $1.2x10^{-3}$) while the other spacings are either comparable or large enough to lead to significant reductions in cross-mode coupling anyway. It is our belief that this addition of core perturbations is novel.

Further to this we investigated for completeness a six LP mode-group design proposed by Sillard et al. [8.6] which has the limitations as in the effective index curves of Figure 8-5.

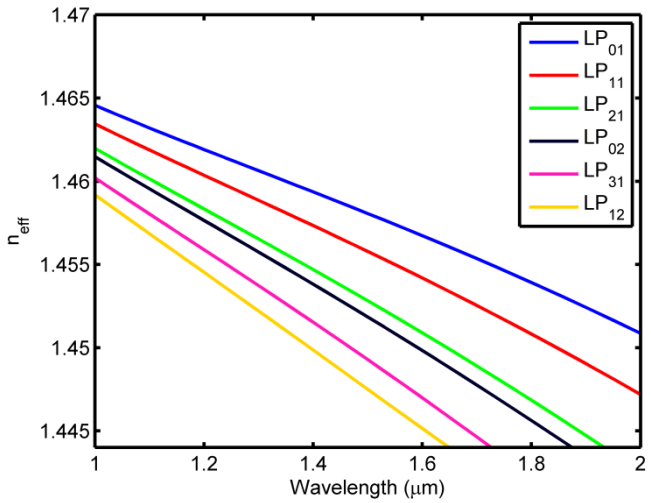

Figure 8-5: Effective index distribution for the Sillard [8.6] four mode-group step index design

We see that both the LP_{21}-LP_{02} and LP_{31}-LP_{12} mode spacings are limited but intuition suggests that six optimised high-index rods could be used to selectively 'lift' the LP_{31} and LP_{21} modes due to the their preferential overlap with the fields as suggested again by (8.1) and illustrated in Figure 8-6.

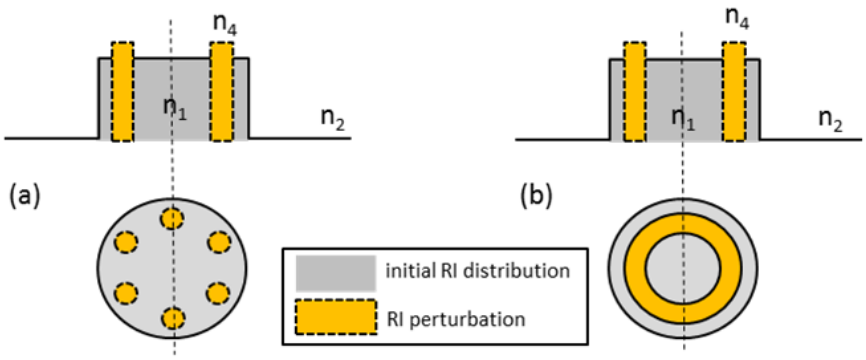

Figure 8-6: Refractive index distribution schematics of a step index fibre with (a) six high-index rod perturbations and (b) a high-high-index ring perturbation

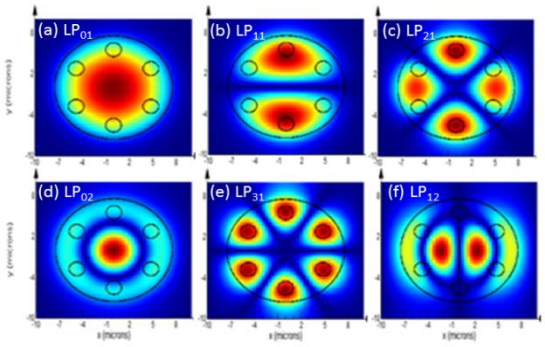

Figure 8-7: Orientation of modes with respect to index modifying rods (a) LP_{01} , (b) LP_{11}, (c) LP_{21}, (d) LP_{02}, (e) LP_{31} and (f) LP_{12}

We perform this perturbation and show graphically in Figure 8-7 the overlaps between the fields and rod perturbations. It can be seen clearly that the fields of the LP_{21} and LP_{31} modes have preferential overlap with the six high-index rods and the high periodicity is such that it suggests that a simple ring might also achieve a very similar effect and the field profile and their overlap with an optimised ring are shown in Figure 8-8 and demonstrate this same behaviour.

The effective index spacings are given in graphical form in Figure 8-9 where it can be seen that the addition of the six high-index rods lifts all modes to some extent but most preferentially the LP_{21} and LP_{31}modes leading to an increase in LP_{21}-LP_{02} and LP_{31}-LP_{12} spacing. It is interesting to note that the data for the high-index ring perturbation provides even better equalisation of mode spacings across the board ($>2x10^{-3}$), with even more significant increases in LP_{21}-LP_{02} spacing than the rod design ($2x10^{-3}$ vs $1.3x10^{-3}$)

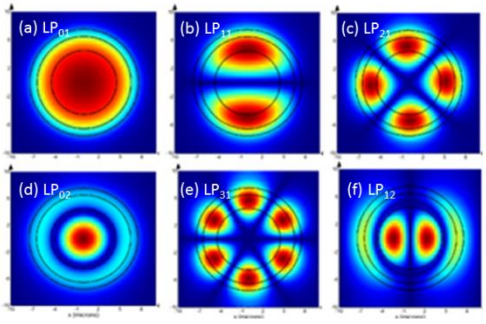

Figure 8-8: Orientation of modes with respect to index modifying ring (a) LP_{01} , (b) LP_{11}, (c) LP_{21}, (d) LP_{02}, (e) LP_{31} and (f) LP_{12}

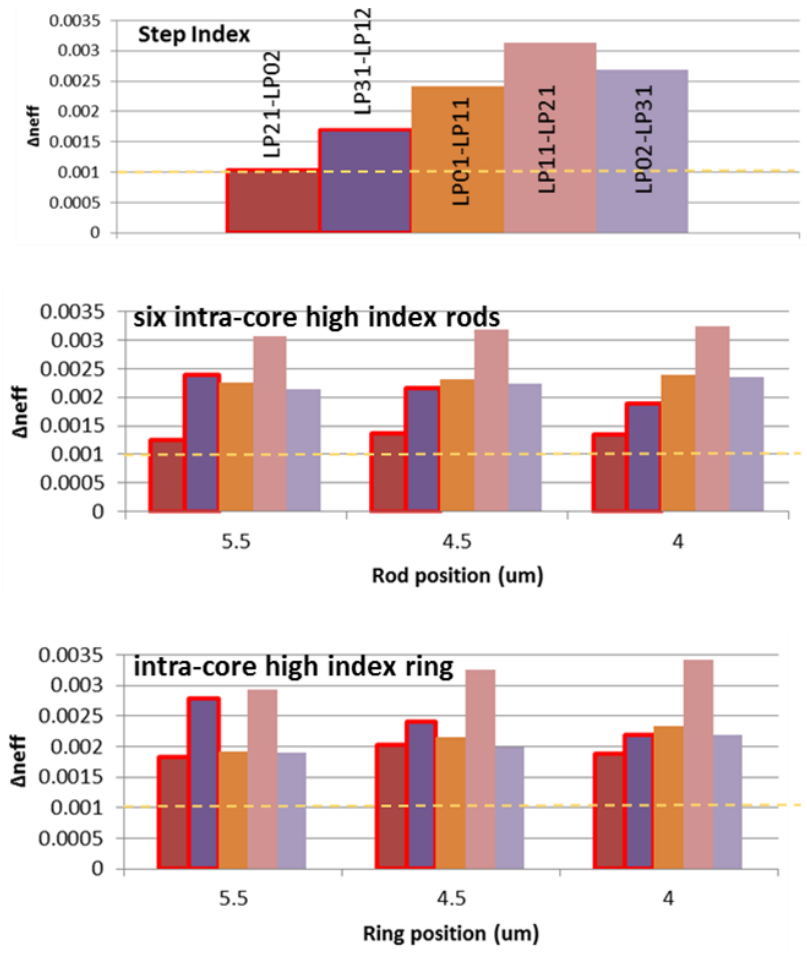

Figure 8-9: Mode spacings for the original Sillard [8.6] six mode-group step index design and the perturbed rod and ring designs with varying positions

8.3 Conclusions

We have proposed new MMF designs for both four and six mode-groups with improved mode spacing, suitable for UC-MDM optical communications. The first four mode-group design involves two steps and is based on fundamental and intuitive waveguide principles. The new design incorporates first an optimised core depression, which affects primarily LP_{01} and LP_{02} mode effective indices. This optimised perturbation increases the LP_{21}-LP_{02} mode spacing but can potentially compromise the fibre micro- and macro-bending behaviour. This effect has been counter-balanced by incorporating four optimally placed thin high-index rods in close proximity with the fibre core. This increases primarily the effective indices of the LP_{21} and LP_{02} modes without affecting significantly their spacing. The small LP_{21}-LP_{02} mode spacing limitation, encountered in standard SI profiles, has been substantially improved by 40-100%. In addition, the new four mode-group fibre design shows increased effective areas, in excess of 150 μm^2 for all supported modes, which is expected to give superior nonlinear performance.

An additional element of this work was the investigation of a six mode-group design by perturbing the step-index design of Sillard [8.6]. Following the introduction of a core depression, the minimum mode spacing, which occurs between the LP_{21} and LP_{02} modes, has increased by 100% through the use of a ring perturbation. This is even an improvement over the six high-index rod design which increased the spacing by 30%. In addition an advantage of this ring design is ease of manufacture by methods such as MCVD. All fibre designs shows increased or comparable effective areas, in for all supported modes, which is expected to give good nonlinear performance.

8.4 References

[8.1] D. J. Richardson, J. M. Fini, and L. E. Nelson, "Space-division multiplexing in optical fibres," *Nat. Photonics*, vol. 7, no. April, pp. 354–362, 2013.

[8.2] M. Bigot-Astruc, D. Boivin, and P. Sillard, "Design and fabrication of weakly-coupled few-modes fibers," *2012 IEEE Photonics Soc. Summer Top. Meet. Ser.*, vol. 1, no. 978, pp. 189–190, Jul. 2012.

[8.3] D. Boivin, M. Bigot-Astruc, M. Travagnin, and P. Sillard, "Weakly-coupled Few-mode Fibers for Single-mode and Mode-division-multiplexed Transmissions," *Opt. Fiber Commun. Conf. Fiber Opt. Eng. Conf. 2013*, p. OTh3K.6, 2013.

[8.4] P. Sillard, M. Astruc, and D. Boivin, "Few-mode fiber for uncoupled mode-division multiplexing transmissions," *ECOC Tech. Dig.*, pp. 38–40, 2011.

[8.5] R. Olshansky, "Mode coupling effects in graded-index optical fibers," *Appl. Opt.*, vol. 14, no. 4, pp. 935–945, 1975.

[8.6] P. Sillard, M. Bigot-Astruc, and D. Molin, "Few-Mode Fibers for Mode-Division-Multiplexed Systems," *J. Light. Technol.*, vol. 32, no. 16, pp. 2824–2829, 2014.

[8.7] K. Jespersen et al., “Measuring distributed mode scattering in long, few-moded fibers,” *Opt. Fiber Commun. Conf. Fiber Opt. Eng. Conf. 2012*, pp. 1–3, 2012.

[8.8] A. Snyder and J. Love, *Optical Waveguide Theory*. London: Chapman and Hall, 1983.

[8.9] R. Stolen, “Modes in fiber optical waveguides with ring index profiles,” *J. Appl. Opt.*, vol. 14, no. 7, pp. 1533–1537, 1975.

Chapter 9: Inverse scattering designs of mode-selective fibre couplers

9.1 Introduction

Recent works have described how supersymmetry (SUSY), which originated in the context of quantum field theory, can be applied to the design of optical structures for integrated optics applications with prescribed eigenmode spectra such as by Miri et al. [9.1] as well as methods for selective mode filtering Heinrich et al. [9.2] and of particular interest to us, applications to the design of optical fibres [9.1]. In each case, SUSY operates on a trunk waveguide and provides a partner which is in some way perfectly phase-matched to the trunk. This perfect phase-matching between waveguides resolves a significant challenge in waveguide design in general. However, as we indicated recently [9.3], a flaw in the SUSY approach is that the partner waveguide cannot incorporate the fundamental mode unless complex refractive index (RI) profiles are utilised as discussed by Miri et al. [9.4], and must in addition contain all other modes supported by the trunk. As such, selective filtering must incorporate all other higher-order modes, and as such any selective filtering must be done through the use of a ladder or cascade of partner waveguides. In addition, there has been no discussion as to quite how the filtering process might be carried out as different phase-matched modes of coupled structures have differing coupling lengths for power transfer.

In this chapter we expand upon our previous works and describe how an alternative approach based upon inverse scattering theory [9.5] can be used to design optical fibres supporting linearly-polarized (LP) modes for which the propagation constants of the modes (the eigenmode spectra) are specified for a fixed azimuthal number l. This differs from the previous SUSY fibre works because we can *selectively* populate the modes of the partner fibre and are not limited to the removal of the fundamental LP_{01} mode at each stage as is the case with real RI profiles using the SUSY approach. We are also not restricted to a partner fibre design for which all higher-order fixed azimuthal value modes are automatically phase-matched and we are able to achieve this for the same fixed value of l (or any other) in the partner, not just l+1 as in the case of SUSY. It should be noted that there does not exist a method by which independent selection of mode azimuthal number l and energy E (propagation constant) can be achieved and typically either l or E is fixed. The most general method that does exist only allows specification along straight lines in the (l^2,E) plane [9.6].

In addition to discussion of the above design of selectively phase-matched partner fibres, we will discuss the potential for equalization of mode coupling lengths such that power transfer occurs at the same length. This follows along the same lines as that described in our previous work in Chapter 7 and is based upon the insight that gain or loss may be carefully used in a coupler to perform total power transfer of a specific mode as suggested by Chen et al. [9.7].

9.2 Selective phase-matching of modes

As discussed in the introduction, the advantage of the IS approach is the ability to *selectively* populate the LP modes of fixed azimuthal value l of a partner fibre and are not limited to the removal of the fundamental LP_{01} mode and the automatic phase-matching of all higher-order modes. We can also phase match the trunk modes to the same azimuthal value l in the partner, which is not the case with SUSY. We illustrate this process by considering a 12-mode step-index (SI) trunk fibre which has the following distribution of modes in Figure 9-2.

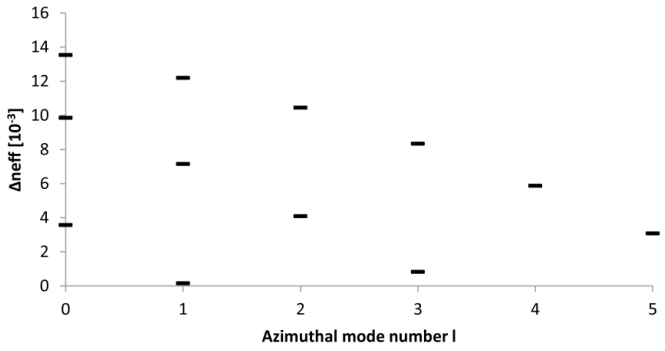

Figure 9-1: Eigenvalue spectra in terms of azimuthal mode number for a 12 mode step-index fibre with $\Delta n=1.44x10^{-2}$, $r_0=10.56$ μm, $n_2=1.444$ and $\lambda=1.55$μm

We now demonstrate the process by creating a partner fibre (design #1) for which we have selectively phase-matched to the l=0 modes LP_{01} and LP_{03} in the trunk fibre (red) to the l=0 modes LP_{01} and LP_{02} in the partner (green) in Figure 9-3. Table 9-1 gives the effective indices of the modes in the trunk and the partner respectively and Figure 9-4 gives its refractive index profile.

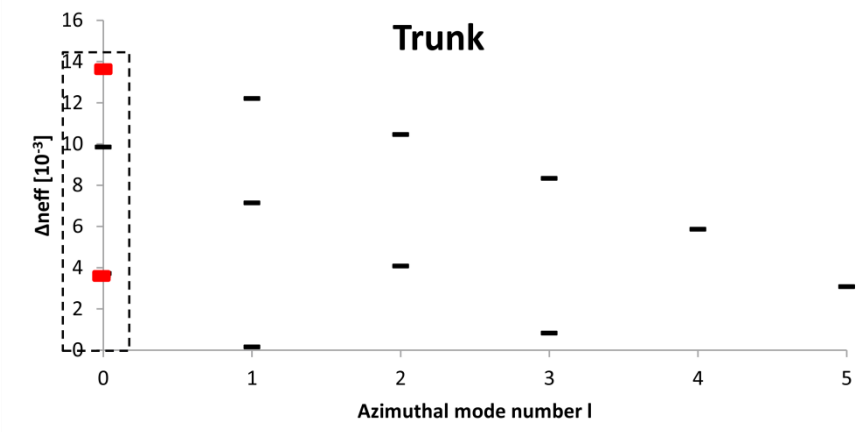

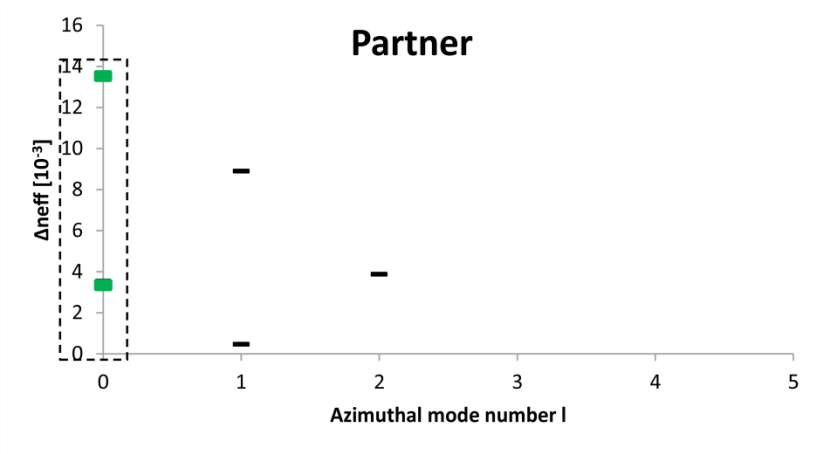

Figure 9-2: Eigenvalue spectra for design #1 - trunk fibre LP_{01} & LP_{03} modes (red) phase matched to the LP_{01} & LP_{02} modes of the partner fibre (green)

Table 9-1: Realised phase-matching modes for design #1

Mode (Trunk)	Mode (Partner)
LP_{01} (1.457528)	LP_{01} (1.457522)
LP_{03} (1.447562)	LP_{02} (1.447580)

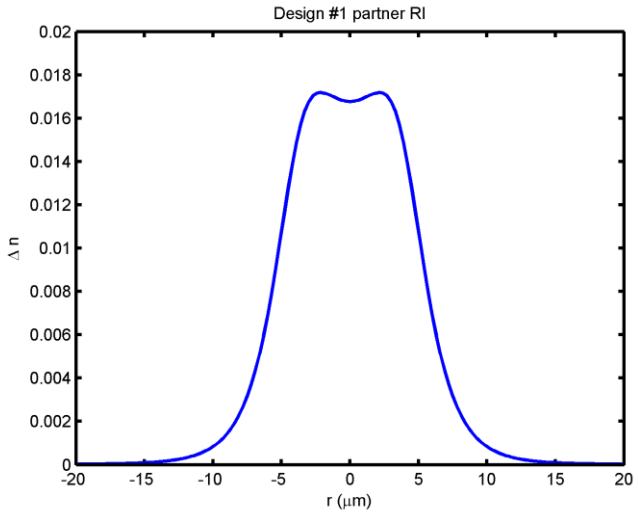

Figure 9-1: Refractive index profile of design #1 partner fibre with $n_{cladding}$=1.444 @ λ=1.55μm

We could also selectively phase match the l=2 modes LP_{21} and LP_{22} 'backwards' to the l=0 LP_{01} and LP_{02} modes of the partner (design #2) as shown in Figure 9-5. Once again, the effective indices

achieved are shown in Table 9-2 and the refractive index profile is given in Figure 9-6. Once again, this could not be achieved with SUSY. It would also be possible to continue this process for any desired l. It is worth noting that all other modes between the trunk and partner, as in the case of SUSY, are disjoint. In each of the cases described, the choice of the arbitrary parameters c_1 and c_2 were chosen (design #1 $c_1=c_2=\sqrt{0.2}$; design #2 $c_1=\sqrt{0.1}$, $c_2=\sqrt{0.2}$) simply by trial and error to produce a 'smooth' refractive index profile and their effect is discussed further in the next section.

We note that the effective indices are in good agreement and any discrepancy is due to the implementation of the finite mesh size, the position of the boundary conditions used in the simulations and the fact that we utilise a fully vectorial solver (MODE Solutions) in this work. We have confirmed that accuracy to within less than $\pm 1\times10^{-6}$ in the effective index can be achieved using a trial version of the LP mode solver (OptiFiber).

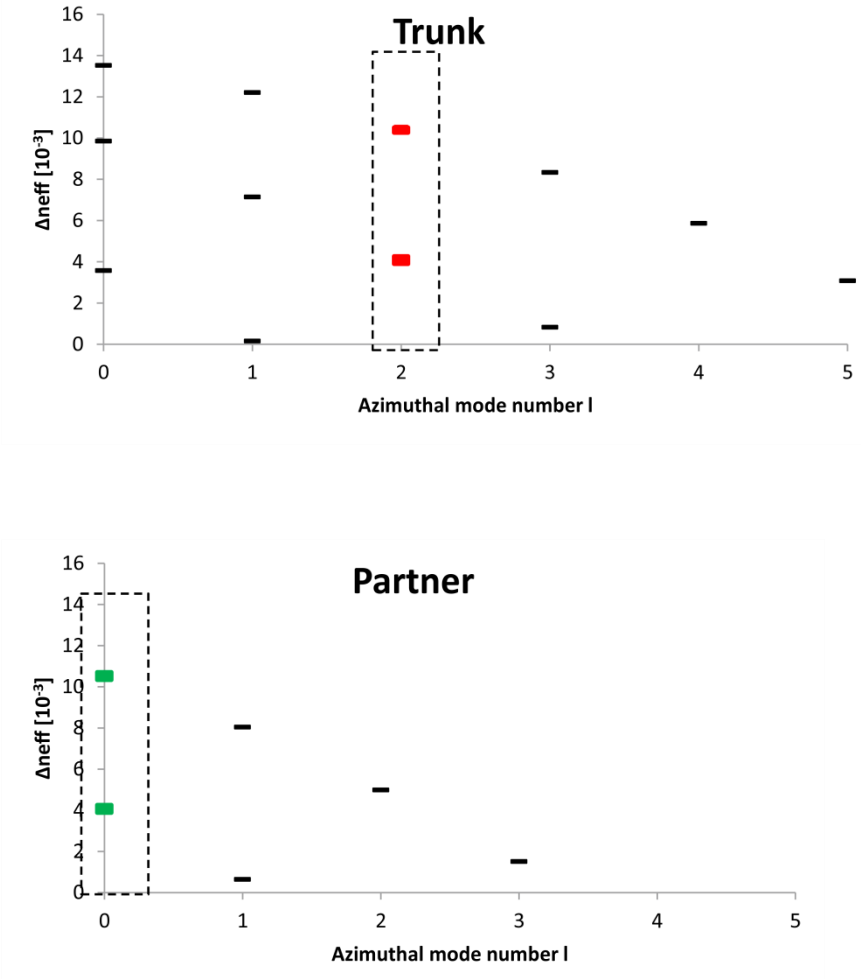

Figure 9-2: Eigenvalue spectra for design #2 - trunk fibre LP_{01} & LP_{03} modes (red) phase matched to the LP_{01} & LP_{02} modes of the partner fibre (green)

Table 9-2: Realised phase-matching modes for design #2

Modes (Trunk)	Modes (Partner)
LP_{21} (1.454448)	LP_{01} (1.454445)
LP_{22} (1.448064)	LP_{02} (1.448071)

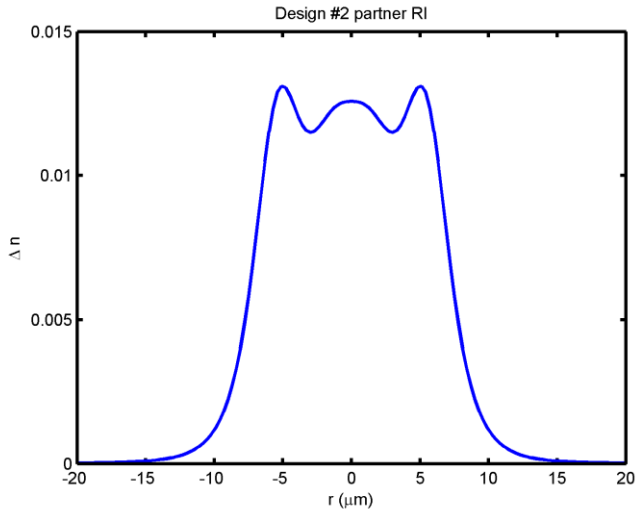

Figure 9-3: Refractive index profile of design #2 partner fibre with $n_{cladding}$=1.444 @ λ=1.55μm

We now proceed to discuss the coupling of modes between the trunk and partner fibres.

9.3 Designs with identical coupling lengths

We begin the process as follows: (1) we start with a trunk fibre that supports a set of guided modes. (2) We choose the azimuthal value l and particular modes from that set we wish to remove and IS design a partner fibre that is phase-matched to these modes. (3) We calculate the coupling coefficients $C_{12,m}$ and $C_{21,m}$ for each phase-matched set of modes. (4) We now solve (7.14) and use (7.15) to determine the optimum combination of (n,q). From this we then determine the optimum mode effective index correction $\Delta_{m,n..}$

Following step (1) we calculate the coupling coefficients in terms of the RI profile, angular frequency ($\omega=2\pi c/\lambda$), permeability of free space μ_0, permittivity of free space ε_0 and the normalized transverse LP mode electric fields E_{yi}, and E_{yj} where F_i indicates that the integral should be performed over the cross section of fibre i.

$$C_{ij} = \omega\varepsilon_0 \int_{F_i} \left(n^2 - n^2{}_j\right) E_{yi}^{*}(x,y) E_{yj}(x,y)\, dxdy \tag{9.1}$$

We note that the normalization of the electric fields here follows that of [9.2] such that, for i=1,2

$$4\times\left[\frac{\beta}{2\omega\mu_0}\int_{F_i}\left|E_y(x,y)\right|^2 dxdy\right]=1 \tag{9.2}$$

As examples we now consider the design of the coupler designs #1 and #2 described at the start of this chapter where in design #1 the LP_{01} and LP_{03} modes are dropped from the trunk and coupled into the LP_{01} and LP_{02} modes of the partner, and in design #2 the LP_{21} and LP_{22} modes are dropped and coupled into the LP_{01} and LP_{02} modes of the partner. It is interesting to note that in recent work Riesen & Love [9.15] discussed mode-selective fibre couplers and the necessity for specific azimuthal orientations of the trunk and partner modes in addition to phase-matching, for optimal power transfer. The coupling coefficient between the trunk LP_{ln} and partner LP_{0m} modes is found to have a cos(lα) dependence [9.15] on the line defined by angle α which is perpendicular to the zero line of the anti-symmetric trunk mode field. Here we assume for simplicity that α=0.

9.3.1 Design #1 – LP_{01} & LP_{03} dropped

As an example, the coupling coefficients are given in Table 9-3 for the case of design #1 involving the phase-matching of the 12-mode SI trunk fibre modes (LP_{01} & LP_{03}) and the IS partner fibre modes (LP_{01} and LP_{02}) with a spacing between profile centres of 22 μm. This was chosen experimentally leading to a relatively low-loss and short length device. The optical power transfer between the trunk and partner fibres are shown in Figures 9-7 & 9-8 respectively. It is observed that, as expected, all the power of the LP_{01} trunk mode is removed in Figure 9-7 after ~66 LP_{03} –LP_{02} coupling lengths due to the disparity in coupling coefficients between the pairs, whereas in Figure 9-8 the removal of LP_{03} power from the trunk occurs at one LP_{03}-LP_{02} coupling length.

Table 9-3: Coupling coefficients for design #1 with two phase-matched modes with trunk-partner spacing 22 μm apart

Modes (Trunk-Partner)	C_{12} / C_{21} (m^{-1})
LP_{01} -LP_{01}	3.33 / 3.33
LP_{03}-LP_{02}	220 / 222

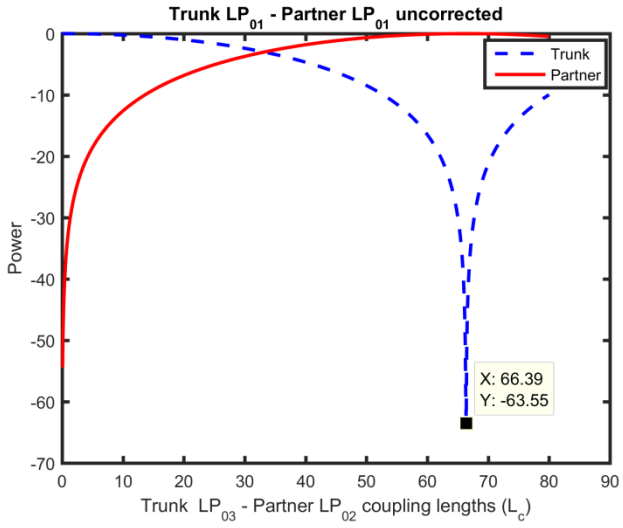

Figure 9-4: Variation in optical power between the design #1 trunk SI LP_{01} and partner IS LP_{01} modes as a function of the LP_{03} –LP_{02} coupling lengths

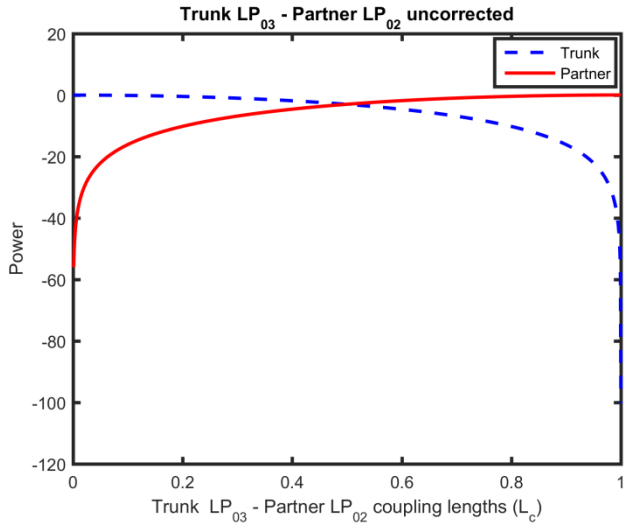

Figure 9-5: Variation in optical power between the trunk SI LP_{03} and partner IS LP_{02} modes as a function of LP_{03}-LP_{02} coupling lengths

From Figure 9-7 we see that the 0^{th}-order coupling length of the LP_{01}-LP_{01} pair is equal to ~66 LP_{03}-LP_{02} coupling lengths and since total transfer of power occurs between the LP_{03}-LP_{02} pair at odd numbers of coupling lengths, the current configuration would not result in total power transfer from the trunk for both the LP_{01} and LP_{03} modes at the same device length. In particular, at ~67 LP_{03}-LP_{02} coupling lengths the remaining LP_{01} power in the trunk is ~-37 dB, which although small in this particular case, does not compare with the <-100 dB level of the LP_{03} mode.

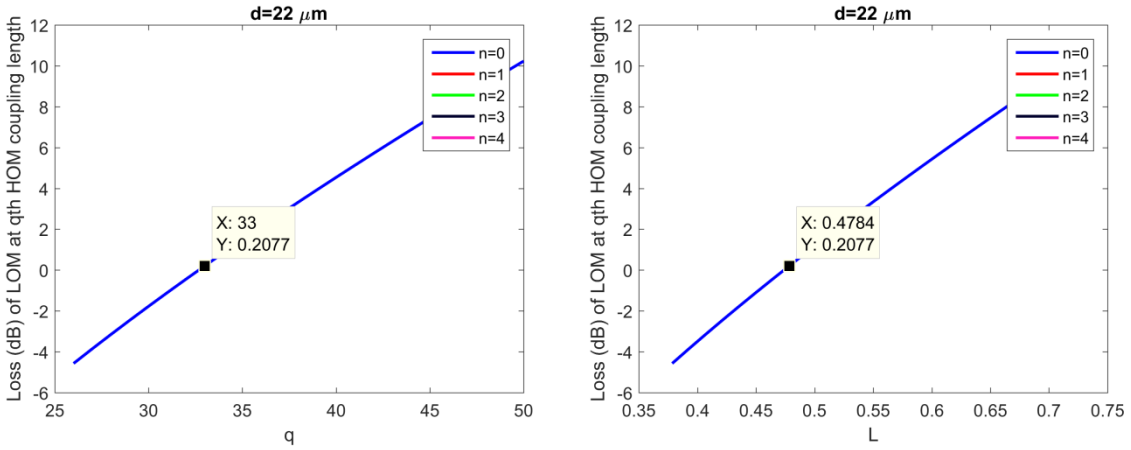

(a) (b)

Figure 9-6: Loss curves for determining the design #1 correction - (a) the (n,q) loss curve showing the loss (dB) at the q'th order coupling length of the LP_{03}-LP_{02} pair for various corrected n'th order LP_{01}-LP_{01} coupling lengths, (b) the same but with length of device in metres

As such we wish to perturb the effective index of the LP_{01} partner mode with gain/loss to correct for this. Using Figure 9-9 we see that the 33rd-order coupling length of the LP_{03}-LP_{02} pair can be equalised to the 0th-order LP_{01}-LP_{01} pair with a loss in power transfer of the LP_{01}-LP_{01} pair of ~0.2 dB. Thus the (n,q) pair is (0,33) and associated using (9.31) with a value of $M_{1,1}$= 0.015 and therefore an effective index correction of $\Delta_{1,1}$=i2.46x10^{-8} . The corrected effective indices of the partner fibre are given in Table 9-4. The resulting coupler design is shown in Figure 9-10 where it can be seen that the refractive index profile of the partner fibre now contains an imaginary component given by the dotted line resulting in the above effective index perturbation. The real part of the refractive index profile remains the same as before the imaginary corrected. The corrected power transfer curves are shown in Figure 9-11 where it can now be seen that the power left in the trunk at [9.33x2+1=67] (478mm device length) coupling lengths is now <-71 dB which is an improvement. In addition, we see that the LP_{01} power in the partner is, as expected, approximately -0.2 dB.

Table 9-4: Corrected partner fibre modes for design #1

Mode (Trunk)	Mode (Partner)
LP_{01} (1.457528)	LP_{01} (1.457528+ i2.46x10^{-8})
LP_{03} (1.447562)	LP_{02} (1.447562)

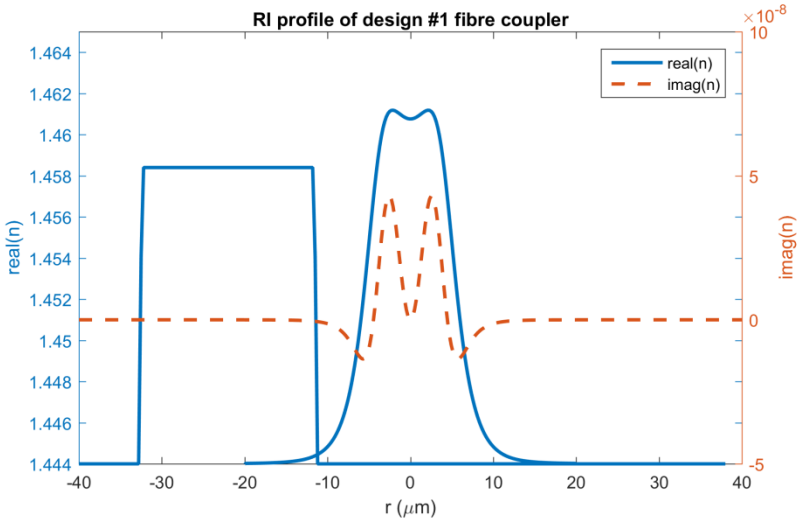

Figure 9-7: Refractive index profile of the design #1 fibre coupler

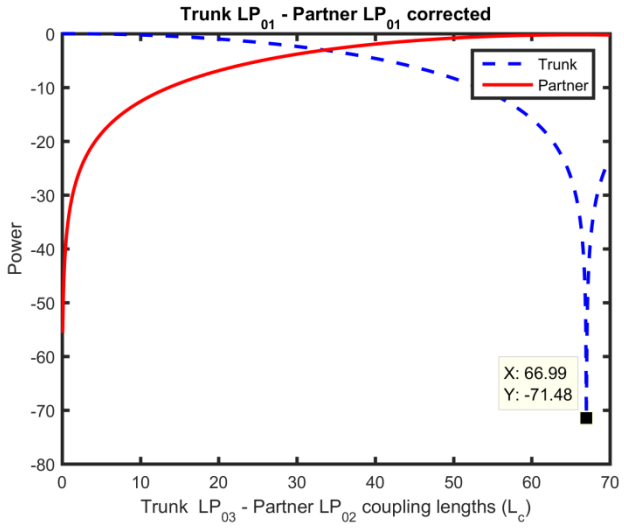

Figure 9-8: Variation in optical power between the corrected design #1 trunk SI LP_{01} and partner IS LP_{01} modes as a function of the LP_{03} –LP_{02} coupling lengths

It is possible to repeat this process for any of the higher-order modes or even a combination of them. We now show this by considering the 'drop' at the LP_{22}-LP_{03} coupling length in design #2 of both the LP_{21}-LP_{01} and LP_{22}-LP_{02} pairs.

9.3.2 Design #2 – LP_{21} & LP_{22} dropped

Here, the coupling coefficients are given in Table 9-5 for the case of design #2 involving the phase-matching of the 12-mode SI trunk fibre modes (LP_{21} & LP_{22}) and the IS partner fibre modes (LP_{01} and LP_{02}) with a spacing of 23 μm. The optical power transfer between the trunk LP_{21} and partner LP_{01} modes are shown in Figure 9-7 where it is observed that, as expected, all the power of the LP_{21}

trunk mode is removed after ~2/6/11 LP_{22} –LP_{02} coupling lengths for the 0th, 1st and 2nd order lengths once again due to the disparity in coupling coefficients between the pairs.

Table 9-5: Coupling coefficients for design #2 with two phase-matched modes with trunk-partner spacing 23 μm apart

Modes (Trunk-Partner)	C_{12} / C_{21} (m^{-1})
LP_{21} -LP_{01}	12.2 / 12.2
LP_{22}-LP_{02}	26.4 / 26.5

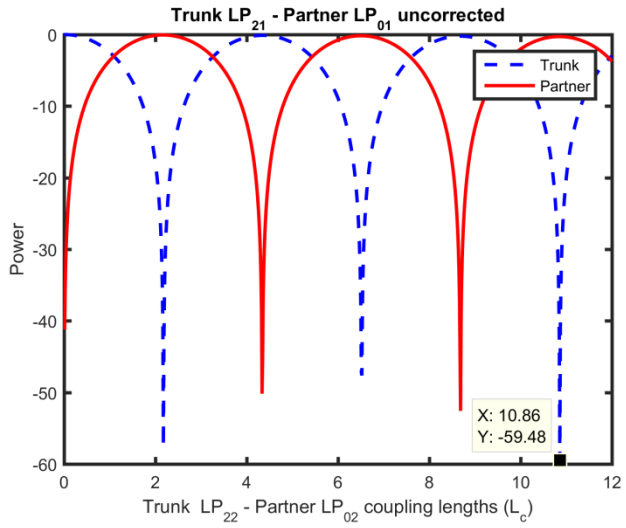

Figure 9-9: Variation in optical power between the design #2 trunk SI LP_{01} and partner IS LP_{01} modes as a function of the LP_{22} –LP_{02} coupling lengths

From Figure 9-12 we see that for odd numbers of the LP_{22}-LP_{02} coupling lengths, the power of the LP_{21} mode remaining in the trunk is at least -5 dB when there is full power transfer of the LP_{22} mode. As such we wish to perturb the effective index of the LP_{01} partner mode with gain/loss to correct for this and we once again use ‘correction curves’ in Figure 9-13 to identify the optimum correction.

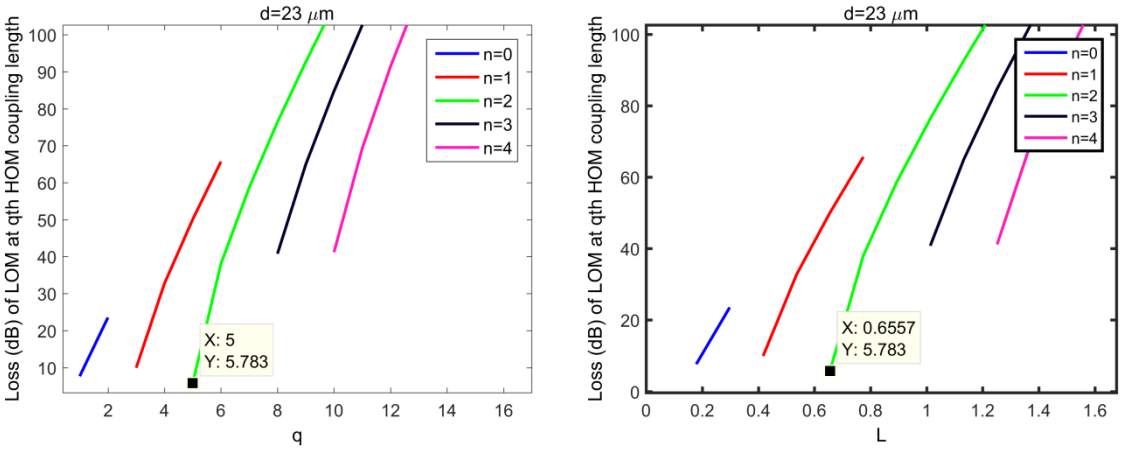

(a) (b)

Figure 9-10: Loss curves for determining the design #2 correction - (a) the (n,q) loss curve showing the loss (dB) at the q'th order coupling length of the LP_{22}-LP_{02} pair for various corrected n'th order LP_{21}-LP_{01} coupling lengths, (b) the same but with length of device in metres

As such we wish to perturb the effective index of the LP_{01} partner mode with gain/loss to correct for this. Using Figure 9-13 we see that the 5th-order coupling length of the LP_{22}-LP_{02} pair can be equalised to the 2nd-order LP_{21}-LP_{01} pair with a loss in power transfer of the LP_{21}-LP_{01} pair of ~5.8 dB. Thus the (n,q) pair is (2,5) and is associated using (9.31) with a value of $M_{1,3}$= 0.0833 and therefore an effective index correction of $\Delta_{1,3}$=i5.00x10^{-7} . The corrected effective indices of the partner fibre are given in Table 9-6. The resulting coupler design is shown in Figure 9-14 where it can be seen that the refractive index profile of the partner fibre now contains an imaginary component given by the dotted line resulting in the above effective index perturbation. The real part of the refractive index profile remains the same as before the imaginary corrected. The corrected power transfer curves are shown in Figure 9-15 where it can now be seen that the power of the LP_{01} mode left in the trunk after [9.5x2+1=11] (655mm device length) coupling lengths is now <-63 dB which is again a large improvement. Once again, the power of the LP_{01} mode in the partner is now ~-5.8 dB as predicted.

Table 9-6: Corrected partner fibre modes for design #1

Mode (Trunk)	Mode (Partner)
LP_{21} (1.454448)	LP_{01} (1.454448+i5x10^{-7})
LP_{22} (1.448064)	LP_{02} (1.448064)

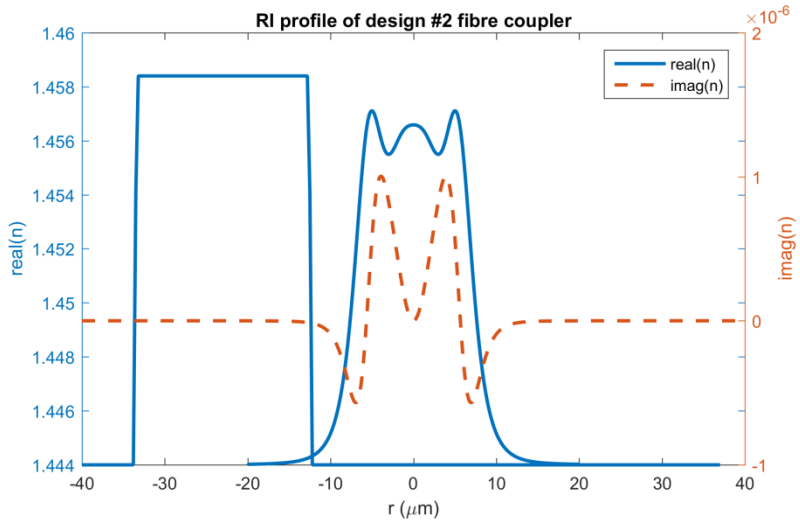

Figure 9-11: Refractive index profile of the design #2 fibre coupler

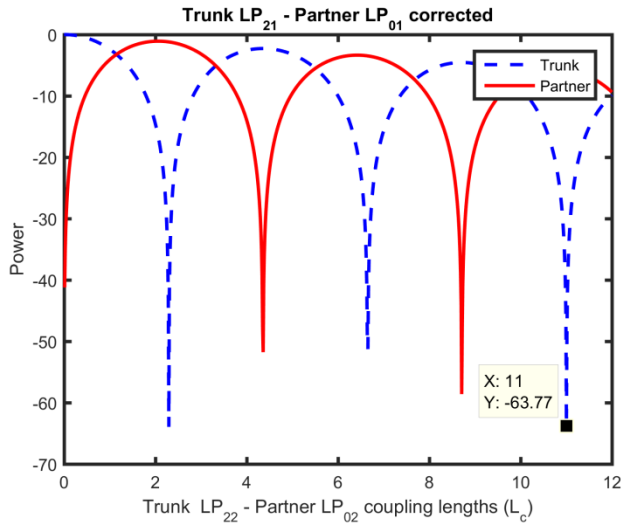

Figure 9-12: Variation in optical power between the corrected design #2 trunk SI LP_{21} and partner IS LP_{01} modes as a function of the LP_{22} –LP_{02} coupling lengths

9.4 Discussion

In this chapter we have demonstrated that it is possible to remove or ‘drop’ selected modes simultaneously from a trunk fibre using a coupled partner fibre which has a calculated imaginary phase-mismatch first suggested by Chen et al. [9.7]. In our case we have limited our discussion to the use of loss in a partner fibre, while it would also be possible to investigate the use of gain, the value of both being calculated using coupled-mode theory, and then implemented using inverse-scattering theory. In each case it was necessary to select the spacing between the trunk and partner

fibres in order to calculate coupling coefficients and in turn the optimum correction. Here we have simply used some intuition and trial and error in order to find devices of reasonable length, but the general pattern to be noted is that smaller trunk-partner fibre spacings tend to lead to shorter equalised devices, though there is always a balance to be had also with respect to the loss in the process. This use of a lossless trunk fibre and a lossy partner has also been considered fairly recently in the context of quantum mechanical PT-symmetry breaking [9.16]. However, it is our belief that this is the first time this has been considered from a more practical point of view with respect to mode-selective couplers, especially in terms of their inverse design. It must be noted that the issues relating to the azimuthal orientation of modes and associated coupling strengths must also be taken into account, but we believe that this work will contribute to the design of mode-selective couplers with a more general and useful approach than that considered in by the use of SUSY.

9.5 References

[9.1] M. A. Miri, M. Heinrich, R. El-Ganainy, and D. N. Christodoulides, "Supersymmetric optical structures," *Phys. Rev. Lett.*, vol. 110, pp. 1–5, 2013.

[9.2] M. Heinrich, M.-A. Miri, S. Stützer, R. El-Ganainy, S. Nolte, A. Szameit, and D. N. Christodoulides, "Supersymmetric optics: Continuous and discrete 1D structures for selective mode filtering," in *CLEO 2013*, p. QM1E.1, 2013.

[9.3] A. R. May and M. N. Zervas, "IS designs for mode selective waveguide couplers," in *23rd Int. Workshop OWTNM*, 2015.

[9.4] M.-A. Miri, M. Heinrich, and D. N. Christodoulides, "Supersymmetric optical waveguides," in *SPIE Photonics West 2014-OPTO: Optoelectronic Devices and Materials*, 2014, vol. 8980, p. 89801F.

[9.5] S. P. Yukon and B. Bendow, "Design of waveguides with prescribed propagation constants," *J. Opt. Soc. Am.*, vol. 70, no. 2, pp. 172–179, 1980.

[9.6] B. Rudyak, A. Suzko, and B. . Zakhariev, "Exactly Solvable Models (Crum-Krein Transformations in the (λ2, E)-Plane)," *Phys. Scr.*, vol. 29, pp. 515–517, 1984.

[9.7] Y. Chen, A. W. Snyder, and D. N. Payne, "Twin core nonlinear couplers with gain and loss," *IEEE J. Quantum Electron.*, vol. 28, no. 1, pp. 239–245, 1992.

[9.8] H. Moses and S. . Tuan, "Potentials with Zero Scattering Phase," *Nuovo Cim.*, vol. 13, pp. 197–206, 1959.

[9.9] I. Gradshteyn and I. Ryzhik, *Table of integrals, series and products*, Seventh Ed. London, UK: Academic Press, 2007.

[9.10] A. Suzko and E. Velicheva, "Supersymmetry and Darboux transformations," *J. Phys. Conf. Ser.*, vol. 343, p. 012120, 2012.

[9.11] R. Sasaki, "Exactly Solvable Quantum Mechanics," *The Universe*, vol. 2, no. 2, pp. 1–32, 2014.

[9.12] A. Yariv, “Coupled-mode theory for guided-wave optics,” *IEEE J. Quantum Electron.*, vol. 9, no. 9, 1973.

[9.13] H. Haus and L. Molter-Orr, “Coupled multiple waveguide systems,” *IEEE J. Quantum Electron.*, vol. 19, no. 5, pp. 840–844, 1983.

[9.14] K. Okamoto, *Fundamentals of Optical Waveguides*. London, UK, 2006.

[9.15] N. Riesen and J. D. Love, “Weakly-guiding mode-selective fiber couplers,” *IEEE J. Quantum Electron.*, vol. 48, no. 7, pp. 941–945, 2012.

[9.16] A. Guo, G. J. Salamo, D. Duchesne, R. Morandotti, M. Volatier-Ravat, V. Aimez, G. A. Siviloglou, and D. N. Christodoulides, “Observation of PT-symmetry breaking in complex optical potentials,” *Phys. Rev. Lett.*, vol. 103, no. 9, pp. 1–4, 2009.

Chapter 10: **Conclusions and Future Work**

10.1 **Inverse scattering designs of optical waveguides**

In this thesis the design of optical waveguides by inverse scattering has been considered and there has been a successful investigation over how dispersion can be controlled through the manipulation of the transverse reflection response of a waveguide. In general, the reflection response can be approximated by a rational reflection coefficient with varying numbers of poles, and here for the first time a larger numbers of poles have been investigated and found to "fine-tune" the waveguide dispersion. To my knowledge this is also the first time that the more general inverse scattering algorithm for rational reflection coefficients devised by Pechnick [10.1] has been applied to waveguides.

Following on from the work of Mills and Tamil [10.2] the design of multimode planar waveguides was considered using Darboux transformations from the point of view of group velocity equalisation [10.3] and the design of mode-selective waveguide couplers [10.4] as an alternative to the recently proposed SUSY approach. The addition of mode-selective gain or loss was then investigated through the use of complex propagation constants [10.5] which for the first time showed theoretically that both gain and loss are required in the refractive index profile for exact equalisation of modal gain. Finally, the combination of arbitrary phase-matching of modes and the addition of tailored loss/gain in trunk-partner designs was used to drop arbitrarily chosen modes and equalise their coupling lengths. By the end of the aforementioned works, it was discovered that the SUSY approach is in fact a particular case of the Darboux transformation approach as discussed in Chapter 2. It is interesting to note that for the reflectionless potentials considered in the design of multimode waveguides above, both the solution to the Gel'fand-Levitan-Marcheko equations and Darboux transformation approach lead to the very same family of potentials [10.6].

This work has shown that inverse scattering techniques open up new previously unexplored possibilities in the design of planar waveguides and we discuss this in the following future work section.

10.2 **Inverse scattering designs of optical fibres**

This thesis began with the aim of applying inverse scattering techniques to the design of optical fibres and although a lot of the achievements to date have been with respect to planar waveguides, much has been learnt in the process. The similarity in mode intensity field profiles between low-order fibre LP modes and that of the TE modes of planar waveguides meant that intuition could be gained from studying the waveguide designs. Initially this led to the design of a few-mode fibre with improved

LP mode spacing [10.7] whereby the core depressions observed in the waveguide designs were carried over to a fibre design. This particular design was further improved through the addition of 'rod-like' features which preferentially 'lift' modes with similar symmetries. This approach is also justified by considering the formula derived by Snyder and Love [10.8] which gives the effective index of a perturbed fibre design in terms of a weighed integral of the perturbation itself and the mode field intensity.

Towards the end of the thesis it was found that previous work performed by Yukon and Bendow [10.9] had investigated the solution of the Gel'fand-Levitan-Marchenko approach in cylindrical coordinates under the weakly-guiding approximation. In particular, phaseless scattering potentials were considered, in an analogous way to the reflectionless potentials of planar waveguides, and explicit solutions were found for specifying the effective index of LP_{lm} modes for m modes of fixed azimuthal value l. While another paper was found by Hooshyar and Tamil [10.10] that discussed another class of the problem, the specification of fixed effective index for varying azimuthal value l, it became clearer that it is not possible to specify freely in advance the effective index of LP modes of varying azimuthal l value, when the paper by Rudyak [10.11] was discovered. Here the aforementioned two different classes of inverse scattering problem were described as being particular cases of their formalism which allowed for the closed-form solution of the problem along arbitrary lines in the (l^2, E) plane. What this showed was that at its most general the problem only had a solution along lines in the (l^2, E) plane and therefore the more general approach that was sought at the start of the work was not achievable.

However, it was found that the approach adopted for fixed l still allowed for the design of fibre couplers based upon the very same trunk-partner formalism adopted in the waveguide designs above. In fact, recent work using SUSY [10.12] had obtained cascades of fibres where the partners always produced phase-matched LP_{lm} modes but with increased order l+1 at each stage. The Gel'fand-Levitan-Marchenko approach, on the other hand, had no such limitation and as discussed in Chapter 9 phase-matching of selected trunk modes is possible for any fixed l. In addition, an attempt to add modal gain/loss to fibre designs was met through trial and error with designs which had very good equalisation of modal gain across the board, simply by specifying the fixed gain and varying the effective indices of the modes. It is interesting to note that iterative variation of the free parameters in the Gel'fand-Levitan-Marchenko design process for fixed effective indices also allows for a certain tailoring of the mode spectra of modes that 'fill the gaps' between the effective indices specified for the fixed l modes. This, due to time constraints, was not included in this thesis, but will be discussed in a future paper. As in the case of waveguide couplers above, the very same approach to coupling length equalisation using the tailoring of gain/loss in the design process is possible.

It is felt that the work performed on fibres here has shown both the benefits and limitations of the inverse scattering approach to fibre design. On one hand the approach described is an alternative and more general one to that of SUSY as described in Chapter 2, while it has been shown that there is no

freedom to obtain fibre designs with arbitrarily prescribed LP modes. However, as above, it has also been shown that variation of free parameters in the design process gives an element of control over the modes that 'fill the gaps'. There is certainly further work possible on the iterative fine-tuning of mode spectra through this approach.

10.3 **Future work**

In the above, some conclusions have been drawn regarding the success of this research work in both the design of planar waveguides and optical fibres. As discussed, the work has shown that there are both more possibilities as well as limitations, particularly in the design of fibres, than previously thought.

While completing this thesis it has come to our attention that considerable work has been carried out on mode selective excitation and gain control in special large-mode area (LMA) fibres known as 'ribbon fibres' [10.13]. These fibres are expected to be used as alternatives to standard circular LMA fibres as they can potentially offer superior bending performance, better heat dissipation and improved power scalability. The work performed in this thesis on the mode-selective tailoring of gain could be applied to this design problem as ribbon fibres are known to utilise high-aspect ratio rectangular cores which are "semi-guiding" in the sense that only one axis is guiding and the other effectively un-guiding which can be approximated by a simple planar waveguide design.

Our novel inverse scattering approaches can also be used to design semiconductor amplifiers and lasers with improved modal properties and output power stability. In this case, gain and loss can be introduced in the waveguiding section by locally pumping the semiconductor. This can be achieved by appropriately patterned electrodes or interference patterns [10.14]-[10.16].

Recent work has shown that ring-core fibre designs [10.17] may be used for a very good standard of gain equalisation and qualitatively similar designs can be obtained without any assumptions as to the form of the rings, from inverse scattering theory and as mentioned above will be published shortly in a paper. It is expected that significant equalisation of gain across a large number of LP mode groups is possible using this approach, even if in an iterative manner.

The design of mode-selective waveguide and fibre couplers could be investigated further but from the point of view of loss-less designs that allow for the incorporation of both loss and gain in both the trunk and partner. This would be timely considering the work using PT-symmetry [10.18] where de-multiplexing using such a design approach has been considered.

Finally, it should added that in the case of optical fibres, the localised gain and loss can be potentially distributed accurately inside the core and/or cladding regions using "pixilation" techniques. In this case, sub-wavelength rods, doped with active ions that can absorb or amplify the signal [10.19] can be optimally assembled and drawn into fibres by a standard "stack-and-draw" technique [10.20].

These fibre drawing techniques have been extensively used in modern advanced active fibre designs [10.21].

10.4 References

[10.1] K. R. Pechenick, "Inverse scattering—exact solution of the Gel'fand-Levitan equation," *J. Math. Phys.*, vol. 22, no. 7, pp. 1513–1516, 1981.

[10.2] D. W. Mills and L. S. Tamil, "Synthesis of Guided Wave Optical Interconnects," *IEEE J. Quantum Electron.*, vol. 29, no. 11, pp. 2825–2834, 1993.

[10.3] A. R. May and M. N. Zervas, "Group velocity equalisation in multimode waveguides using inverse scattering designs," in *Sixth International Conference on Optical, Optoelectronic and Photonic Materials and Applications (ICOOPMA '14)*, 2014.

[10.4] A. R. May and M. N. Zervas, "IS designs for mode selective waveguide couplers," in *23rd Int. Workshop OWTNM*, 2015.

[10.5] A. R. May and M. N. Zervas, "Inverse scattering designs of active multimode waveguides with tailored modal gain," *J. Sel. Top. Quantum Electron.*, 2015.

[10.6] R. Sasaki, "Exactly solvable potentials with finitely many discrete eigenvalues of arbitrary choice," *J. Math. Phys.*, vol. 55, 062101, pp.1-11, Jun. 2014.

[10.7] A. R. May and M. N. Zervas, "Few-Mode Fibers with Improved Mode Spacing," in *European Conference on Optical Communication (ECOC)*, 2015.

[10.8] A. Snyder and J. Love, *Optical Waveguide Theory*. London: Chapman and Hall, 1983.

[10.9] S. P. Yukon and B. Bendow, "Design of waveguides with prescribed propagation constants," *J. Opt. Soc. Am.*, vol. 70, no. 2, pp. 172–179, 1980.

[10.10] M. Hooshyar and L. S. Tamil, "Inverse scattering theory at fixed energy and the design of circular optical waveguides," *J. Math. Phys.*, vol. 33, pp. 663–669, 1992.

[10.11] B. Rudyak, A. Suzko, and B. Zakhariev, "Exactly Solvable Models (Crum-Krein Transformations in the (λ2, E)-Plane)," *Phys. Scr.*, vol. 29, pp. 515–517, 1984.

[10.12] M. A. Miri, M. Heinrich, R. El-Ganainy, and D. N. Christodoulides, "Supersymmetric optical structures," *Phys. Rev. Lett.*, vol. 110, pp. 1–5, 2013.

[10.13] J. R. Marciante, V. V. Shkunov, and D.A. Rockwell, "Semi-guiding high-aspect-ratio core (SHARC) fiber amplifiers with ultra-large core area for single-mode kW operation in a compact coilable package," *Opt. Express*, vol. 20, no. 18, pp. 20238-20254, 2012.

[10.14] R. Herrero, M. Botey, M. Radziunas, and K. Staliunas, "Beam shaping in spatially modulated broad-area semiconductor amplifiers.," *Opt. Lett.*, vol. 37, no. 24, pp. 5253–5255, 2012.

[10.15] S. Kumar, R. Herrero, M. Botey, and K. Staliunas, "Suppression of modulation instability in broad area semiconductor amplifiers," *Opt. Lett.*, vol. 39, no. 19, pp. 5598–5601, 2014.

[10.16] R. Herrero, M. Botey, N. P. Kumar, and K. Staliunas, "Improving beam quality in broad area semiconductor amplifiers," in *Proc. of SPIE*, 2012, 843222.

[10.17] Q. Kang, E.-L. Lim, F. P. Y. Jung, C. Baskiotis, S. Alam, and D. J. Richardson, "Minimizing differential modal gain in cladding-pumped EDFAs supporting four and six mode groups," *Opt. Express*, vol. 22, no. 18, pp. 21499-21507, 2014.

[10.18] H. Benisty, A. Lupu, and A. Degiron, "Transverse periodic PT symmetry for modal demultiplexing in optical waveguides," *Phys. Rev. A*, vol. 91, no. 5, pp. 1-11, 2015.

[10.19] J. Townsend, "The development of optical fibres doped with rare-earth ions," PhD Thesis, University of Southampton, 1990.

[10.20] W. Wadsworth, R. Percival, G. Bouwmans, J. Knight, and P. Russell, "High power air-clad photonic crystal fibre laser.," *Opt. Express*, vol. 11, no. 1, pp. 48–53, 2003.

[10.21] A. Benoit, R. Dauliat, K. Schuster, S. Grimm, R. Jamier, F. Salin, and P. Roy, "Optical fiber microstructuration for strengthening single-mode laser operation in high power regime," *Opt. Eng.*, vol. 53, no. 7, 071817, pp. 1–6, 2014.